

POLYMER/CLAY NANOCOMPOSITE SELF-ASSEMBLY FOR GAS BARRIER
FILMS APPLICATION

By

Maedeh Dabbaghianamiri

A dissertation submitted to the Graduate Council of
Texas State University in partial fulfillment
of the requirements for the degree of
Doctor of Philosophy
with a Major in Materials Science, Engineering, and Commercialization
December 2017

Committee Members:

Gary W. Beall, Chair

Clois E Powell

William Chittenden

Christopher Rhodes

Farhad Ameri

COPYRIGHT

by

Maedeh Dabbaghianamiri

2017

FAIR USE AND AUTHOR'S PERMISSION STATEMENT

Fair Use

This work is protected by the Copyright Laws of the United States (Public Law 94-553, section 107). Consistent with fair use as defined in the Copyright Laws, brief quotations from this material are allowed with proper acknowledgement. Use of this material for financial gain without the author's express written permission is not allowed.

Duplication Permission

As the copyright holder of this work I, Maedeh Dabbaghianamiri, authorize duplication of this work, in whole or in part, for educational or scholarly purposes only.

DEDICATION

For mom and dad

ACKNOWLEDGEMENTS

The work reported in this dissertation was supported by the National Science Foundation (PREM Center for Interfaces, DMR-1205670), and the Graduate College, Doctoral Research Support Fellowship. Moreover, my special thanks are for the College of Science and MSEC program for financial support.

Special thanks to my advisor Dr. Gary Beall, who provided me with the opportunity to work in his research group during the past three years.

I would also like to thank Dr. Powell for his excellent guidance and giving me the opportunity to work in his polymer lab to get more hands-on experience.

I would also like to thank my committee members, Dr. Powell, Dr. Chittenden, Dr. Rhodes, and Dr. Ameri for their excellent advice.

I would like to thank the postdoctoral fellows of Dr. Beall's group, Dr. Sayantan Das, Dr. Shazly Duria, and Dr. Abbas Fahami for their help and support during my research.

Finally, I want to say many thanks to my husband, Javad and my parents for their support to help my dream come true.

TABLE OF CONTENTS

	Pages
ACKNOWLEDGEMENTS	vii
LIST OF TABLES	xi
LIST OF FIGURES	xii
ABSTRACT	xvi
CHAPTER	
I. INTRODUCTION	1
1.1 Background and Motivation	1
1.2 Dissertation Overview and Research Objectives	7
II. DEPOSITION AND CHARACTRIZATION TECHNIQUES.....	9
2.1 Deposition Techniques.....	9
2.2 Characterization Techniques.....	12
2.2.1 X-ray Diffraction (XRD)	12
2.2.2 Oxygen Transmission Rate (MOCON 2/60)	14
2.2.3 Transparency Measurement (UV-Vis spectrometer)	16
III. POLYMERS AND MMT NANOCLAY.....	18
3.1 Introduction.....	18
3.2 Different Polymers.....	18
3.2.1 Polyvinylpyrrolidone (PVP)	18
3.2.2 Polyethylene Glycol (PEG)	19
3.2.3 Polyacrylic Acid (PAA).....	20

3.2.4 Polyvinyl Acetate (PVA), Ethylvinyl Alcohol (EVOH) and Polyvinyl Alcohol (PVOH)	20
3.3 Role of Entropy in Polymer-nanoparticles	22
3.4 Different Polymers and MMT Nanoclay	25
3.4.1 XRD and OTR of Different Polymers and MMT Nanoclay	26
3.5 Role of Different Hydrolyzation Levels (DHL) in PNCs.....	31
 IV. CLAYS AND NANOFILLERS IN PNC	34
 4.1 Introduction.....	34
4.2 Different Clays and Nanofiller in Gas Barrier Applications	34
4.2.1 Saponite Clay	39
4.2.3 Humic Acid.....	40
4.2.4 Hydrotalcite	41
4.2.5 Vermiculite Clay (VMT)	42
4.2.6 Hectorite Clay	43
4.2.7 Laponite Clay.....	44
4.3 Modeling	48
 V. ANNEALING AND HUMIDITY IN PNC	50
 5.1 Introduction.....	50
5.2 Annealing Time Relationships in PNC.....	50
5.3 Oxygen Transmission Rate and Humidity Relationship.....	53
5.4 Polymer Molecular Weights Role in PNCs	60

VI. INKJET PRINTING AND COATING APPLICATION	63
6.1 Introduction.....	63
6.2 Comparison between Printing and Spraying Deposition	63
6.3 Transparency and PNCs Thickness	76
6.4 Edible Coating Application.....	76
VII. CONCLUSION AND RECOMMENDATION FOR FURTHER RESEARCH	80
7.1 Results and Conclusion.....	80
7.2 Recommendation for Future Research.....	82
APPENDIX SECTION	83
REFERENCES	87

LIST OF TABLES

Table	Page
3. 1: Hydrolyzation level of PVOH with MMT and OTR relation.....	32
4. 1: Relative permeation for different clays in Tortuous Path model.....	48
6. 1: Comparison of composite transmittance films used with various materials, OTR and transparency in range of visible light (400 nm -700 nm) via UV-Vis spectrometer.....	75

LIST OF FIGURES

Figure	Page
1. 1: LbL technique procedure	2
1. 2: Intercalated and Exfoliated nanocomposites structure	4
2. 1: (a) Ink-jet Printing deposition, (b) Experiment procedure (polymer/clay nanocomposite)	10
2. 2: (a) Spraying deposition, (b) Experiment procedure (polymer/clay nanocomposite).....	11
2. 3: XRD device.....	12
2. 4: X-ray diffraction pattern of MMT solution on PET substrate	13
2. 5: XRD pattern of an exfoliated clay-polymer composite	14
2. 6: MOCON 2/60 device	14
2. 7: Comparison of composite barrier films in different thicknesses acquired via various methods	15
2. 8: Different polymers and clays tested. Modified from [26]	16
2. 9: UV-Vis spectrometer device.....	17
3. 1: Molecular structure of polyvinylpyrrolidone ((C ₆ H ₉ NO) _n)	19
3. 2: Molecular structure of PEG (C _{2n} H _{4n+2} O _{n+1}).....	19
3. 3: Molecular structure of PAA ((C ₃ H ₄ O ₂) _n).....	20
3. 4: Molecular structure of PVA (C ₄ H ₆ O ₂) _n	20
3. 5: Molecular structure of EVOH(C ₂ H ₄ O-C ₂ H ₄) _n	21
3. 6: Molecular structure of PVOH [CH ₂ CH(OH)] _n	21
3. 7: Schematic of displacing water mole with polymer molecule	24

3. 8: Wide angle XRD pattern of a 3-bilayer composite of PVP and MMT. Modified from [26]	25
3. 9: XRD comparison between different polymers and MMT clay ((a):PAA-MMT;(b)EVOH-MMT;(c)PVP-MMT;(d)PVOH-MMT).....	26
3. 10: Overall OTR comparison between polymers and MMT clay.....	29
3. 11: XRD for PVAc-MMT PNC.....	30
3. 12: OTR rate for PVAc-MMT PNC	30
3. 13: (a) TGA of pure PVA; (b) TGA of dried PVA as a function of temperature.....	31
3. 14: XRD of DHL of PVOH	33
4. 1: (a) Schematic of the tortuous path model showing the high-aspect ratio clay plates increasing the path; (b) Schematic diagram of around the clay plate is the constrained polymer region	35
4. 2: Overall classification of clays	38
4. 3: XRD of Saponite alone and PVOH- Saponite PNC	40
4. 4: XRD of PVOH-Humic acid(HA) PNC.....	41
4. 5: XRD of PVOH-Hydro PNC	42
4. 6: XRD of PVOH-VMT.....	43
4. 7: XRD of PVOH-HEC PNC.....	44
4. 8: XRD of different polymers with LP clay.....	45
4. 9: OTR comparison between different polymers and LP Nano clay	46
4. 10: OTR comparing of PVOH with different nanofillers	47
4. 11: Comparison of OTR values for a series of different size smectite clays with PVOH.....	49

5. 1: XRD results for PVOH-MMT after 4 hrs annealing below T _g	51
5. 2: OTR results for (a) PVOH-MMT (b) PVOH-MMT after 4 hrs annealing below T _g	52
5. 3: OTR results for (a) PVP-MMT (b) PVP-MMT after 4 hrs annealing below T _g	53
5. 4: Comparing different composites in 0% humidity and (2) in 45% humidity	55
5. 5: The effect of humidity on the OTR of PVOH-MMT nanocomposite	56
5. 6: 3 BL printed PVO-MMT film and annealing above T _g and in 100% Humidity.....	57
5. 7: 1 BL PVOH-MMT PNC in 0% humidity and annealed above T _g and in 100% Humidity	58
5. 8: PVP-MMT PNC (1BL) in different humidity percentages	59
5. 9: (a) 1BL PEG-MMT PNC;(b) 1BL PAA-MMT PNC in 0% humidity and annealed above T _g and in 100% Humidity	60
5. 10: (a) XRD; and (b) OTR comparison of different molecular weights of PEG with MMT clay (PEG (1) MW:2000; PEG (2) MW:8000)	61
5. 11: (a) XRD; (b) OTR comparison of different molecular weight of PVP with MMT clay (PVP (1) MW:160000; PVP (2)360000)	61
6. 1: XRD results for PVP-MMT (a) printing, (b) spraying	64
6. 2: XRD results for PAA-MMT (a) printing, (b) spraying	64
6. 3: Oxygen Transmission Rate comparison of (a) PVP-MMT _(P) , (b) PVP-MMT _(S) , (c) PAA-MMT _(P) , and (d) PAA-MMT _(S) . (P: Printing, S: Spraying)	65
6. 4: OTR comparison of PET, several deposited nanocomposites and previous [26] work via inkjet-printer	67
6. 5: Comparison among materials that affect oxygen barrier.....	68

6. 6:(a) Photograph of PVOH-MMT;(b). Cross-section SEM image of 6 BL PVOH-MMT composite	69
6. 7: (a) SEM surface picture (b) ion milled part of surface	70
6. 8: Morphological features of (a) 6B PVOH-MMT;(b) narrow size of MMT palates.....	71
6. 9: Effect of film thickness on OTR for PVOH-MMT PNC.....	72
6. 10: Transparency measurement via UV-Vis spectrometer	73
6. 11: Cross-section picture of PVOH-Lap 5 BL printed	74
6. 12: (a) OTR of printed PVOH-Lap in 5 BL;(b) Transparency measurement.....	74
6. 13: Transparency improvement in less thickness	76
6. 14: Shelf life extension for selected fruits and vegetables (in days).....	78
6. 15: Comparison of coated and uncoated tomatoes at 35 days after purchase.....	79

ABSTRACT

A polymer which has nanoparticles dispersed in its matrix is called a polymer nanocomposite (PNC). A common type of PNC includes smectic clays such as montmorillonite (MMT). These clay minerals increase the mechanical properties of conventional polymers and improve barrier properties. Layer-by-Layer assembly (LbL) is a common method for depositing thin films to improve barrier properties. LbL methods are tedious, time consuming, and produce large quantities of waste. Inkjet printing and spraying coating techniques were employed to make self-assembled gas barrier films. These techniques are industrially scalable and efficient. These methods do not need a rinsing step and drying step as required in LbL. A new highly ordered self-assembly intercalated polymer/clay nanocomposite system was developed. The systems appear to be driven by entropic forces. They are nanostructured and self-assemble at the micron scale. These systems display excellent gas barrier properties which don't follow the tortuous path model of diffusion. This behavior can be explained by constrained polymer theory. Structural characteristics of the intercalates and gas barrier properties of films produced with the intercalated systems are described. A novel approach for food packaging is demonstrated.

CHAPTER I. INTRODUCTION

1.1 Background and Motivation

Decher and Hong [1] introduced spontaneous adsorption of nanoparticles for producing spontaneously ordered structure and self-assembly. Self-assembled nanocomposites involve the use of surfactants or block copolymers as soft templates with nanoparticles. Composites with well-dispersed nanoparticles in the polymer matrices are called nanocomposites. Incorporating nanomaterial into a polymer (polymer nanocomposites [PNCs]) improves its physical properties and barrier performance [2-13]. Nanoparticles have at least one dimension less than 0.1 μm (100 nm) [14]. Nanocomposites have been introduced in response to a growing need for surface coatings in microelectronic, and flexible packaging industries. According to recent assessments [15], global market size of flexible packaging will be \$293 billion in 2022 [16].

Gas barrier properties are dependent on the particle shape, size, volume percentage, and particle dispersion. Graphite, carbon tubes, and clays are common nanoparticles for enhancing gas barrier performance. Graphite sheets are disk-like nanoparticles. Graphene is one layer of graphite which is used in gas barrier applications. There is a limitation to mass-production of graphene [17]. Carbon nanotubes (CNTs) have been used to improve gas barrier properties [18-20]. Improving orientation and dispersion of CNTs enhance gas barrier properties. Both graphene and carbon nanotubes are expensive. Polymers with carbon nanotubes are black, and not transparent. Clays are used in PNCs for improving gas barrier properties. They are naturally abundant, safe, and have low cost [21]. Nanocomposites having highly oriented clay platelets are oxygen

barrier providers and are transparent. They are employed in food, biomedical, and electronics packaging applications [22].

Gas permeability is determined by the absorption rate of gas molecules into the matrix at the atmosphere/polymer boundary [23]. By employing the Layer-by-Layer (LbL) deposition technique, materials with unique physical properties can be produced. The LbL fabrication method allows the design of ultrathin gas barrier films [15]. (see Figure 1.1)

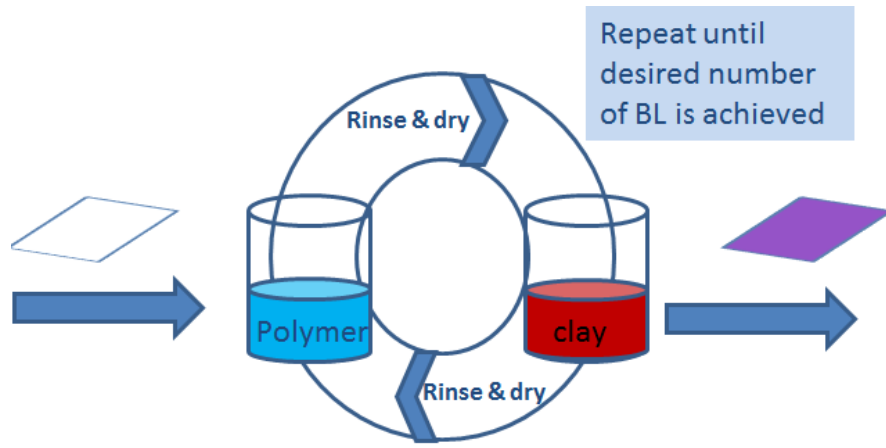


Figure 1. 1: LbL technique procedure

Regarding the study of LbL assemblies with clay, Nielsen proposed the Tortuous Path concept [24-27]. Because the filler materials are impermeable inorganic crystals, gas molecules must diffuse around them rather than taking a straight line (mean) path that lies perpendicular to the film surface. The amount of oxygen gas that passes through a substance over a given period is measured as the Oxygen Transmission Rate (OTR). Adding impermeable inorganic nanoparticles to bulk polymer films reduces OTR [28].

The transport gas mechanism within the polymer matrix follows Fick's Law. The polymer matrix maintains the same characteristics of the neat bulk polymer. According to

Soltani et al. [14], decreases in OTR are ascribed to the increases in the diffusive pathway (tortuosity) derived from nano-brick obstacles.

$$P = S \times D \quad (1.1)$$

In the limit of Fick's law, P is permeability, S is solubility, and D is diffusivity. Reducing polymer matrix volume or constraints on the polymer mobility can cause a decrease in solubility of nanocomposites. A decrease in diffusion can occur because of a more tortuous path for the diffusing molecules.

In semi-crystalline polymers, the size, shape, structure, and the crystallinity degree influence the permeation process. The crystalline domains don't allow gases to diffuse through them readily [11]. To avoid the behavior associated with semi-crystalline polymers, amorphous polymers are selected for study because of the lack of changes in crystalline microstructure [29].

Figure 1.2 shows two types of intercalated and exfoliated nanocomposite. When polymers enter the gallery spacing of the clay plates, and the plates remain associated, it is an intercalated nanocomposite [30]. Intercalated structures can be spontaneously formed when they are thermodynamically driven [29]. Exfoliated nanocomposites are clay plates that are dispersed individually in the polymer matrix.

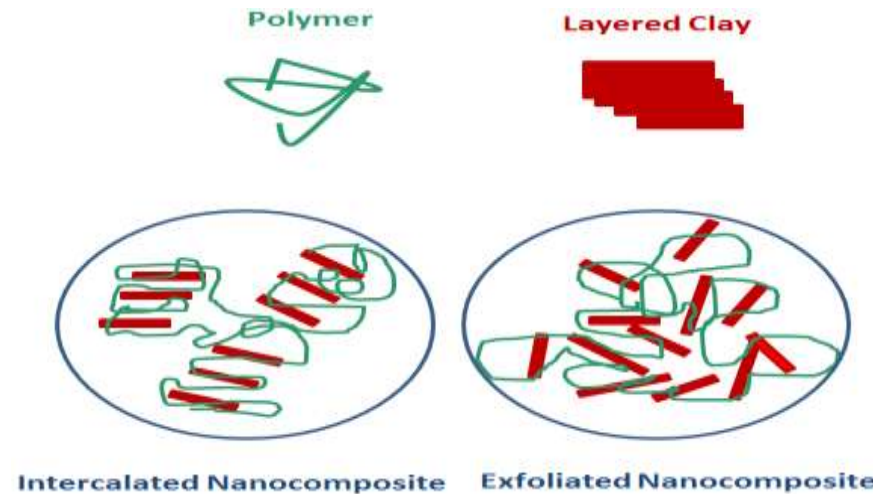


Figure 1. 2: Intercalated and Exfoliated nanocomposites structure

Electrostatic attraction is needed for an effective hybrid organic-inorganic (HOI) LbL coating. Natural nanoclays, such as montmorillonite (MMT) has a negative charge on each platelet face. They are utilized in LbL coatings. MMT (tradename Cloisite Na⁺) can be used as an anionic clay. Montmorillonite is classed in the smectite group. The MMT structure consists of two fused tetrahedral layers of silica sandwiching an octahedral layer of alumina and magnesia [31-34]. MMT layered silicates are ceramic platelets with a high aspect ratio. MMT layer thickness of each platelet is around 1 nm with lateral dimensions varying from 30 nm to several microns. The layers associate on top of each other like the pages of a book. Between the layers, Van der Waals gaps are created by the counterions. These are called galleries. The isomorphic substitution of the octahedral or tetrahedral cations, e.g., the substitution of Al³⁺ with Mg²⁺ or Mg²⁺ with Li¹⁺, generates negative charges. They are counter balanced by alkaline and alkali earth cations located inside the galleries [26]. Ion exchange reactions of the counter ions with other counter ions can alter the nature of the montmorillonite surface and increase the basal spacing. This can improve the access to the galleries by polymers.

Examples of the use of MMT to reduce gas permeability included polyimide/layered silicate nanocomposites with 8% MMT by weight in a polyimide system. The composite had 80% reduction in gas permeability [34-36]. Nylon 6-MMT nanocomposites with 18% modified MMT by weight decreased gas permeability by 60% [37].

Soltani et al. [15] demonstrated oxygen permeability reduction in a polyelectrolyte by increasing the concentration of MMT nanoclay. Adding a higher concentration of fillers to PNCs did not improve gas barrier performance. The majority of the work on nanoclay barrier films has been focused on low nanoclay content with 10% by weight or less [29].

Gas permeability is a function of polymer type. The research focused on the preparation of LbL barrier films includes different substrates and coating materials. High gas barrier flexible films have been developed for flexible electronic devices, pharmaceuticals, and food packaging [23]. The traditional procedure for making gas barrier films includes dipping a substrate into a polymer solution repeatedly followed by dipping the polymer-coated substrate into nanoparticle dispersions to create alternating organic/inorganic layers (usually more than 50). There are rinsing and drying steps between each dipping. This approach produces a large amount of waste rinse water, and is tedious. This LbL technique is difficult and expensive to implement on a commercial scale [38]. A critical issue for the commercial use of nanocoating technology is reducing the number of processing steps required while achieving high gas barrier. To reduce the permeability of gases such as O₂ or CO₂ and water vapor, several coating techniques can be employed [39]. Different substrates are used to test oxygen transmission rates in gas

barrier applications in food packaging. Oriented polypropylene and polyethylene terephthalate have good gas barrier performance [40]. PET (179-micron thickness), for example, has an oxygen transmission rate (OTR) around $8.6 \text{ cc/m}^2 \cdot \text{day.atm}$ [26].

Polymer-clay nanocomposite (PCNCs) films produced by LbL assembly have high transparency and high oxygen barrier properties [22]. Many layers are needed to achieve low oxygen transmission. Barrier coatings are very important in packaging [38, 41-44]. Oxygen-sensitive food requires an oxygen transmission rate (OTR) of less than $1 \text{ cc/m}^2 \cdot \text{day.atm}$ (e.g., for coffee and high-fat snacks). Flexible organic light-emitting devices require an OTR below $10^{-5} \text{ cc/m}^2 \cdot \text{day.atm}$ [45].

In 2014, Cook et al. [46] used Drop on Demand (DOD) inkjet printing to produce highly ordered nanocomposites on a PET substrate with PVP (Polyvinylpyrrolidone: k-15) and MMT. The polymer-clay dispersion spontaneously intercalated via entropy driven self-assembly. The nanocomposite was highly ordered. The film thickness was 15.5 microns. The oxygen transmission rate was below the detection limit of the Mocon measuring device.

In 2014, Wong et al. employed a spray-coating method for manufacturing self-assembled thin, flexible, and transparent epoxy films containing zirconium phosphate nanoplatelets. The spray-coated a-ZrP/epoxy films had 10 times the OTR reduction when compared with the uncoated film [48]. Suarez -Martinez et al. showed that a fabrication method using spray-coating of a BPEI/MMT (BPEI: branched polyethylenimine) composite (thickness $\approx 400 \text{ nm}$) reduced the OTR by a factor of 5 lower than PET alone [49]. The large-scale production of making gas barrier films by spraying is easy to achieve.

1.2 Dissertation Overview and Research Objectives

This research will be focused on depositions of different polymers to determine if other polymers beside PVP will self-assemble via an entropy driven mechanism and if other nanoparticles can form these self-assembling systems. This research will determine the structure property relationships in these self-assembling systems. The research is aimed at understanding the relative role of tortuous path and constrained polymer models in gas barrier performance. This research will provide the extension of this newly identified polymer intercalation chemistry to other polymers and nanoparticles. Polymer intercalation will be demonstrated with a variety of new polymers, smectite clays, and provide confirmation of the constrained polymer theory. The commercial applications of these intercalates will be discussed.

In **chapter I**, the introductory topics and the motivations of this research are described. The concept and structure of polymer/clay nanocomposites are described in this chapter. The materials and techniques for the preparation of clay nanocomposites are introduced. The overview and research objectives are presented in detail.

In **chapter II**, the deposition techniques for creating polymer/clay nanocomposite films are explained. Applied characterization techniques are discussed.

In **chapter III**, the effect of using different polymers and MMT nanoclay in polymer nanocomposites will be discussed. The role of entropy in self-assembly and the underlying principles of gas barrier technology for advanced applications will be demonstrated.

Chapter IV will demonstrate the effect of using different fillers and nanoclays other than montmorillonite clay.

In **chapter V**, the relation between XRD morphology and annealing time will be discussed. The role of polymers with different molecular weight on ordering and gas barrier properties will be discussed. The relation between different molecular weight (MW) polymers and annealing needs to be considered in the temperatures above and below glass transmission temperature (T_g). The effect of temperature variation on the oxygen permeation rate and crystal structure will be investigated. The influence of relative humidity (RH) on the gas barrier of films will be examined for different PNCs.

In **chapter VI**, different deposition techniques will be compared for enhanced commercial viability. Traditional self-assembled gas barrier systems use LbL techniques have many steps and results in material waste. The novelty of this research is in the development of self-assembled gas barrier films with inkjet printing and spraying techniques and their efficiency as gas barriers. The effect of polymer/clay coating on different fruits will be demonstrated.

Chapter VII shows the conclusion of the research, results, and gives suggestions for future work.

CHAPTER II. DEPOSITION AND CHARACTRIZATION TECHNIQUES

This chapter introduces the techniques for PNC film deposition and characterization.

2.1 Deposition Techniques

Different deposition techniques will be studied for enhanced commercial viability of self-assembling coatings. Traditional self-assembled gas barrier systems use the LbL technique. LbL requires many steps and results in material waste. The novelty of this research is in the development of self-assembled gas barrier films with inkjet printing and spraying techniques and studying their efficiency as gas barriers. Different polymers and clays in various weight percentages (0.1%-0.5%) were prepared by dispersing measured quantities of the compound into deionized water and stirring for 5 hours utilizing ultrasound dispersion before usage. Deposition techniques were performed by Drop on Demand (DOD) inkjet printing (Fujifilm Dimatix DMP-2831) and paint spraying.

The resolution of Inkjet-printed patterns is controlled by the hydrodynamics of the jetted micro droplets and the volatility of the ink constituents [50]. The fluid physical characteristics to achieve optimum performance is viscosity, low volatility, particle size and pH of the fluid. The viscosity is preferred to be 10-12 centipoise at jetting temperature. Low volatility is preferred with boiling points higher than 100°C. For all fluids filtration is recommended to be 0.2 µm. A pH-value between 4 and 9 is recommended [51]. The solutions of the individual polymers and clay were placed in Fujifilm Dimatix DMP-2831 print heads with 100 dpi resolution. A print head contains

16 nozzles spaced 254 μm apart. Each nozzle of the print head can generate droplets as small as 1 picoliter (pl) [52].

Figure 2.1 illustrates the DOD printer. Several bilayers can be created by the inkjet printer.



Figure 2. 1: (a) Ink-jet Printing deposition, (b) Experiment procedure (polymer/clay nanocomposite)

The spray-coating deposition allows for fast, efficient application of coatings on a substrate and is scalable (Note: spray technique was done in bilayers). A simple paint sprayer was used. The pressure and the amount of liquid were controlled by the nozzle orifice. The sprayer produces fog droplets that will coat the surface uniformly. The pressure of the exiting drops was controlled by the nozzle. The nozzle of the spray gun was placed about 10 cm away from the surface and oriented 90° from the surface. Figure 2.2 illustrates the spray deposition technique.

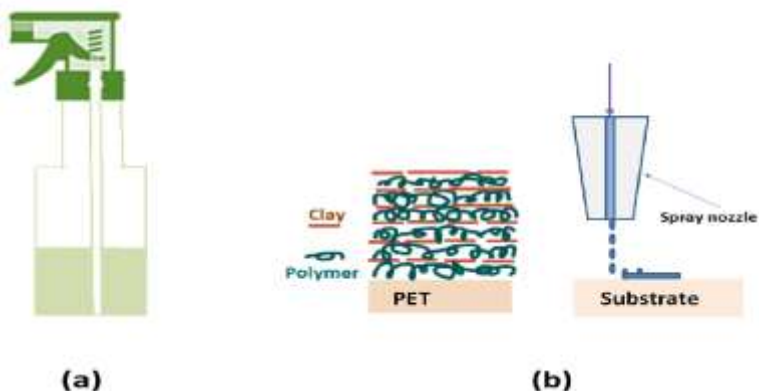


Figure 2. 2: (a) Spraying deposition, (b) Experiment procedure (polymer/clay nanocomposite)

Several bilayer (BL) films were created by ink jet printing and spraying. For each composite, we created six square samples ($6.35\text{ cm} \times 6.35\text{ cm}$) for maximum throughput and efficiency. Different solutions (PVP, PAA, PVOH, PAC, and MMT) were deposited as Bilayers (BL) (where a bilayer, BL, refers to one polymer layer and one nanoclay layer) on Mylar (PET; Poly (ethylene terephthalate) substrates by DOD. We let each layer dry at room temperature (usually 5 min). The PET sheet (8.5 in. \times 11 in., CG5000) has 110-micron thickness. PET film was acquired from 3M Manufacturing Company. This film was used because of its transparency and to promote ink adherence to the surface. PET film was pre-cleaned before use by rinsing multiple times with iso-propanol (IPA) and deionized (DI) water.

2.2 Characterization Techniques

2.2.1 X-ray Diffraction (XRD)



Figure 2. 3: XRD device

A full exfoliation and alignment of MMT in polymer–clay nanocomposites give optimal properties. Exfoliation between the particles and polymer matrix produces the maximum interfacial interaction. For measuring the exfoliation or intercalation, one of the ideal analytical methods is X-ray diffraction (XRD) [53-54]. Bragg's law in XRD provides the atomic dimensions in the crystalline lattice. Peaks as a function of the x-ray angle depends on the atomic spacing in the lattice. Bragg law is:

$$2(d \sin \theta) = n\lambda \quad (2.1)$$

where the wavelength of the X-ray used is λ , and the atomic plane spacing is d , the reflection order is n , and the angle of diffraction beam to the atomic plane is Θ .

Because of the detector geometry related to the X-ray source, the angle observed is 2Θ . According to the literature [56-57], the smectite clays have XRD patterns on 00l or hk0 reflections. The individual clay plates are turbostratic. In Figure 2.4, there is an example of MMT nanoclay dried from a water solution. It has a 00l reflection. The basal spacing between the clay plates of approximately 1.4 nm. [56-58].

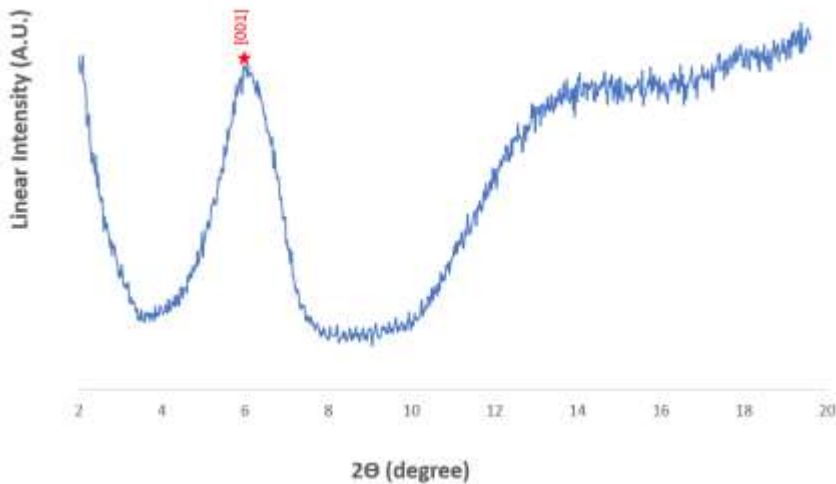


Figure 2. 4: X-ray diffraction pattern of MMT solution on PET substrate

XRD characterization can be used for determining the level of exfoliation or intercalation by observing change or disappearance of the basal spacing peak [31].

In some of the cases in the polymer-nanocomposite study, the XRD peaks may disappear. This implies an exfoliated system or disordered tactoids. XRD alone cannot be used for quantifying the level of exfoliation. Microscopy methods such as transmission electron microscopy should be used in conjunction with XRD. When the polymer has entered the gallery of clay plates, and the plates are stable in their position, the composites are called intercalated systems. The spacing of the gallery of clays measured by XRD is referred to as the basal spacing [31].

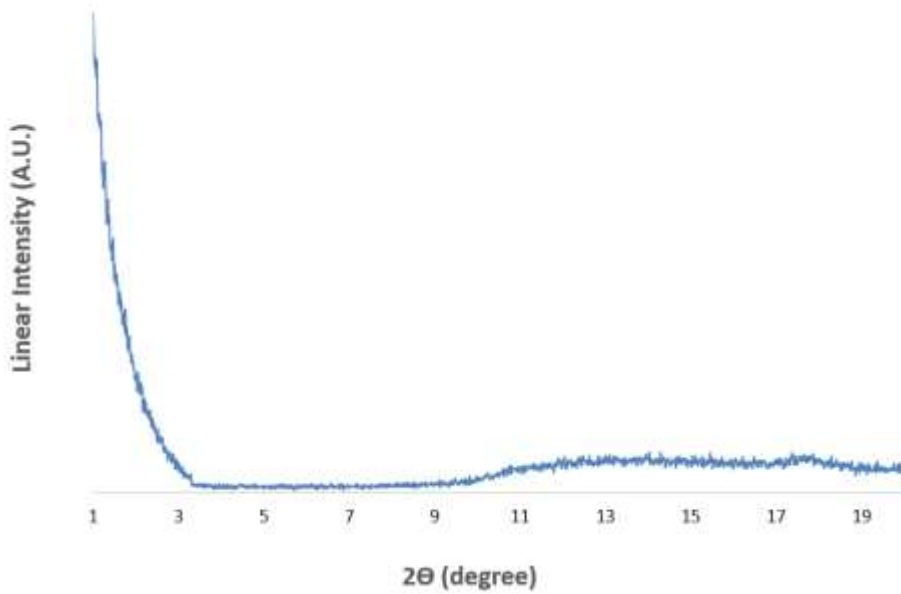


Figure 2. 5: XRD pattern of an exfoliated clay-polymer composite

2.2.2 Oxygen Transmission Rate (MOCON 2/60)

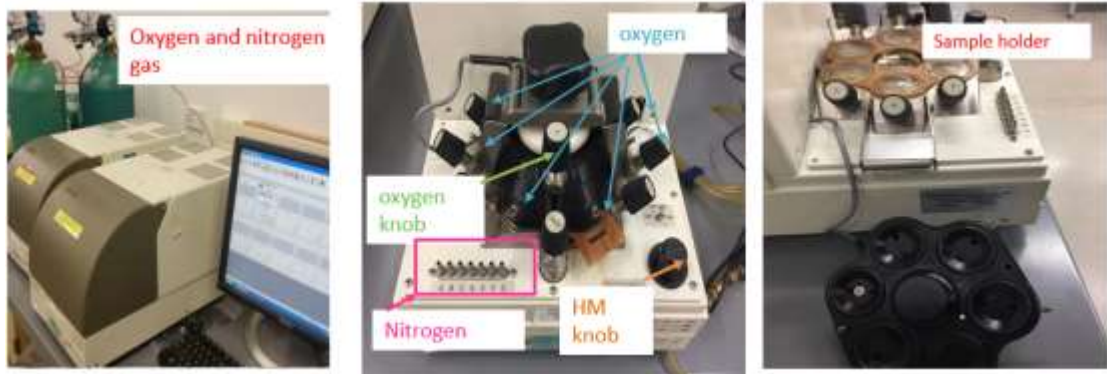


Figure 2. 6: MOCON 2/60 device

The gas permeability is related to the rate of diffusion and solubility of the gases in the polymer nanocomposites. Our composites are intercalated systems according to the results of XRD analysis. The rate of their permeation of print-coated and spray-coated films was evaluated using the Mocon Ox-Tran 2/60. The Oxygen gas barrier property of nanocomposite films was determined via the permeation rate of the films. PET provides

a good barrier to oxygen (O_2 permeability of PET is an average $14 \text{ cc/m}^2.\text{day.atm}$).

Incorporating nanoparticles into the polymeric matrix improves the oxygen barrier performance [33].

Figure 2.7 compares the permeation rate of different deposition techniques in the literature. The smallest thickness with excellent OTR can be achieved by dipping, rinsing, and drying techniques (known as LbL). These techniques need many deposition layers.

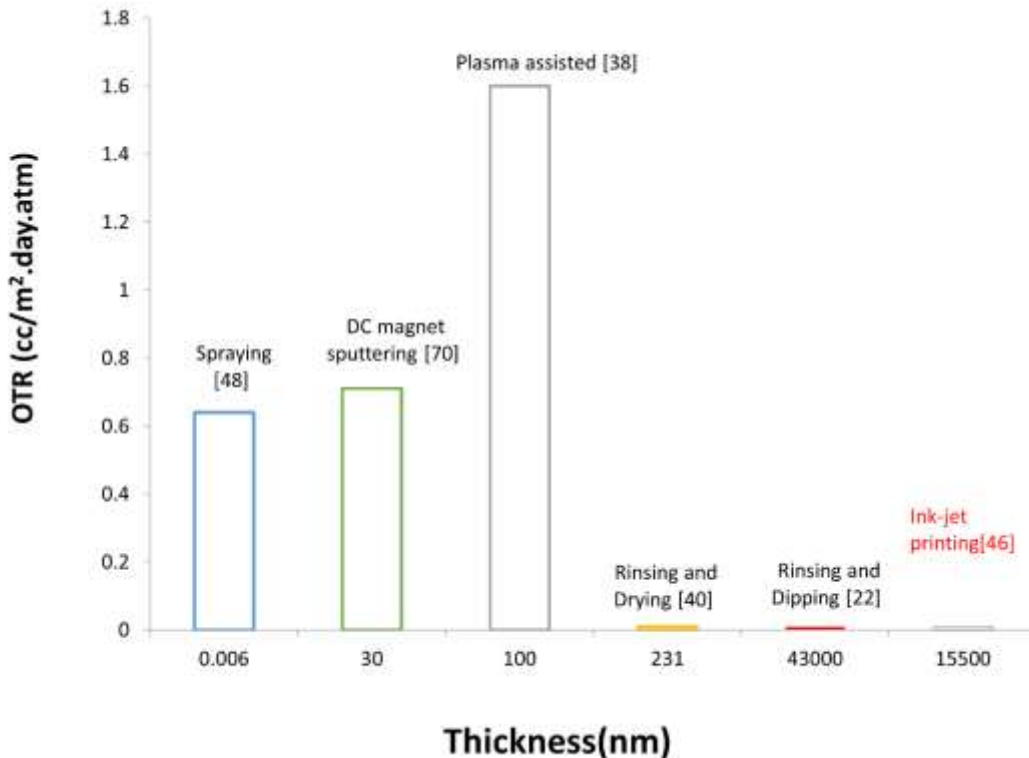


Figure 2.7: Comparison of composite barrier films in different thicknesses acquired via various methods

Cook et al. [46] compared different polymers and nanofillers (see Figure 2.7). They achieved a zero-transmission rate for oxygen utilizing the inkjet printer and PVP-MMT nanocomposite with 6 Bilayers (15.5-micron thickness).

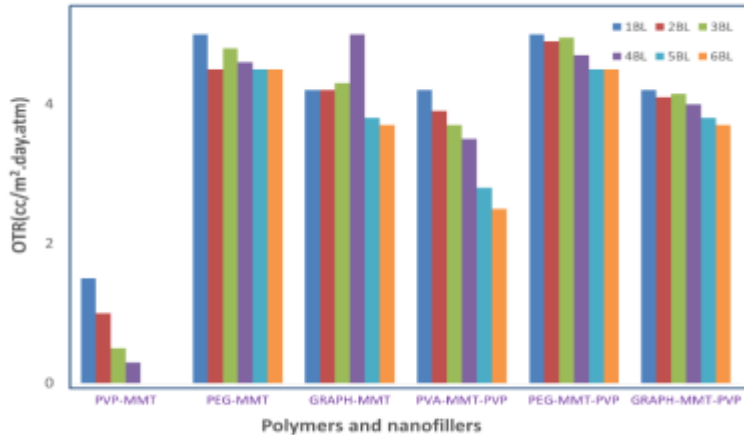


Figure 2. 8: Different polymers and clays tested. Modified from [26]

2.2.3 Transparency Measurement (UV-Vis spectrometer)

Transparency was measured for different nanocomposites with different thicknesses. The thickness of assembled films varies by pH, molecular weight, solution, and environmental factors such as temperature or relative humidity [59].

The barrier properties of PNCs have several important applications. The most common application of PNCs is to prevent H_2O vapor and oxygen from exposure to food and drugs. PNC protects the food from wasting. The shelf life of food increases significantly. It helps monitor food freshness. Because of the size and refractive index of the clay, the packages made from PNC are transparent. The clay particles are too small to

diffract visible light. The refractive index of MMT is close to the polymer's refractive index [56, 60].

Transparent packaging increases food appeal and allows monitoring of degradation [61-63]. Higher transparency allows for more textures to be identified inside the packages [64].

The UV-Vis spectrometer employed to measure transparency was the UV-2501PC set in transmittance mode in the range of visible light (from 400 nm to 700 nm).



Figure 2. 9: UV-Vis spectrometer device

CHAPTER III. POLYMERS AND MMT NANOCLAY

3.1 Introduction

In this chapter, the barrier performance of different polymers (other than PVP) and nanoclays (other than montmorillonite) will be measured. The role of entropy in self-assembly and the underlying principles of gas barrier technology for advanced applications is demonstrated. Self-assembly is driven by entropy in systems where small molecules on the surface of the nanoparticle are displaced by higher molecular weight polymers during intercalation [38].

3.2 Different Polymers

Self- assembled nanocomposites involve the use of surfactants or block copolymers as soft templates with nanoparticles [30,65,66-67]. In this section, we are conducting research on several polymers and their structure property relationships in order to demonstrate the wider applicability of the barrier composites first identified by Cook et al. [46].

3.2.1 Polyvinylpyrrolidone (PVP)

PVP (polyvidone or povidone) is a water-soluble polymer. It is made from the monomer N-vinylpyrrolidone. The polar group of PVP is a carbonyl and a ternary nitrogen. A carbonyl group is a functional group composed of a carbon atom double bonded to oxygen (C=O) [68].

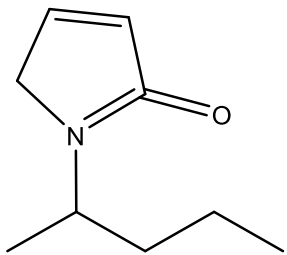


Figure 3. 1: Molecular structure of polyvinylpyrrolidone ($(C_6H_9NO)_n$)

Cook et al. [69] demonstrated the bulkiness of the pyrrolidone ring causes the polymer backbone to be linear. Once the rings on one side of the polymer bonds to the exchangeable cation, the rings on the opposite side have difficulty bonding to another clay plate; This strongly influences the intercalation/exfoliation character of this polymer. This polymer exhibits very poor gas barrier properties. It was surprising when the intercalate with MMT exhibited high barrier performance. This polymer was included in the research as a benchmark.

3.2.2 Polyethylene Glycol (PEG)

PEG is known as polyethylene oxide (PEO) or polyoxyethylene (POE). PEG has many applications in manufacturing. PEG is a polyether compound. An ether group is an oxygen atom connected to two alkyl or aryl groups (R-O-R'; C-O-C). (the polar group is the oxygen). PEG molecular backbone is extremely flexible. It exists in solution as a highly coiled bundle.

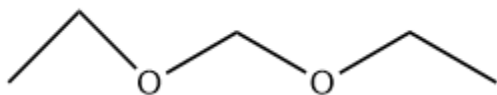


Figure 3. 2: Molecular structure of PEG ($(C_{2n}H_{4n+2}O_{n+1})$)

3.2.3 Polyacrylic Acid (PAA)

PAA is a synthetic high molecular weight polymer of acrylic acid (Carbomer).

PAA is an anionic polymer at pH higher than 7. The polar group of PAA is carboxyl.

PAA is most water loving in the salt form. Sodium carboxylate is an example.

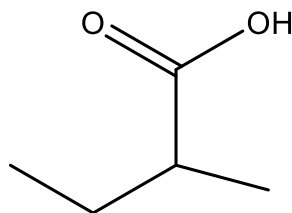


Figure 3. 3: Molecular structure of PAA ($(C_3H_4O_2)_n$)

3.2.4 Polyvinyl Acetate (PVA), Ethylvinyl Alcohol (EVOH) and Polyvinyl Alcohol (PVOH)

PVA (PVAc, poly (ethenyl ethanoate)) is utilized to make white glue, school glue, or Elmer's glue. PVA belongs to family of polyvinyl esters.

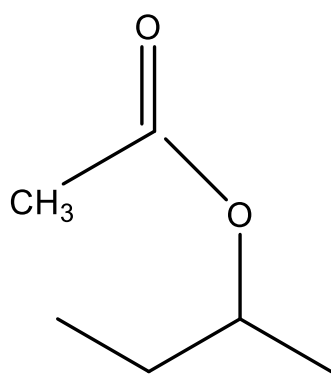


Figure 3. 4: Molecular structure of PVA ($(C_4H_6O_2)_n$)

EVOH and PVOH are prepared from poly vinyl acetate. Both polymers are hydrolyzed forms of poly vinyl acetate.

EVOH is a copolymer of vinyl alcohol and ethylene. EVOH is prepared by polymerization of ethylene and vinyl acetate followed by hydrolysis. EVOH is specified by the mole % ethylene content. When EVOH has lower ethylene content, the material will have higher barrier properties. (Note: The ethylene group is hydrophobic)

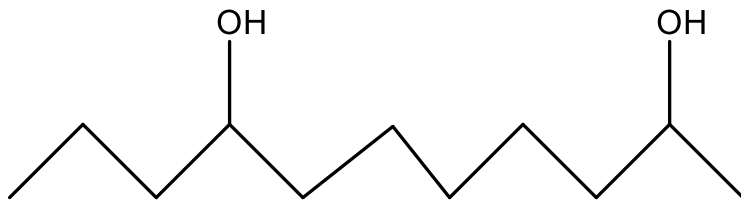


Figure 3. 5: Molecular structure of EVOH($\text{C}_2\text{H}_4\text{O}-\text{C}_2\text{H}_4\text{n}$)

One of the water-soluble synthetic polymers is PVOH (PVA, or PVAI). PVOH has applications in papermaking and coatings. PVOH is made by polymerizing vinylacetate followed by varying degrees of hydrolysis. Alcohol in chemistry means any organic compound with a hydroxyl functional group ($-\text{OH}$) bound to a saturated carbon atom. The polar groups for EVOH and PVOH are alcohol.

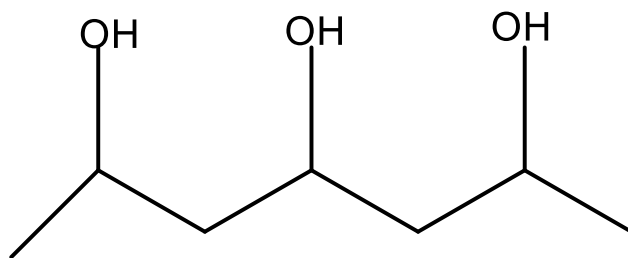


Figure 3. 6: Molecular structure of PVOH [$\text{CH}_2\text{CH}(\text{OH})\text{n}$]

PEG is the most flexible and can bond easily to both sides of the MMT gallery. PVOH is slightly less flexible and bonds across the gallery if the charge density of the dispersed phase is high enough [69].

3.3 Role of Entropy in Polymer-nanoparticles

Self-assembly is the interaction between entropic and enthalpy properties of nanoparticles. This interaction can be driven by entropy to self-assembled polymer-nanoparticle composites (PNC) by adjusting the nature of ion or molecule bonding on the nanoparticle surfaces. The entropic interactions between the nanoparticles and the polymer can be used for creating coatings [70].

A self-assembled system tends to minimize its free energy to achieve its lowest free energy thermodynamically. Intermolecular forces (IMFs), between nanoparticles can drive self-assembly. Changing the functionality of a nanoparticles side groups, and having weak and specific intermolecular forces will encourage self-assembly that orders the particles spontaneously. Intermolecular forces such as hydrogen bonding or Van der Waals forces can provide interparticle interactions. IMFs can mediate interactions between molecules. These can be attraction or repulsion forces that act between molecules, and other neighbor particles (e.g., atoms or ions) [71]. Ion exchange of smectic clays with quaternary ammoniums has facilitated a major industry. The available number of commercial quaternaries is limited. However, there is an alternate method of clay intercalation which is via ion-dipole bonding of polar organic molecules with the exchangeable cations in the galleries of the clay sheets. This approach is a classic test for identification of smectite clays and it has been recognized for many decades.

As an example, for verifying how entropy involves in self-assembly, we looked at to PVP-MMT PNCs which has the excellent gas barrier (consider PVP with 15000 molecular weight). According to Cook et al. [69], entropy is the energy driver for

self-assembled gas barrier film. When clay particles are added to polymer nanocomposite structure, polymer entropy decreases. But, the entropy increases for three hundred moles of water for each mole of PVP which is displaced by the ion-dipole bonding of polymer to the exchangeable cations on the surface of the clay in the gallery. For example, in MMT clay, “the exchangeable cation on the surface has a significant partial positive charge that is normally accommodated by approximately three water molecules of hydration per sodium cation” (Note: MMT clay exchange capacity is 97 meq/100grm) [69] (Note: Molecular modelling of this system indicates that this intercalated system has three layers of PVP in the gallery with two being associated with the clay surface on the two sides of the gallery and a third in the middle associating with the two bonding polymers).

In PVP-MMT PNC, the enthalpic energy of the bond formed between the carbonyl on the pyrrolidone group is essentially the same as the water ion-dipole bonded to the sodium.

The entropy increase (real energy) occurs when the “three water molecules” are displaced by the intercalating PVP molecule. We are assuming that “every second pyrrolidone group bonds to the surface,” for each mol of PVP molecule (MW= 15000) would displace over 270 moles of water.

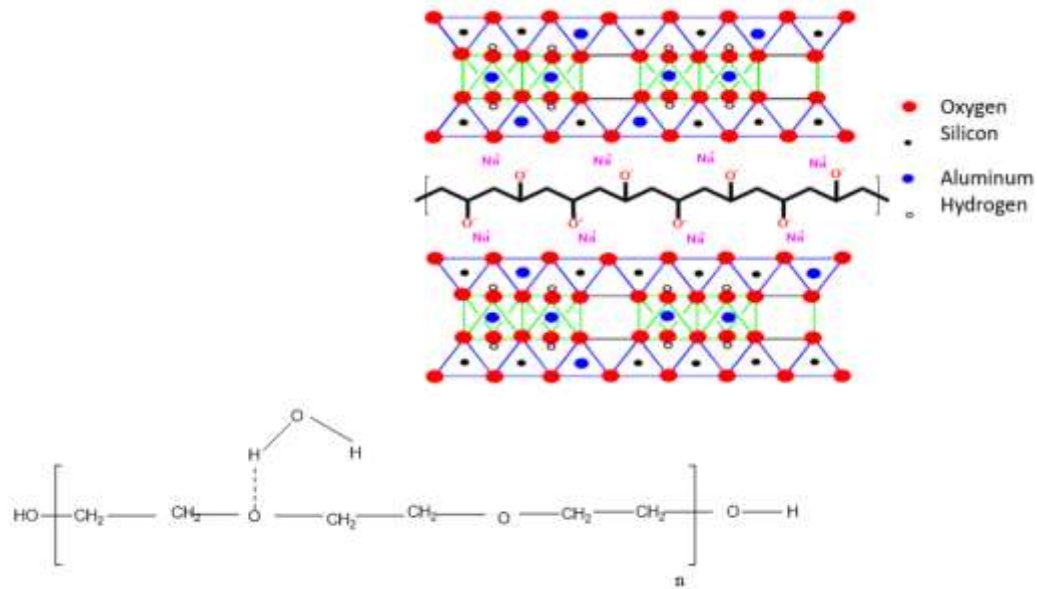


Figure 3.7: Schematic of displacing water mole with polymer molecule

Calculation: $(C_6H_9NO)_n$:

$$15000 \times \frac{2}{3} = 10000 \text{ gr}$$

$C_6=12 \times 6 = 72$; $H_9=1 \times 9 = 9$; $N = 14$; $O=16 \Rightarrow (72+9+14+16=111 \text{ gr/mol})$

$$\frac{10000 \text{ gr}}{111 \text{ gr/mol}} = 90 \text{ mol}$$

$90 \times 3 = 270 \text{ mol}$ of water be displaced with each mole of PVP

Therefore, the entropy will be increased by the hundreds of displaced water molecules [69].

Another factor to help to have a high degree of ordering is using ink-jet printing and spraying deposition techniques. Because of surface tension effects drops for inkjet printing evaporate quickly and in spraying deposition drops spreading quickly. As the film dries the platy nanoparticles align parallel to the PET surface due to the water surface tension.

These mentioned scenarios in this part for depositing PVP-MMT PNC via inkjet printing and spraying can be extended to other polymers (PVOH, PAA, EVOH, and PEG) and clays (MMT, Laponite).

3.4 Different Polymers and MMT Nanoclay

The literature study shows several examples demonstrating the relationship between crystallinity and permeability. Permeability decreased by the increase of crystallinity [56]. Figure 3.8 shows an example of an intercalated system [46].

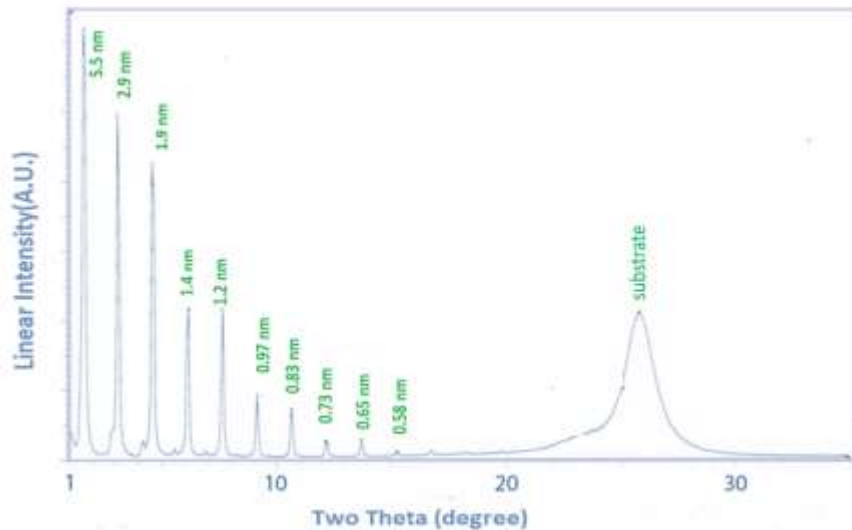


Figure 3. 8: Wide angle XRD pattern of a 3-bilayer composite of PVP and MMT. Modified from [26]

3.4.1 XRD and OTR of Different Polymers and MMT Nanoclay

With the unusually ordered nanostructured intercalates formed between PVP and MMT and their extreme barrier performance it is of interest to demonstrate that the self-assembly phenomena can be extended to other polymers and smectite clays [46]. In this section, we investigate the XRD morphology of a series polar polymers (PVP, PAA, PVOH, PEG, PAC, EVOH) with MMT nanoclay. We deposited all films in 1BL and with spraying technique.

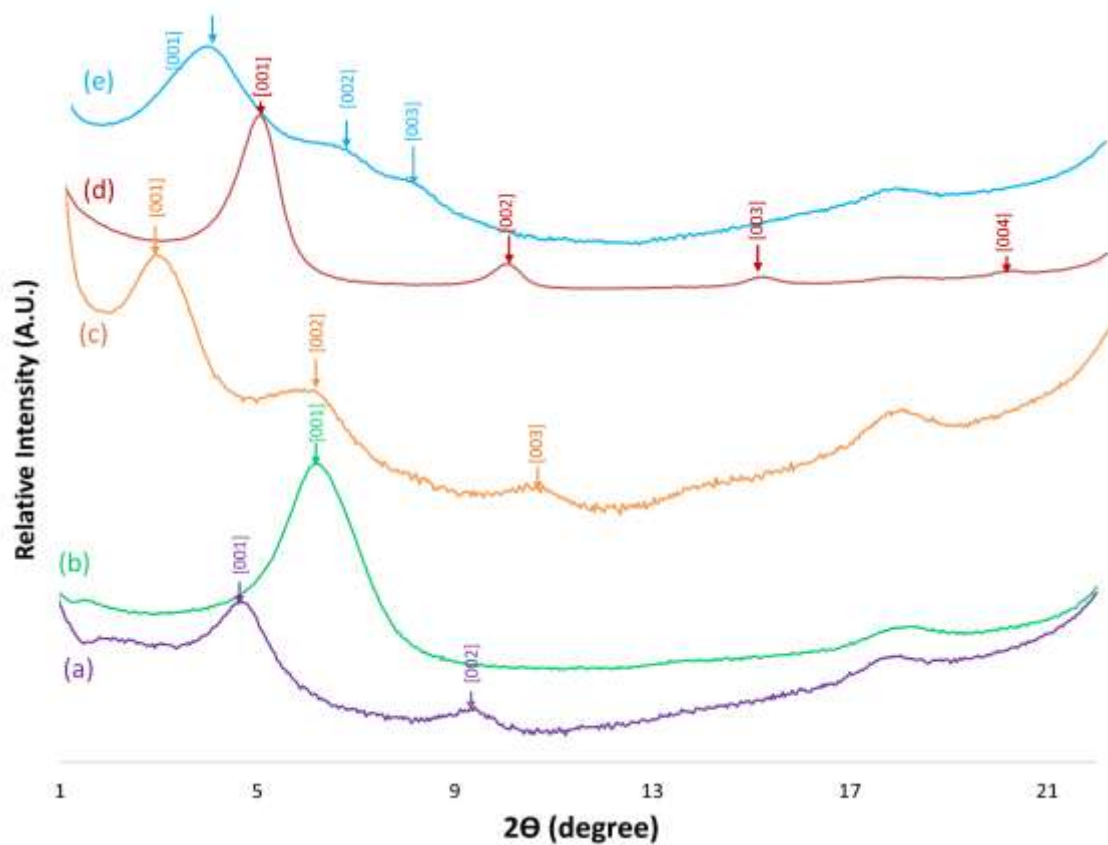


Figure 3. 9: XRD comparison between different polymers and MMT clay ((a):PAA-MMT;(b):EVOH-MMT;(c):PVP-MMT;(d):PVOH-MMT)

The x-ray diffraction patterns for these films can be seen in Figure 3.9. In this figure, we have several orders of reflection for polymers and MMT nanoclay and all the polymers have formed intercalated systems with MMT.

The PVP-MMT intercalate has a highly ordered pattern exhibiting 4 to 5 orders of reflection with a basal spacing 5.89 nm. It is significant that these films are nanostructured but bridge across the micron scale of the dried films. This system molecular modelling displays that this intercalated system has “three layers of PVP in the gallery with two being associated with the clay surface on the two sides of the gallery and a third in the middle associating with the two bonding polymers” [46].

The PVOH-MMT intercalate has 3 to 4 orders of reflection with a basal spacing of 2.1 nm. This would indicate a bilayer structure with independent molecules coating both sides of the gallery or more likely the polymer zig zags across the gallery randomly and bonds with the other side.

The PEG-MMT intercalate shows 4 orders of reflection and has a basal spacing of 1.8 nm. Because of the high degree of flexibility of PEG, PEG molecule is most likely zig zagging in the gallery and bonding across the gallery.

The PAA-MMT complex only showing 2 orders of reflection and a basal spacing of 1.91 nm. This would indicate similar molecular arrangement as seen in PEG and PVOH.

The intercalate formed between EVOH-MMT is quite different from all the others. It has only a single broad peak with a basal spacing of 1.44 nm. This is only enough space for one molecule to lay flat between the plates.

We need to investigate oxygen permeation of different polymers and MMT nanoclay to verify which one works better. Each of the intercalated films were then tested for their oxygen transmission rate (OTR). In these tests a single bilayer was printed in each case. The OTR for all different deposited films can be seen in Figure 3.10. From Figure 3.10 we can understand that most of used polymers are hydrophilic, but some of them have more hydrophobic chains than other polymers. The OTR for the uncoated PET is $14 \text{ cc/m}^2 \cdot \text{day} \cdot \text{atm}$. It is surprising that all of the intercalated systems except one gave OTR's with better than a 50% reduction in gas permeability.

It is an interesting point that PVP and PAA are not recognized for being oxygen barrier polymers but, PVOH and EVOH are recognized to be good barrier polymers but quite sensitive to humidity. This could be a sign that the constrained polymer phenomenon has a role in the barrier performance of these intercalated systems especially in PVP and PAA.

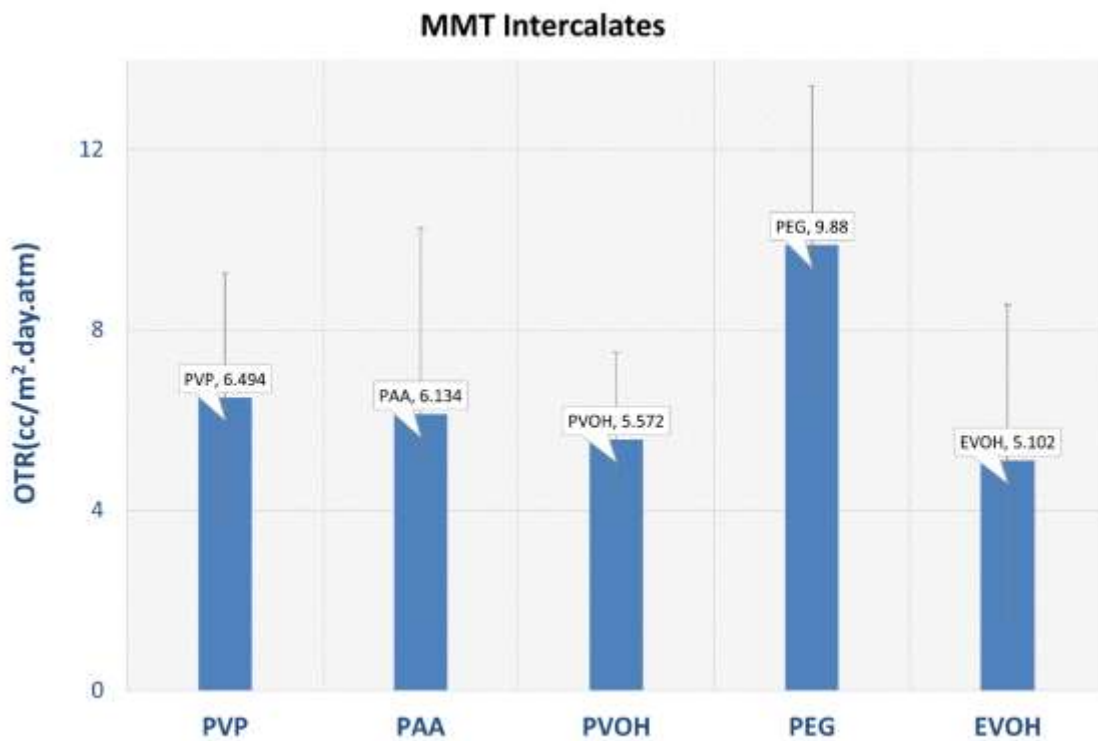


Figure 3. 10: Overall OTR comparison between polymers and MMT clay

We investigated on the gas barrier property of Elmer's glue. We deposited one BL of PVAc-MMT with spraying. First, we needed to see its lattice morphology with MMT nanoclay. In Figure 3.11, we can see PVAc is intercalated with MMT, and we have two reflections.

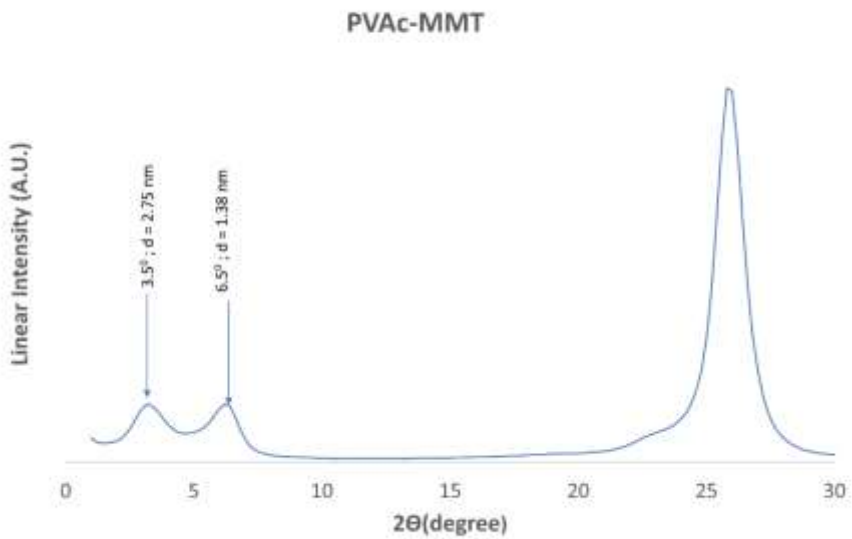


Figure 3. 11: XR for PVAc-MMT PNC

After investigating the crystal morphology, we did a permeation test. In Figure 3.12, we can see we have 16 times less oxygen permeation rate than PET uncoated alone.

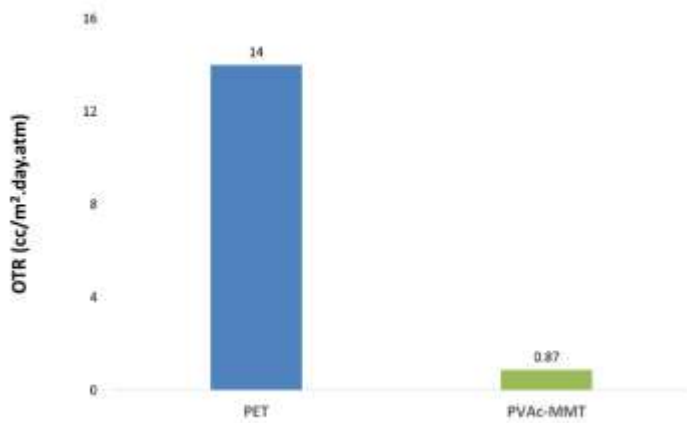


Figure 3. 12: OTR rate for PVAc-MMT PNC

We did reverse engineering to investigate on the percentage of PVAc in this solution. So, we did thermal analysis with TGA (TA Q50 Thermogravimetric Analyzer) during heating in an argon atmosphere at a rate of 10 °C/min from room temperature to 800 °C.

Figure 3.13 shows the thermogravimetric analysis (TGA) of pure PVA (glue) and dried PVA (glue) degradation mechanism from room temperature to 800 °C. According to TGA graph, the thermal decomposition process elimination of water structure happens in less than 200 °C. The first mass loss of 60% occurred between around 53 °C, and 159 °C and it may be related to the elimination of water in PVA solution (glue solution).

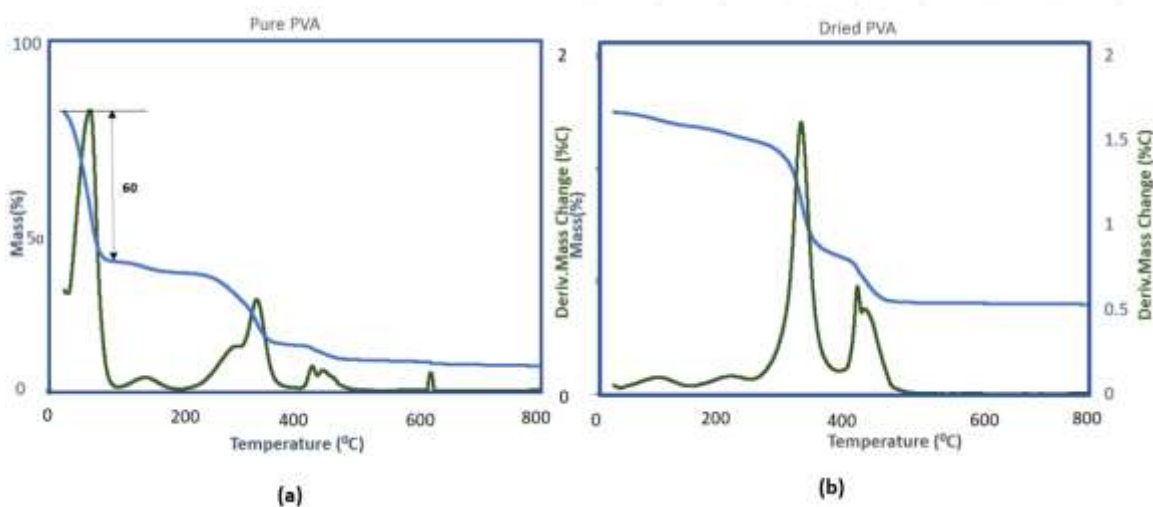


Figure 3. 13: (a) TGA of pure PVA; (b) TGA of dried PVA as a function of temperature

Overall, having a good amount of oxygen barrier has 40 % wt. of PVAc in its structure.

3.5 Role of Different Hydrolyzation Levels (DHL) in PNCs

In previous section, we found that PVA-MMT nanocomposite has a good barrier property. We were not able to make a gas barrier film with PVAc because we could not

dissolve it in water (100% hydrolyzed). Therefore, in this section, we investigated the effect of different hydrolyzation of poly vinyl alcohol (PVOH) [72].

Hydrolysis is a process when polymers are breaking down into monomers. It can happen by applying an enzymatic catalyst and water molecules. The polymer will break into two components. When components are unionized, one part obtains a hydrogen atom (H) from a split water molecule, the other part obtains a hydroxyl group (OH⁻) [73].

PVOH is a water-soluble polymer which has excellent properties such as water-solubility, adhesion strength, and gas barrier. For producing poly vinyl alcohol, the process is made from vinyl acetate monomer through polymerization and saponification processes. PVOH exists in many grades according to different degrees of hydrolysis and polymerization. It is respectively controlled in the saponification processes and polymerization [74]. So, in this part of this research, we investigated on several levels of hydrolyzation of PVOH and its effect on gas barrier properties, while we know from the last section that poly vinyl acetate-MMT nanoclay is working well in gas barrier properties. Table 3.1 shows the usage of different hydrolyzation levels of PVOH with MMT and verifying their effect on XRD which shows their morphologies.

Table 3. 1: Hydrolyzation level of PVOH with MMT and OTR relation.

Different PVOH	Different Hydrolyzation Level(DHL)	OTR(cc/m ² .day.atm) PVOH-MMT
Kuraray 5-74	72.5~74.5	5.1
Kuraray 3-80	78.5~81.5	5.5
Denka B-20	87.0~89.0	4.6
Denka H-17	95.0~96.0	5.6

PVA performance changing is dependent on polymerization and hydrolysis degrees. The results show hydrolyzation levels do not affect gas permeability significantly. Their OTR are approximately the same ($SD=\pm 0.5$), and all DLH of PVOH are hydrophilic. Figure 3.20 shows the XRD, and all the nanocomposites have three reflection orders.

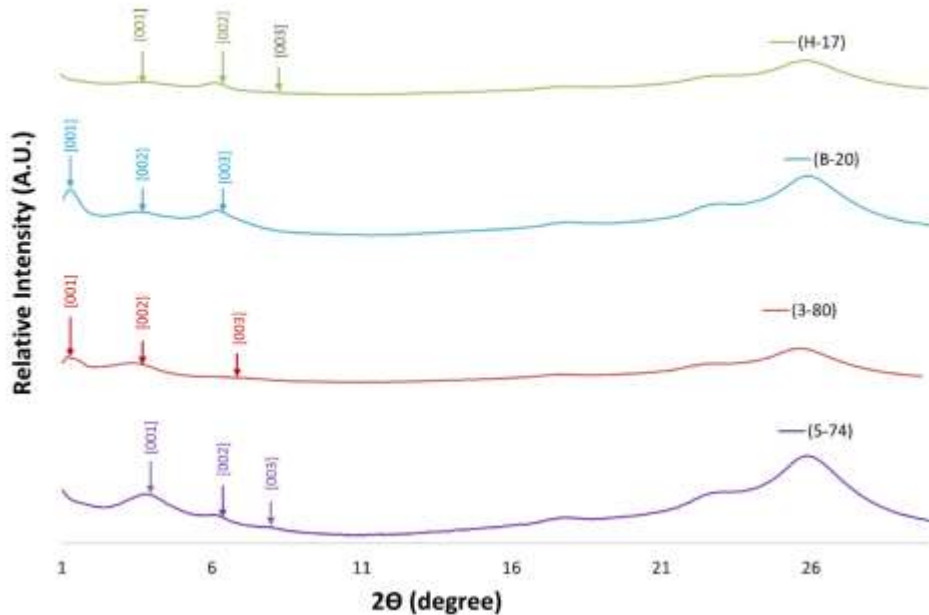


Figure 3. 14: XRD of DHL of PVOH

CHAPTER IV. CLAYS AND NANOFILLERS IN PNC

4.1 Introduction

Electrostatic attraction is needed for an effective hybrid organic-inorganic coating. Natural nanoclays such as montmorillonite (MMT), have a negative charge on each platelet face [65, 75]. In this section, we will perform a study on different clays and nanofiller that can be used in PNC gas barrier application. We compare the performance of various smectites with different plate dimensions for examining the tortuous path versus constrained polymer models.

4.2 Different Clays and Nanofiller in Gas Barrier Applications

Nielsen gas diffusion theory of nanocomposites employs a tortuous path around the clay particle to describe the improved barrier properties. Clay nanoparticles behave as impermeable barriers to gas molecules in a simple two-dimensional model [76]. In the Nielsen theory, a longer path length depends on the high aspect ratio of the clay filler and volume % of the filler in the composite [31]. Nielsen's equation for permeability is:

$$\frac{P_c}{P_p} = \frac{V_f}{[V_{ff} \left(\frac{L}{2T} \right) + 1]} \quad (4.1)$$

Where: P_c = the composite permeability coefficient, P_p = pristine polymer permeability coefficient, V_f = the polymer volume fraction, V_{ff} = the filler volume fraction, L = the Length on average (i.e., longest dimension of the clay nanoparticle) and T = the thickness of the filler on average (i.e., the smallest dimension of the clay nanoparticle). (Note:

Assume that the clay particle morphology in cross-section is a rectangle) (see figure 4.1(a)). It is clear from this simple model that the relative permeability of a composite will strongly depend on the lateral dimensions of the platy particle (i.e. the larger the aspect ratio the higher the barrier).

The Tortuous Path model is applicable for crystalline and semi-crystalline polymer nanocomposites such as Low-Density Polyethylene (LDPE) and Ionomer. If amorphous polymers are used to prepare nanocomposites, this model is not appropriate as pointed out by Adam et al. [31] (Note: Tortuous Path model cannot account for the effects of humidity on gas permeability). There are many examples where amorphous polymers exceed the barrier performance predicted by this model. The region of constrained polymer caused by interaction with the nanoparticle contributes to the gas barrier performance [31]. Thin polymer association between clay layers can be considered an expanded state of intercalation [26].

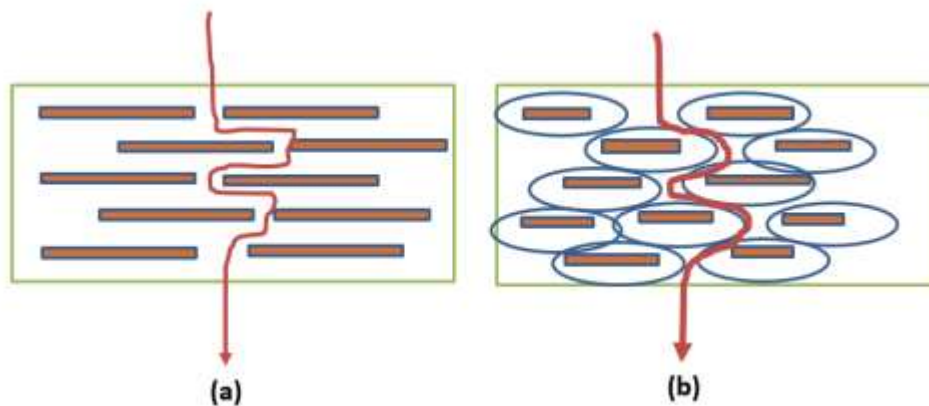


Figure 4. 1: (a) Schematic of the tortuous path model showing the high-aspect ratio clay plates increasing the path; (b) Schematic diagram of around the clay plate is the constrained polymer region

Beall et al. [56, 77] found when looking at clays aspect ratios in the range of 100 to 200 nm loading of 5 wt.%, there is an improvement in decreasing the relative permeability, and this is because of forming a constrained polymer region around the platy clay nanoparticles. This region causes deviations from the Tortuous Path model. In Tortuous Path model, the size of the constrained region and the diffusion coefficient within the constrained region were not considered. Therefore, Beall et al. [31,69] proposed a conceptual model, which corrected the effect of the change in the diffusion coefficient and the size of the constrained region of the tortuous path equation. This model helps to forecast the shape and value of the relative permeability curves of clay loading.

For the clay plates which have gas barrier effect, the “Tortuous Path Model” is the common model which works for many PNCs. For improving the deviations from the “Tortuous Path Model”, the second complex model was proposed, and it is related to a constrained polymer region.

In literature [77], this model fits more composites but includes several variables such as the constrained region size, shape, and its value diffusion coefficient. In this model, there is an assumption for existing four individual phases: constrained phase, polymer phase, clay phase, and surface modifier phase. Gas permeability still can be modeled by the “Tortuous Path Model” considering the surface modifier region has a negligible effect on the gas permeability of the composite.

The constrained phase has a gas diffusion coefficient different than the bulk polymer. The polymer in this region will either have a lower free volume (lower diffusion coefficient) or lower solubility for the permeating gas. For the constrained polymer region, this

conceptual model gives a correction factor (V_f) that can be used to the Nielson model (Eq. (1)).

$$V_f = V_{unp} + \left(\frac{V_{cp}}{R_{cu}} \right) \quad (4.2)$$

Where:

Volume fraction of unconstrained bulk polymer = V_{unp} ;

Volume fraction of constrained polymer = V_{cp} ;

Ratio of the diffusion coefficient of the constrained and Unconstrained = R_{cu}

Adame et al. [31] measured the constrained polymer region size by using nylon 6 and MXD6. They put their samples in high humidity to swell because they assumed that the constrained region would swell less than other regions. In this conceptual model, they assume 5wt.% of clay plates are dispersed well, and so the distance between plates could be 50 nm approximately. But, the “constrained polymer region” needs to extend from the surface minimum of 25 nm. Constrained polymer region size as low as 5% loading of clay is approximately 98% (They used AFM to verify composite morphology).

Amorphous polymers show this constrained polymer effect on high barrier effect. In amorphous polymers, because of the lower free volume or lower solubility, they have the largest effect of constrained polymer regions.

As mentioned earlier adding nanofillers will improve the polymer properties. Clay chemistry involves non-covalent interactions with various hydrophilic polymers. A composition which contains an anionic silicon compound is called silicate. Silicates are the most common type of mineral in majority of Earth's crust [78].

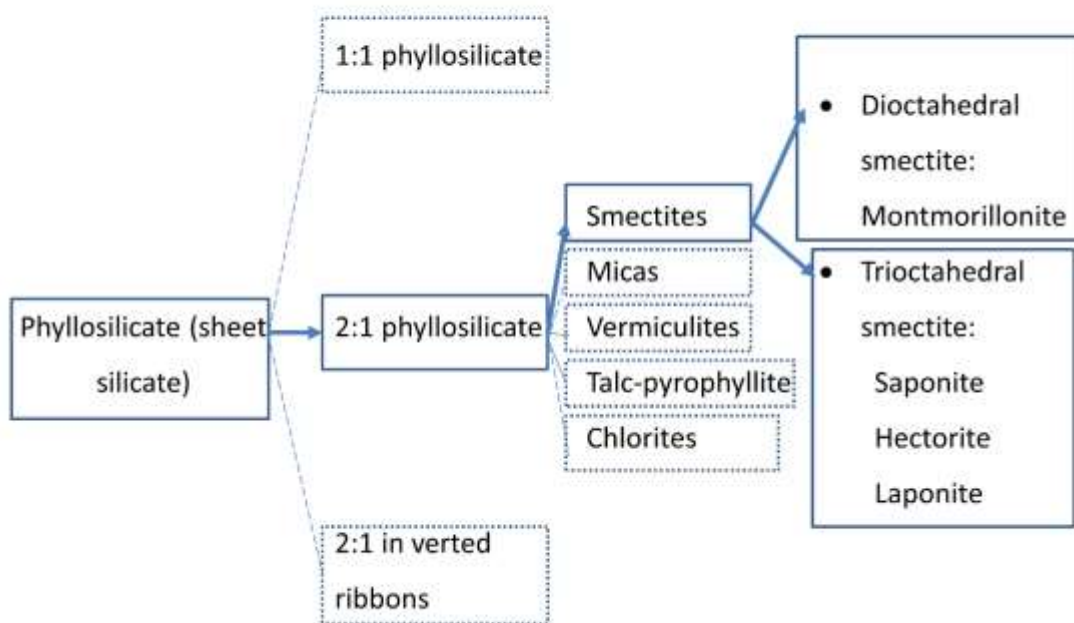


Figure 4. 2: Overall classification of clays

Smectite clays are a class of plate like silicates that are approximately one nanometer thick but tens to hundreds of nanometers in the other two dimensions. These plate like nanoparticles occur in nature in large deposits all over the world.

These minerals are commonly referred to as 2:1 clays where a central octahedrally coordinated metal (Al, Mg) is sandwiched between two tetrahedrally coordinated silicon layers. These individual layers are crystallographically turbostratic exhibiting no crystal symmetry between plates. The smectite group of Dioctahedral is more negatively charged than Trioctahedral smectite. Dioctahedral smectite group has Al in the middle and Trioctahedral smectite group has Mg in the middle

The most common and commercially viable minerals of this type of clay are montmorillonite ($\text{Al}_2\text{Si}_4\text{O}_{10}(\text{OH})_2$) and Hectorite ($\text{Mg}_3\text{Si}_4\text{O}_{10}(\text{OH})_2$). In both minerals substantial isomorphous substitution occurs that impart cation exchange capacity to the minerals. In montmorillonite the most common substitution is Mg for Al and in hectorite it is Li for Mg. This substantial cation exchange capacity has been utilized to produce a whole family of intercalated complexes utilizing quaternary ammonium compounds that substitute for the exchangeable cation in the space between the plates referred to as the gallery [79]. The substitution quaternary ammonium compound containing long alkyl chains for the cation changes the character of the surface from being hydrophilic to hydrophobic

These four clays were chosen to have a wide variation of lateral dimensions. Laponite is very small at 30 nm, hectorite at 80 nm, MMT at 150 nm and VMT at 1000 nm. This series is a good test of the tortuous path model of Nielsen since the lateral dimensions of the particles strongly affect the gas permeability with small particles having little effect [80].

4.2.1 Saponite Clay

Saponite is a trioctahedral mineral from the smectite group. The average dimensions of Saponite (Sap) are 300-1000 nm in length and 1 nm in thickness. $((\text{Ca}_{0.25}(\text{Mg},\text{Fe})_3((\text{Si},\text{Al})_4\text{O}_{10})(\text{OH})_2 \cdot n(\text{H}_2\text{O}))$ [62]. Ebina et al. [81] showed that synthetic smectite saponite with a binder additive, carboxymethyl cellulose sodium salt or polyacrylic acid sodium salt have heat-durability and light-transmission above 90 %. Also, oxygen gas-barrier properties of the films were measured under dry conditions, and

the permeability of the saponite film containing 20 wt. % of polyacrylic acid sodium salt was $0.074 \text{ cm}^3 \text{ m}^{-2} \text{ day}^{-1} \text{ atm}^{-1}$ and it had 10-micron thickness [81]. In Figure 4.3, we have an intercalated system with adding saponite to PVOH.

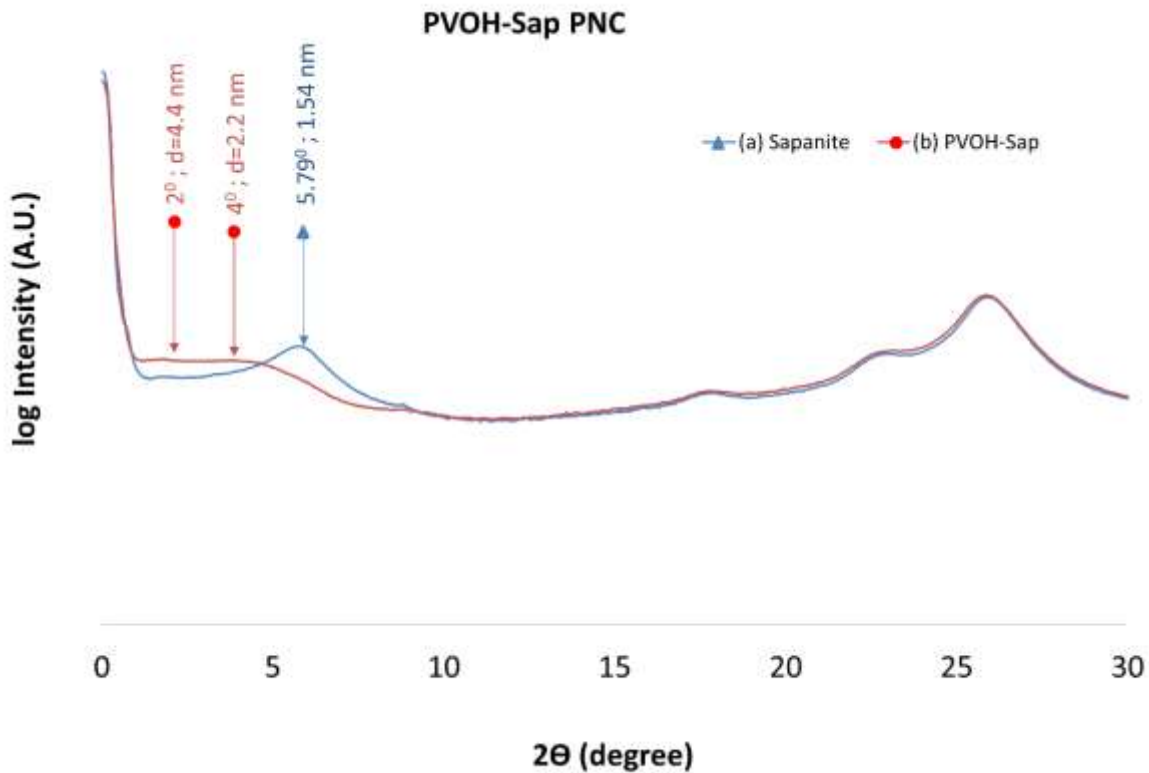


Figure 4. 3: XRD of Saponite alone and PVOH- Saponite PNC

4.2.3 Humic Acid

The main component of humic materials is Humic acids (HA) which are the primary organic constituents of soil and coal. Humic acid is a mixture of many different acids containing carboxyl and phenolate groups. Having carboxylate and phenolate groups help the humic acids to form complexes with ions such as Mg^{2+} , Ca^{2+} , Fe^{2+} and Fe^{3+} [61]. The effect of adding this nanofiller to PVOH also was investigated in this research. In Figure

4.4, we can see adding Humic acid to PVOH will give us one reflection, and we have an intercalated system here as well.

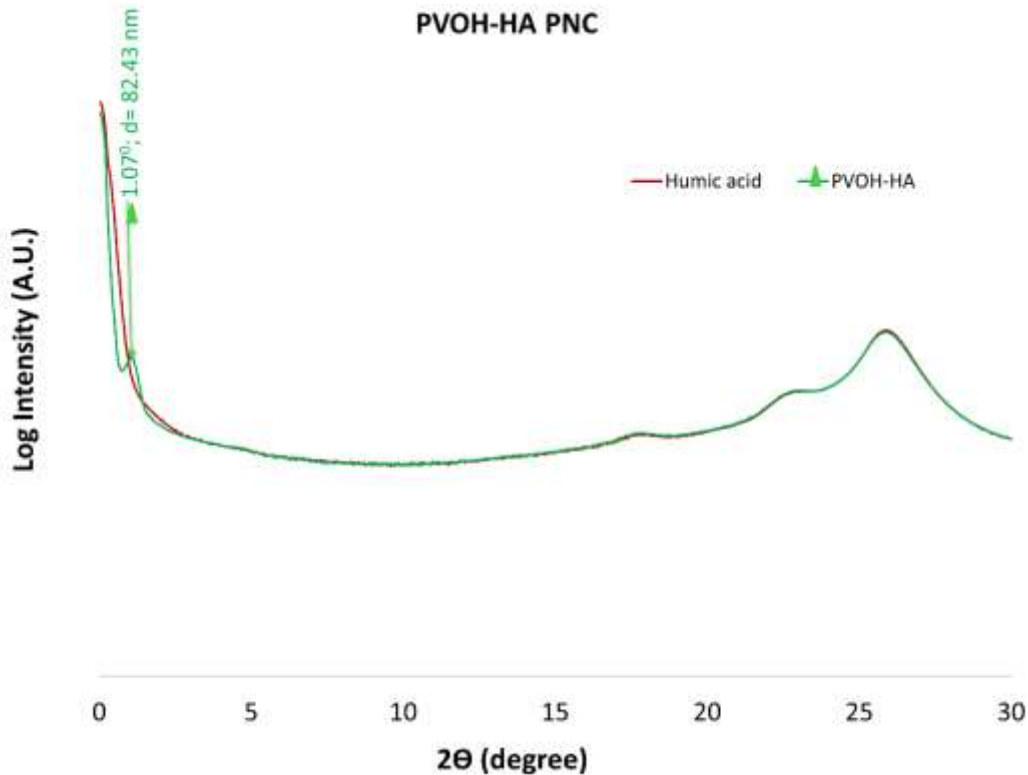


Figure 4. 4: XRD of PVOH-Humic acid(HA) PNC

4.2.4 Hydrotalcite

A layered double hydroxide is Hydrotalcite (Hydro) ($Mg_6Al_2CO_3(OH)_{16.4}(H_2O)$), and this name comes from its similarity with talc and having high water value. Layered double hydroxides are famous for their anion exchange capabilities [64]. We verified this exchange capacity by adding Hydro to PVOH and verifying in crystal morphology as seen in Figure 4.5 there are not any changes.

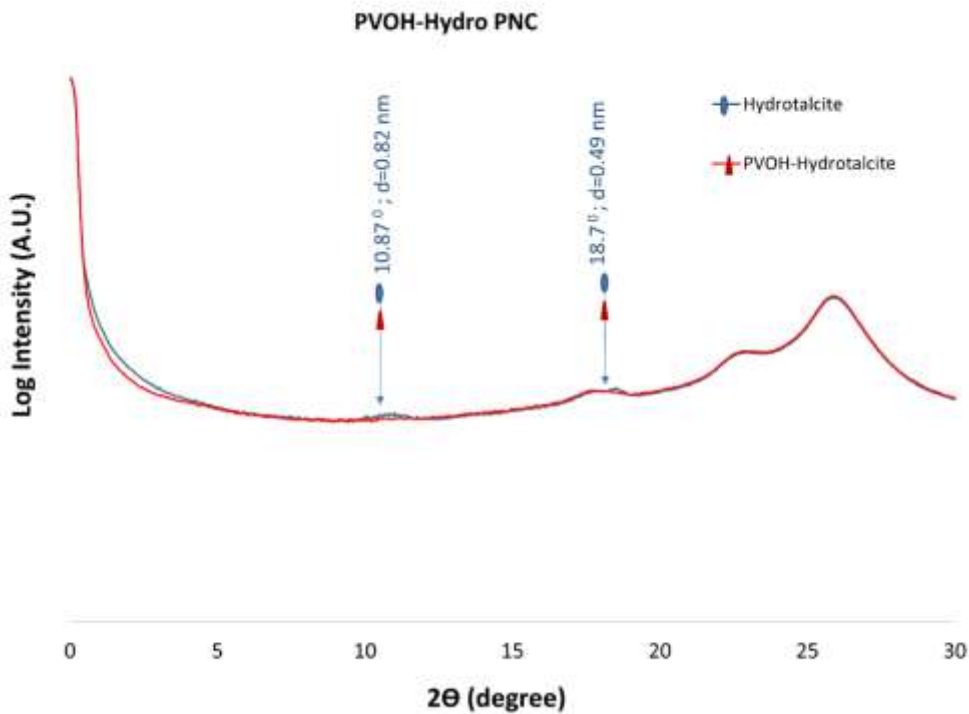


Figure 4. 5: XRD of PVOH-Hydro PNC

4.2.5 Vermiculite Clay (VMT)

Vermiculite (VMT) is a mineral kind of hydrous phyllosilicate. In VMT, there are two tetrahedral sheets for any octahedral sheet (2:1 clay). Vermiculites (VMT) among other discussed clays have larger aspect ratios (between 1500 and 3000). VMT has a good cation exchange capability. VMT on average has a thickness less than 75 nm.



In 2012, Priolo et al. [82] deposited branched polyethyleneimine (PEI) and VMT (>96 wt.%) film by using (LbL) assembly which has transparency over 95%, and has less amount of oxygen permeation ($\text{OTR} = 0.017 \text{ cc/m}^2 \cdot \text{day.atm}$), and has 165 nm thickness. The high gas barrier results from a highly aligned, Nano brick wall structure (which exceeding tortuosity for gas molecule diffusion). So, in this research, we investigated

adding VMT to PVOH to see its reaction. As seen in Figure 4.6, the influence and effect of having VMT in PVOH polymer matrix, we have several reflections after adding it to PVOH. It would appear that only a portion of the VMT has been intercalated with the peak at 1.22 nm being unintercalated VMT.

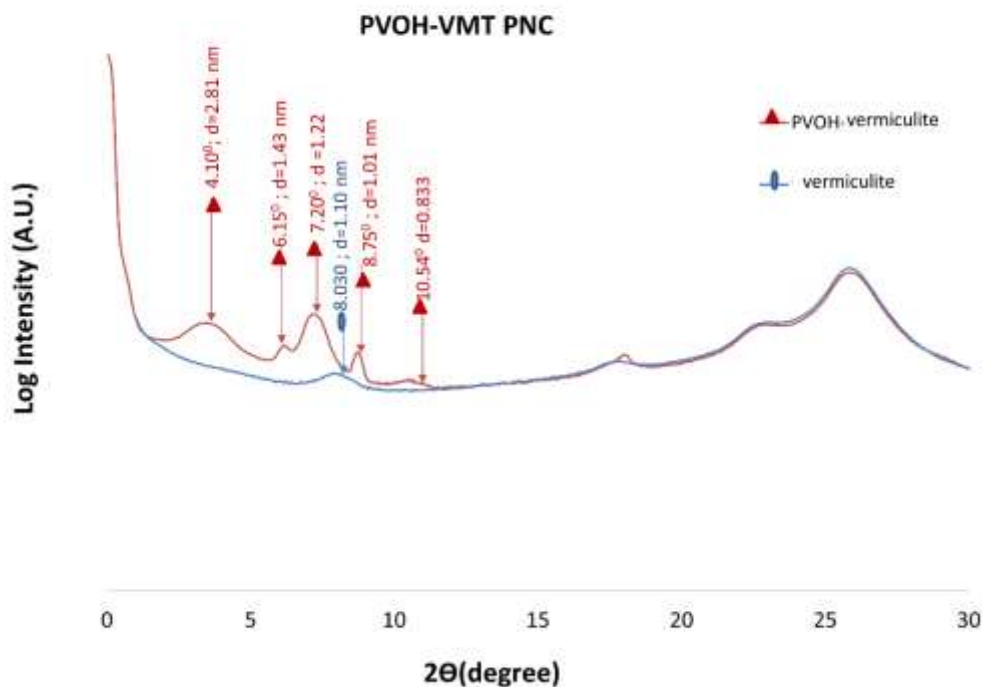


Figure 4. 6: XRD of PVOH-VMT

4.2.6 Hectorite Clay

Hectorite (HEC) is a white clay mineral with a chemical formula of $\text{NaO}_3(\text{Mg}, \text{Li})_3\text{Si}_4\text{O}_{10}(\text{OH})_2$ (0.1-micron aspect ratio and 1 nm thickness) [83].

We investigated on adding HEC to PVOH, and Figure 4.7 shows how this clay is reacting and can have an intercalated system with PVOH.

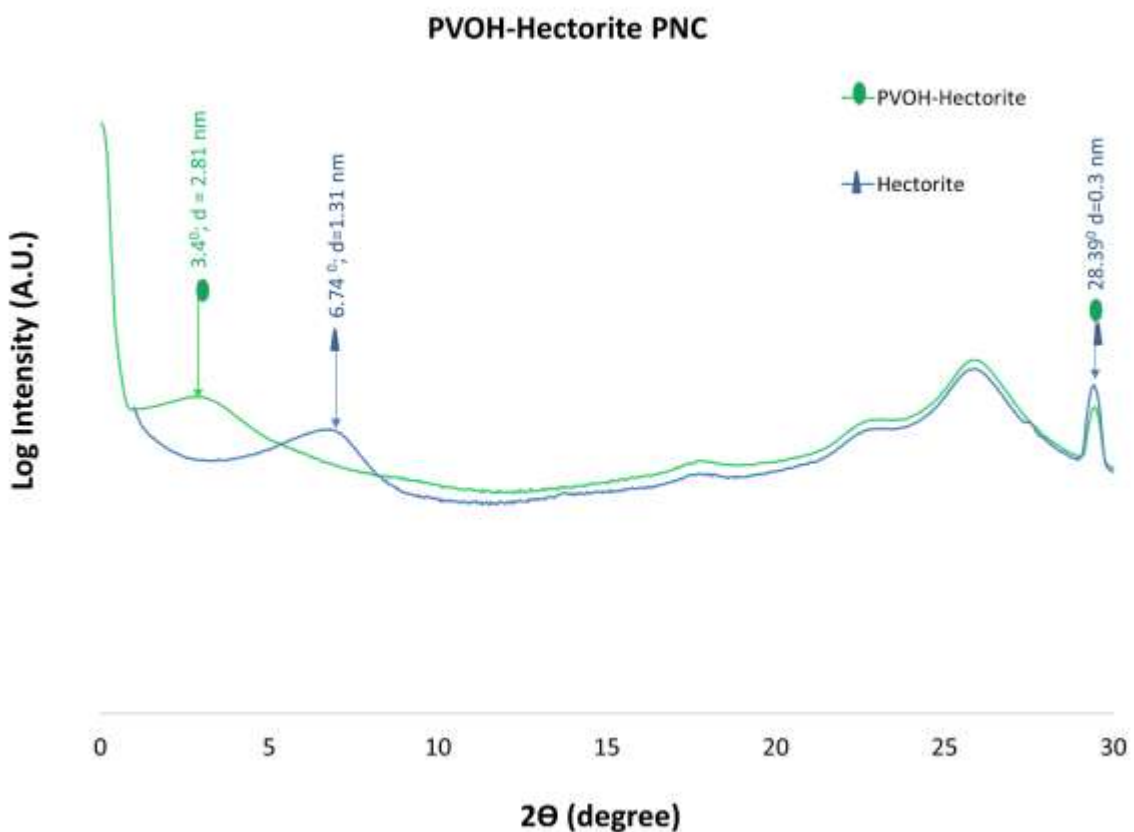


Figure 4. 7: XRD of PVOH-HEC PNC

4.2.7 Laponite Clay

Laponite clay (LP) has a diameter = 25 nm and thickness = 1 nm. It is a synthetic layered silicate with a low heavy metals content. It swells in water and gives the colorless colloidal dispersions in water. U. Tritschler et al. [84] showed that liquid crystal (LC) polymer with Bio-inspired Laponite (LP) composite (high fractions more than 80%) exhibit a promising behavior of reduced oxygen transmission. The obtained gas barrier PNC performance can be used in nanostructure of the coatings [84].

In this research, we investigated the effect of using amorphous polymers with LP to study their gas barrier performance.

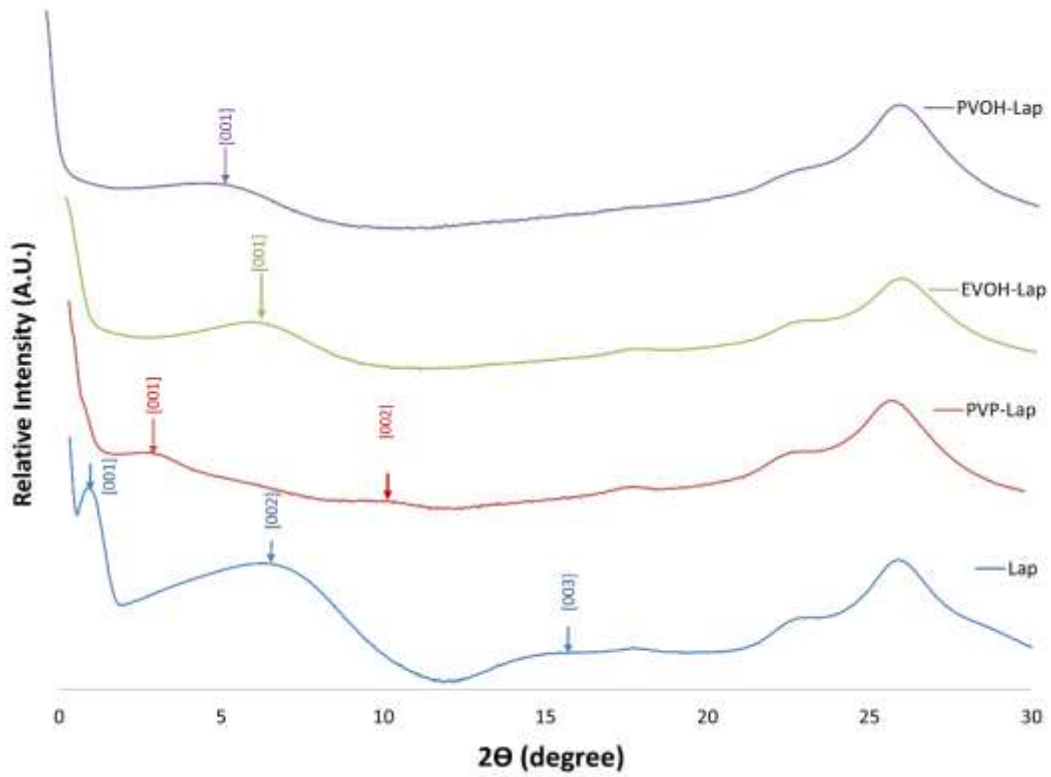


Figure 4. 8: XRD of different polymers with LP clay

As mentioned earlier in this chapter about a constrained region of polymer and the small size clay may work in an amorphous polymer matrix and give less amount of oxygen permeation. So, in Figure 4.9, we investigate to use LAP clay with other amorphous polymers, and we measured their oxygen permeation rate.

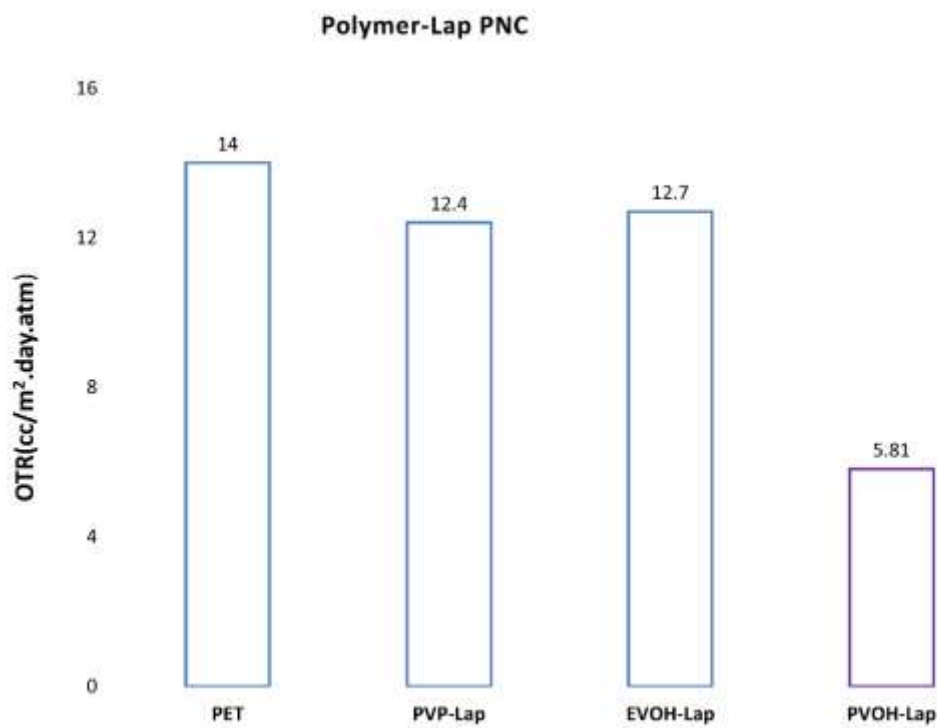


Figure 4. 9: OTR comparison between different polymers and LP Nano clay

PVOH-Lap PNC gives us the minimum amount of OTR in comparison to others.

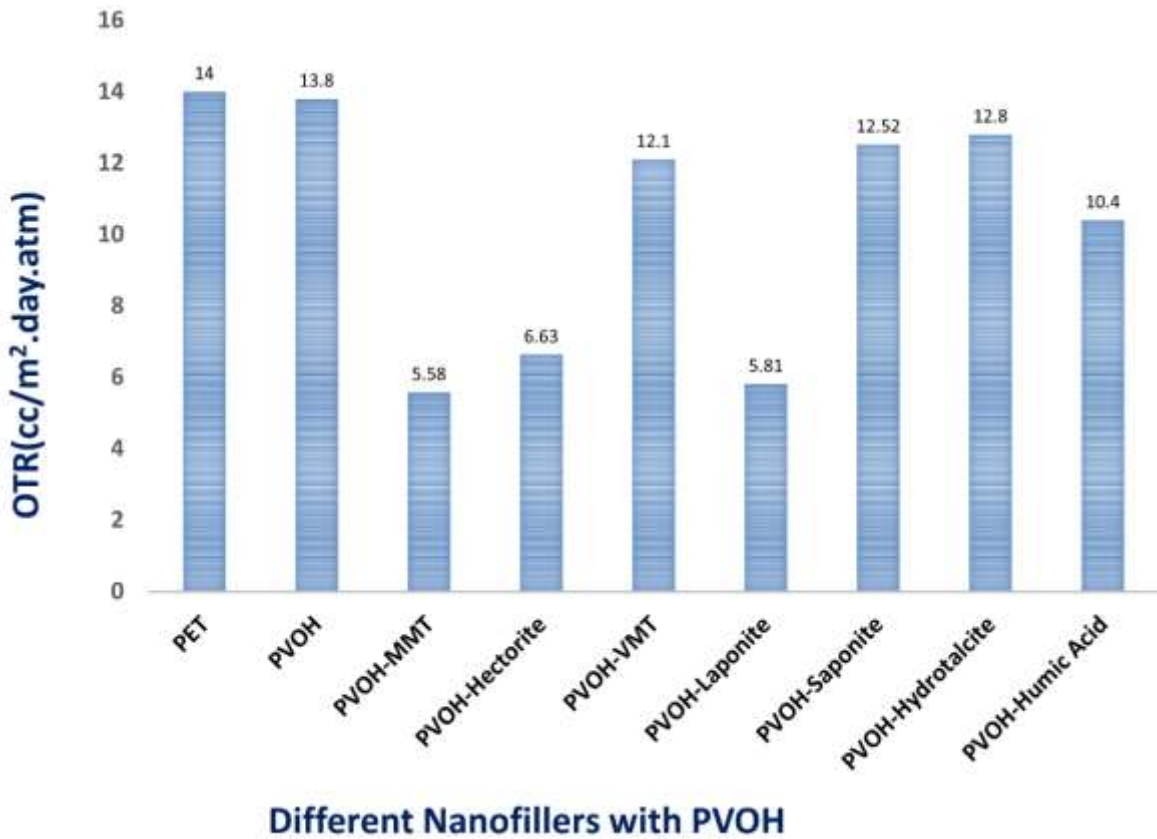


Figure 4. 10: OTR comparing of PVOH with different nanofillers

Figure 4.10 shows the amount of OTR for different nanofillers in PVOH polymer matrix. The results are rather surprising. The LAP complex performed as well as the MMT and the VMT performed the worst. The VMT results can be explained by the fact that the x-ray diffraction pattern indicates that the VMT was only partially intercalated with PVOH. In addition, the print head of the ink jet printer kept getting stopped up due to the large particle size. The VMT results can be discounted based upon these factors. The relative performance of the MMT and LAP are much more difficult to rationalize using just the tortuous path model for barrier properties. The very unusual performance of LAP however can easily be accommodated with a modified Nielsen model where the effect of constrained polymer is accounted for in the calculations [31].

Overall, we can conclude that all negatively charged clay and all nanoclays which have 1 nm thickness works better than other used nanofillers.

4.3 Modeling

In this section we want to test the applicability of various permeation models in predicting gas permeability.

From Nielsen's equation for permeability (4.1), for different clays in different lateral dimension, we have Table 4.1.

Table 4. 1: Relative permeation for different clays in Tortuous Path model

Clays	Lateral Dimension (nm)	P _c /P _p
VMT(vermiculite)	1000	0.4 %
MMT(Montmorillonite)	150	2.6 %
HEC(Hectorite)	80	4.7%
LAP(Laponite)	30	11.2%

According to our calculation in Table 4.1, MMT has 4 times less permeation rate than LAP. Then, we compared our calculation data with our experimental data in Figure 4.11

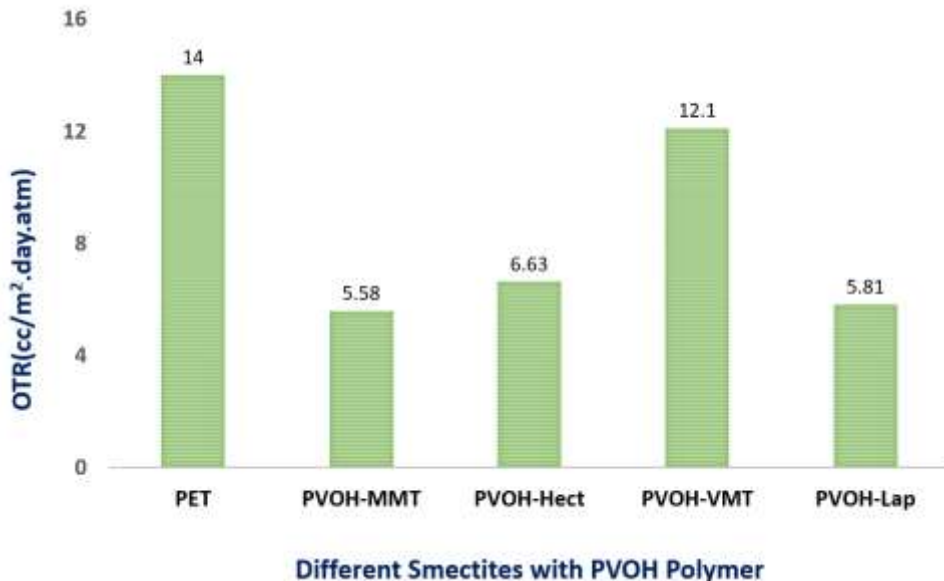


Figure 4. 11: Comparison of OTR values for a series of different size smectite clays with PVOH

Figure 4.11 contains the OTR results for different smectic clays with PVOH. The results are rather surprising. The LAP complex performed as well as the MMT. The very unusual performance of LAP can easily be accommodated with a modified Nielsen model where the effect of constrained polymer is accounted for in the calculations. From comparing our calculated data from the Nielsen model (tortuous path model) and our experimental data, we found that tortuous path model does not work for different clays in polymer nanocomposite. Because, Tortuous Path model, the size of the constrained region and the diffusion coefficient within the constrained region were not considered (Note: VMT is not fully intercalated because of having large aspect ratio).

CHAPTER V. ANNEALING AND HUMIDITY IN PNC

5.1 Introduction

It has been observed in previous work [69] on PVP/clay self-assembled films that the films were highly ordered. This part of research reveals that films appear to order more with time and temperature variations. The relation between different molecular weight (MW) polymers and annealing needs to be considered in the temperatures above and below glass transmission temperature (T_g) for various polymers. Then, the effect of temperature variation on the oxygen permeation rate and crystal structure will be investigated.

Moreover, in this section, the influence of relative humidity (RH) on the gas barrier films will be investigated in different PNCs via different deposition techniques.

5.2 Annealing Time Relationships in PNC

Incorporating nanomaterial into a polymer improves the barrier performance. We examined the annealing time relation on PVOH-MMT PNC. The XRD pattern for higher molecular weight polymers depends on increasing the annealing time to have sharp peaks. For example, in part (a) of Figure 5.1, there is an intercalated system pattern of PVOH-MMT, and in part (b) XRD characterization was done after putting the nanocomposite in an oven for 4 hours at 40 °C. As seen in part (b) of Figure 5.1, we have sharp peaks with higher intensity when compared with part (a). Achieving sharper XRD peaks for higher molecular weight polymers needs longer annealing time. Long-term annealing time improves the crystallinity [84]. Different molecular weight polymers and annealing conditions result in different XRD patterns [49]. The effect of different

molecular weight (MW) polymers on the kinetics of the crystal growth were investigated in the literature. For example, the rates of the crystal growth of felodipine in the presence of different MWs of PVP were reported to be different under various combinations of concentration (0.5-4.5 wt. %) and temperatures (70-110 °C) [85].

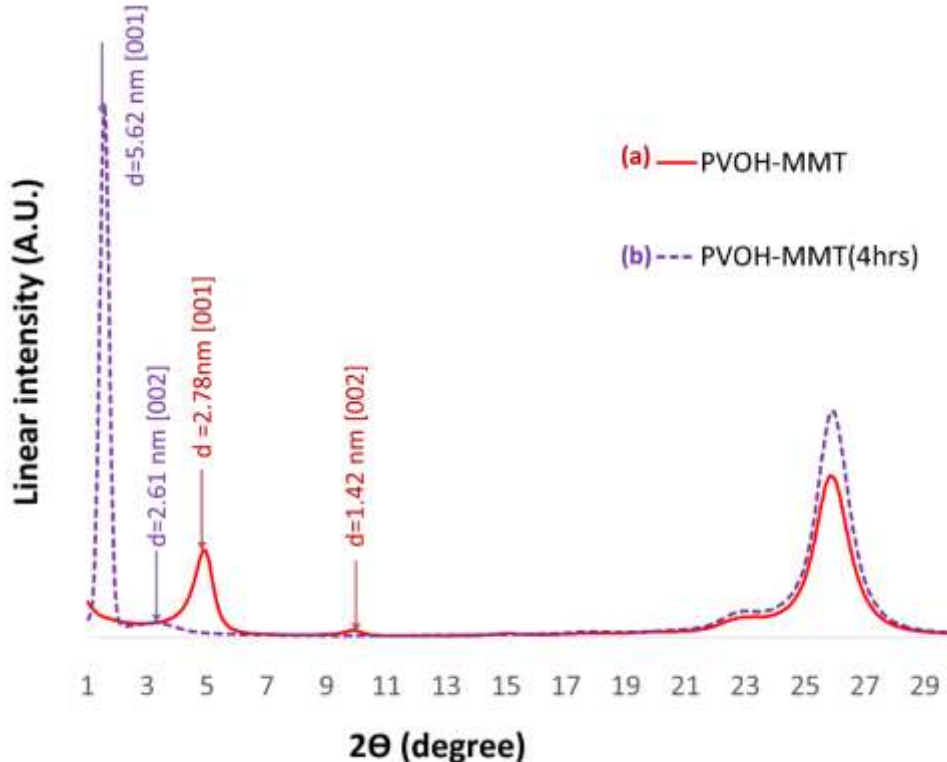


Figure 5. 1: XRD results for PVOH-MMT after 4 hrs annealing below T_g

Then after observing annealing effect on OTR, we investigated the effect of annealing time (less than T_g) on oxygen permeation. Annealing increase the peak distance of XRD because without annealing polymers are uncoiled but after annealing polymers going to be recoiled. Furthermore, annealing helped to have ordered system. We can see in Figure 5.2, that annealing of PVOH-MMT nanocomposite will give lower

OTR (Note: we annealed PVOH-MMT PNC above T_g but, it had not the main effect on OTR reduction, and it was 5.68 cc/m².day.atm).

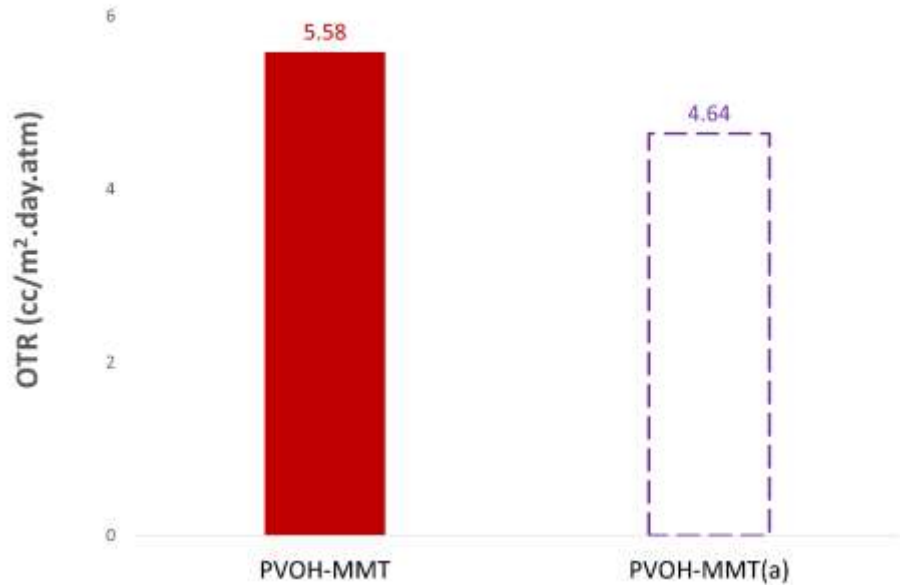


Figure 5. 2: OTR results for (a) PVOH-MMT (b) PVOH-MMT after 4 hrs annealing below T_g

We also investigated annealing effect on PVP-MMT PNC and PVP with high molecular weight (PVP=360000), and in Figure 5.3, we can see observed OTR reduction.

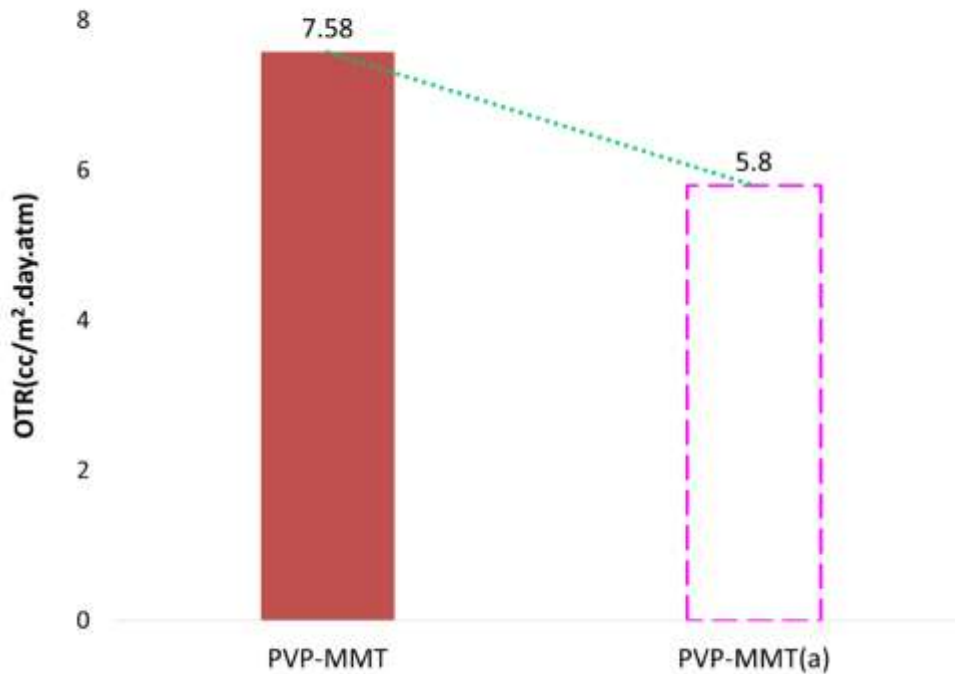


Figure 5. 3: OTR results for (a) PVP-MMT (b) PVP-MMT after 4 hrs annealing below T_g

Overall, we can conclude that annealing polymer nanocomposites in temperatures less than T_g will increase oxygen barrier property of PNC.

5.3 Oxygen Transmission Rate and Humidity Relationship

In the majority of polymer and nanocomposites, the gas barrier property decreases with increasing humidity [86-88]. Relative humidity (RH) is obtained by the following ratio:

$$RH\% = \frac{a}{b} \times 100 \quad (5.1)$$

a = Amount of water vapor present in air; b = maximum amount of water the air can hold at the current temperature and pressure.

A more specific definition of relative humidity requires Dalton's law of partial pressures [89].

In humid environments, the films deposited with hydrophilic materials will swell [90]. In clay-based materials, humidity increases OTR because of swelling [91,38]. A thicker polymer between clay layers improves gas barrier performance [38]. PVP swells significantly at high humidity when deposited with MMT [92]. Holder et al. [92] showed that LbL deposition of PVP-MMT improves the gas barrier property at high humidity. A longer Tortuous Path is created at the higher humidity because there is close packing and greater spacing between the clay layers (H-bonding between polymer and clay is not strong). OTR of the PVP-MMT composite was dramatically decreased as a function of RH. At 0% RH, a 40-BL film has an OTR of 3.9 cc/ (m².day.atm and at 100% RH, OTR was 3.5

In Figure 5.4, we investigated the effects of having Humidity (HM) in PNC. Therefore, we compared having PNC in 0% HM and 45% HM (2). We can see in Figure 5.4, the effect of HM on PVOH-Lap and EVOH-MMT PNC caused greater permeation rates. In the case of the MMT and Hectorite intercalates the humidity had no effect. The only system affected was the small particle laponite. For the PVOH-MMT the OTR at 100% relative humidity did not change at all. This again indicates that the constrained polymer effect is at work in these systems.

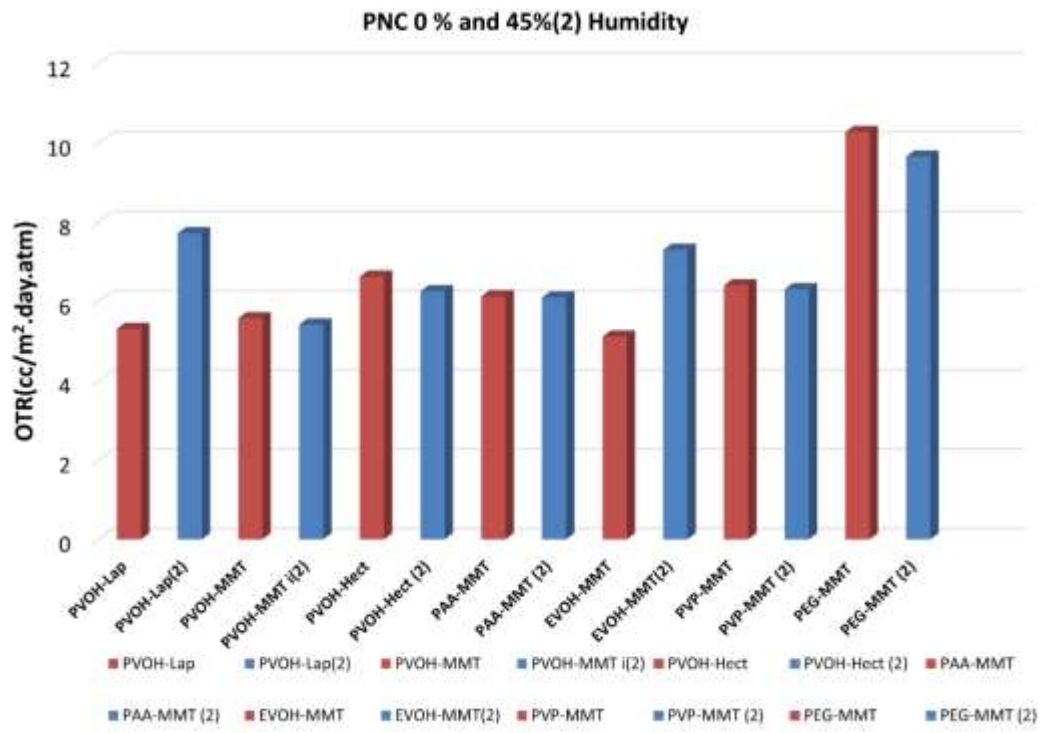


Figure 5. 4: Comparing different composites in 0% humidity and (2) in 45% humidity

PVOH is a known polymer for its low cost and its good gas-barrier properties [93]. PVOH barrier properties are sensitive to humidity. It must be protected by polymer overcoats such as polypropylene. In 2014, Dou et al. showed that incorporating LDH (layered double hydroxides) nanoplates in PVA can reduce oxygen transmission of PET to 0.72 (cc /m².day. atm) with an approximate 420 nm thickness and 20 bilayers [94]. We investigated the effect of adding MMT nanoclay with the ink-jet printer on gas barrier performance of PVOH.

The influence of relative humidity (RH) on the gas barrier films needs to be investigated in other PNCs as a function of different deposition techniques. PVOH (polyvinyl alcohol) is a barrier polymer against gases [95]. At high relative humidity, PVOH permeability increases [96]. Adding MMT nanoclay to PVOH with a DOD printer

in 6 BL had zero OTR at 0% RH. Different levels of RH were utilized to measure PVOH-MMT nanocomposite barrier performance as a function of RH. In Figure 5.5, the effect of different humidity on PVOH-MMT nanocomposite barrier performance is summarized.

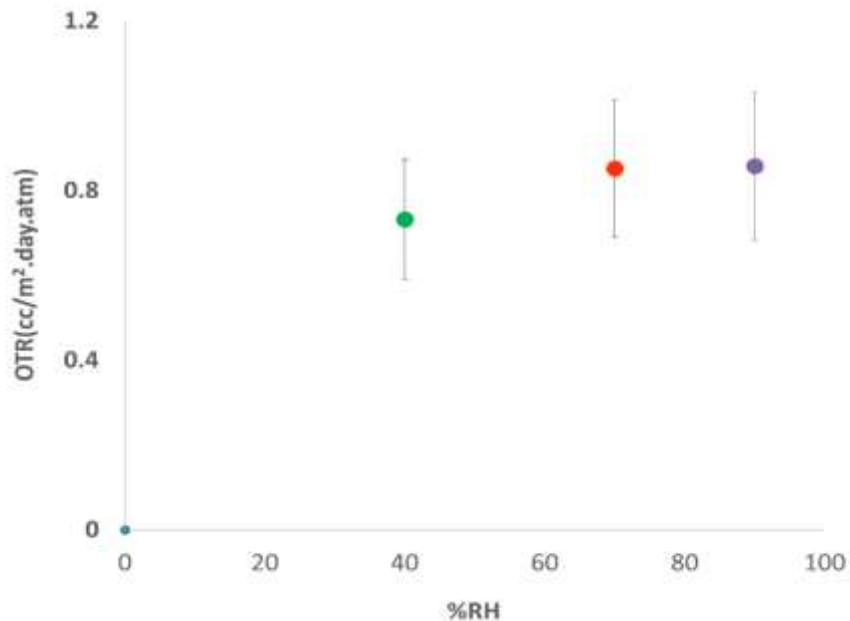


Figure 5. 5: The effect of humidity on the OTR of PVOH-MMT nanocomposite

Figure 5.5 shows the effect of humidity on the OTR of PVOH-MMT nanocomposite as a function of increasing RH values. All average an OTR less than 1 cc/m².day.atm.

Increasing temperature (in Tg) in polymer nanocomposite is not related to its morphology, but higher molecular weight polymers need to be annealed for having polymer nanocomposite in exfoliation structure [10,97]. In literature [98], gas barrier behavior in most polymers and composite materials reduces at high humidity. These water and gas barrier properties depend on the crystallinity of the polymer layer [99].

We considered another example for verifying the effect of annealing and humidity on PVOH-MMT, PEG-MMT, and PAA-MMT nanocomposite above Tg (PVOH Tg is 85°C). In Figure 5.6, we can see crystal morphology of PVOH-MMT in different temperatures and have it in 100 % humidity.

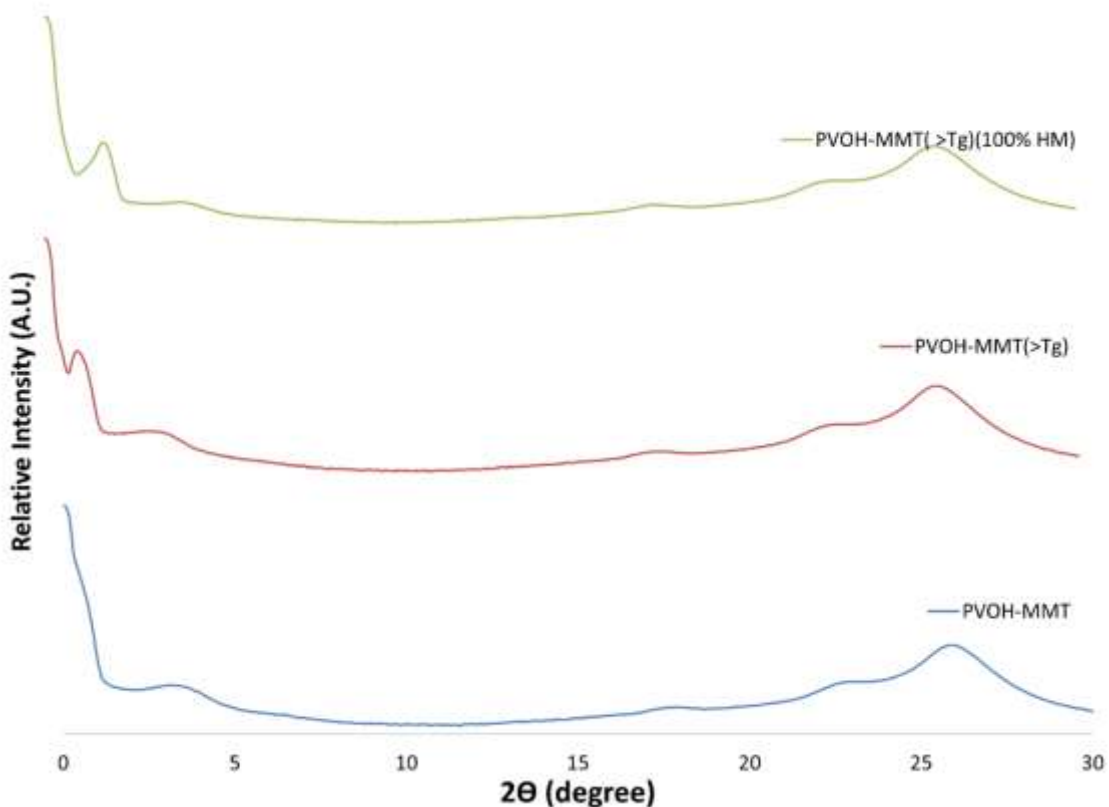


Figure 5. 6: 3 BL printed PVO-MMT film and annealing above Tg and in 100% Humidity

In Figure 5.7, we annealed PVOH-MMT PNC below Tg and put it in 100% humidity. We also compared the PVOH-MMT at room temperature with 0% humidity. The results show there is no permeation difference in both.

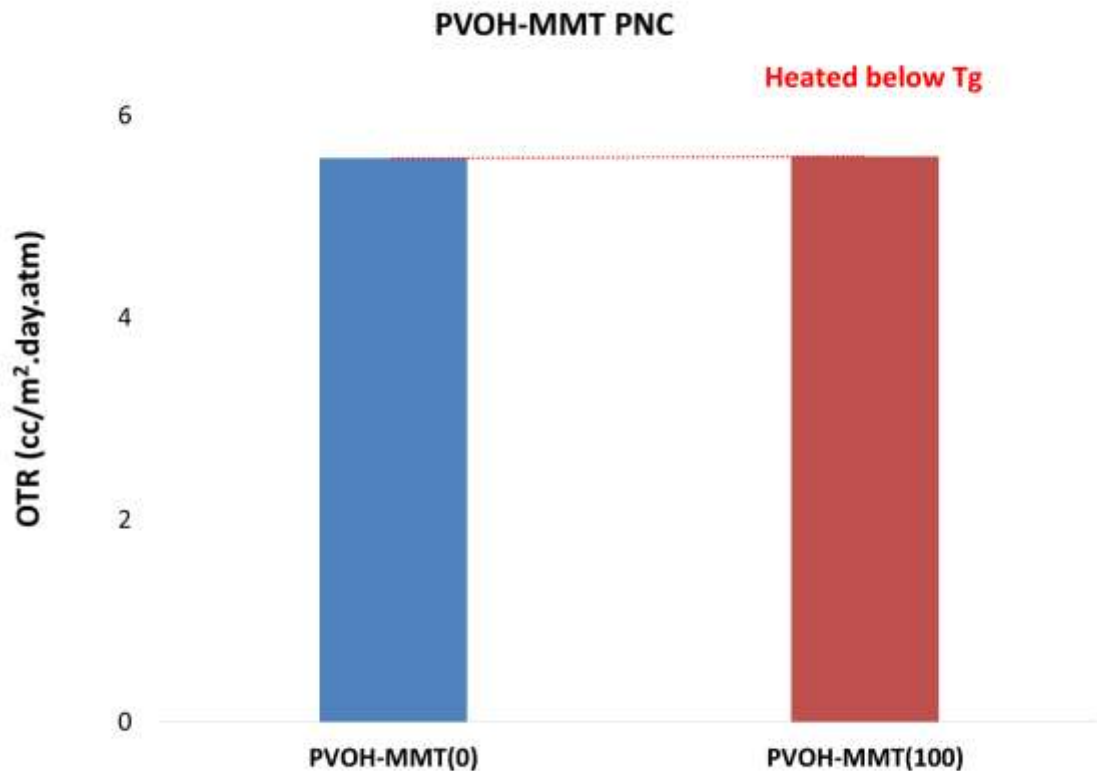


Figure 5. 7: 1 BL PVOH-MMT PNC in 0% humidity and annealed above Tg and in 100% Humidity

Messersmith et al. [100] showed 80% reduction permeability to water vapor for poly(ϵ -caprolactone) (PCL) and delaminated organic aluminosilicates made by in situ intercalative polymerizations.

In 2012, Holder et al. [101] showed that PVP/MMT PNC has an interesting reaction under humidity and lower than Tg of the PVP (Temperature transitions from a glassy state to a less glassy, or rubbery state) because PVP swells and forms hydrogen bonding with water.

When PVP swells (denser), the clay layers are not swelling and instead maintain their tight lateral packing between polymer layers. Therefore, we can see the effect of constrained polymer regions help to have less gas permeation rate

For example, a PVP/MMT PNC (a clay concentration of 74 wt. %) under humidity environment will give greater spacing. Therefore, oxygen barrier improves at high humidity [101].

We considered the effect of humidity on our PVP-MMT nanocomposite which made in 1 BL and deposited with spraying in Figure 5.8 (PVP Tg = 170 °C).

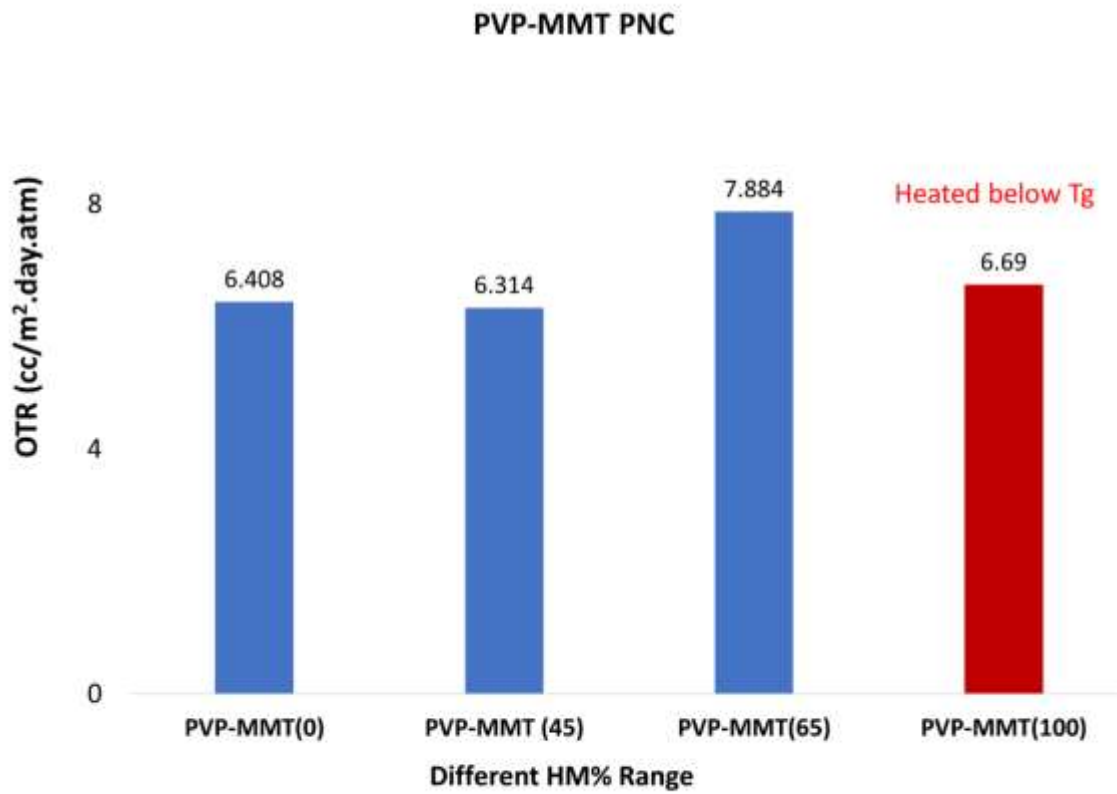


Figure 5. 8: PVP-MMT PNC (1BL) in different humidity percentages

Considering having different ranges of humidity in PVP-MMT does not affect oxygen permeation rate.

We annealed PEG-MMT and PAA-MMT in 100 % humidity, and the result shows in Figure 5.9, both PNCs, having this mentioned condition increases oxygen permeation rate.

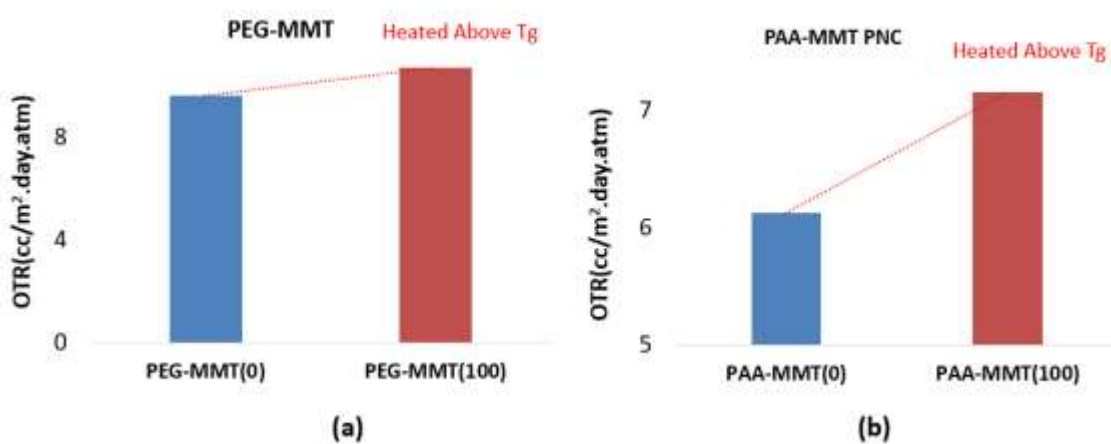


Figure 5. 9: (a) 1BL PEG-MMT PNC;(b) 1BL PAA-MMT PNC in 0% humidity and annealed above Tg and in 100% Humidity

5.4 Polymer Molecular Weights Role in PNCs

We investigated on verifying the effect of using the different molecular weight of polymers on gas barrier properties. We deposited 1BL PNC with spraying PEG-MMT and PVP-MMT in different molecular weights. In Figure 5.10 (a) and 5.11(a), We can see XRD morphology of PEG and PVP MMT PNC. In both figures, we can see that usage of the lower molecular weight polymer has more intensity. In Figure 5.10 (b) and 5.11 (b), we can understand the lower molecular weight with higher intensity has lower amount of

OTR. (PEG (1) MW:2000; PEG (2) MW:8000) and (PVP (1) MW:160000; PVP (2)360000).

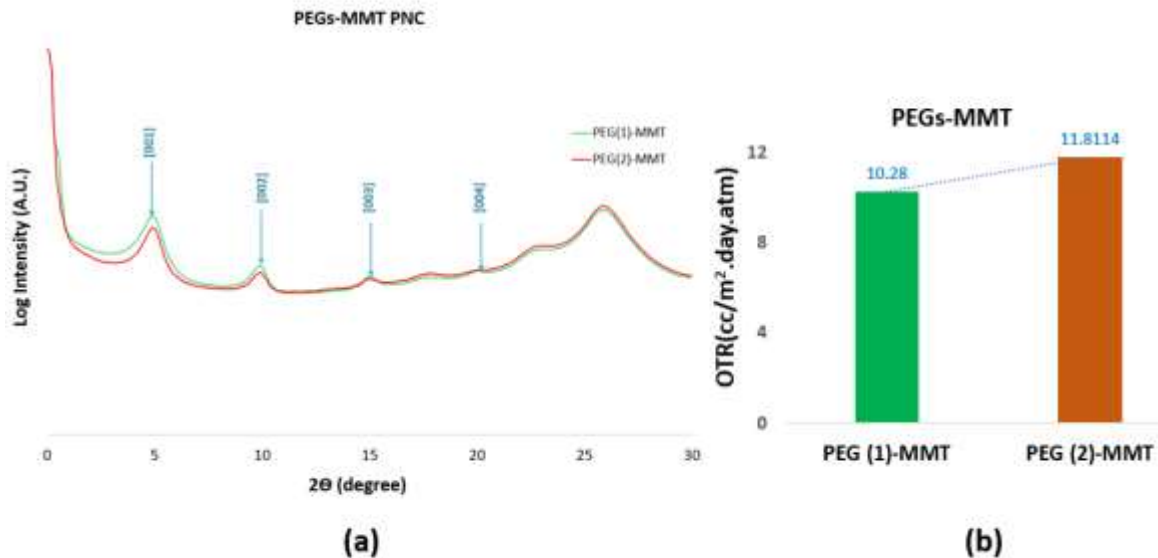


Figure 5. 10: (a) XRD; and (b) OTR comparison of different molecular weights of PEG with MMT clay (PEG (1) MW:2000; PEG (2) MW:8000)

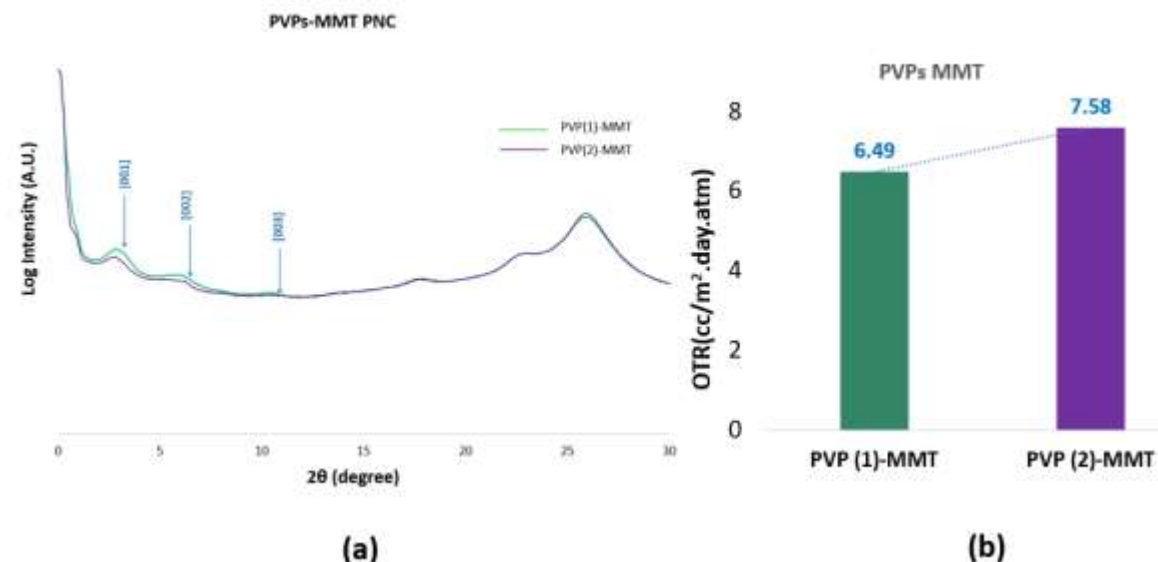


Figure 5. 11: (a) XRD; (b) OTR comparison of different molecular weight of PVP with MMT clay (PVP (1) MW:160000; PVP (2)360000)

We conclude that lower molecular weight polymer appears to self-assembled slightly better and give better OTR.

CHAPTER VI. INKJET PRINTING AND COATING APPLICATION

6.1 Introduction

Different PNCs were deposited via spraying and printing, and their OTR and XRD were investigated. In the end, we printed a PVOH-MMT PNC in 6 BL with printing technique and did comprehensive characterization study on it.

6.2 Comparison between Printing and Spraying Deposition

The deposited films with PVP-MMT and PAA-MMT via printing and spraying techniques were analyzed using XRD to verify whether any spontaneous self-assembly had occurred. In x-ray diffraction, the angle of peaks and their intensity can be used to identify the structure of nanocomposites. The wide layer separation in the exfoliated nanocomposites causes the disappearance of any diffraction peak.

For intercalated nanocomposites, the increase of the distance between layers causes the peaks to move to lower angles. The intercalated Polymer/clay films should have several orders of reflection. The intensity and high amount of orders are due to the self-assembly of ordered layers of clay intercalated by a polymer. This intercalation is mediated by ion-dipole bonding of the exchangeable cation to the montmorillonite surface. For entering the confined space of the gallery, the polymers must uncoil in the intercalation process. Polymer entropy decreases at the beginning of the process. Entropy will increase for the displacement of thousands of water molecules by the polymer-ion dipole bonding to exchangeable cations on the surface of the clay [46]. If there is not a MMT pattern in the XRD pattern, exfoliated or intercalated nanocomposite structure has occurred. According to Priolo et al. [26], the primary scattering peak of the neat MMT

clay is at 8.37° spacing (d_{001}) of 1.056 nm. Figure 6.1 and Figure 6.2 show XRD patterns for deposited films of PVP-MMT and PAA-MMT. The position, intensity, and broadness of the peaks of different composites with different concentrations and layers will have changed in x-ray patterns.

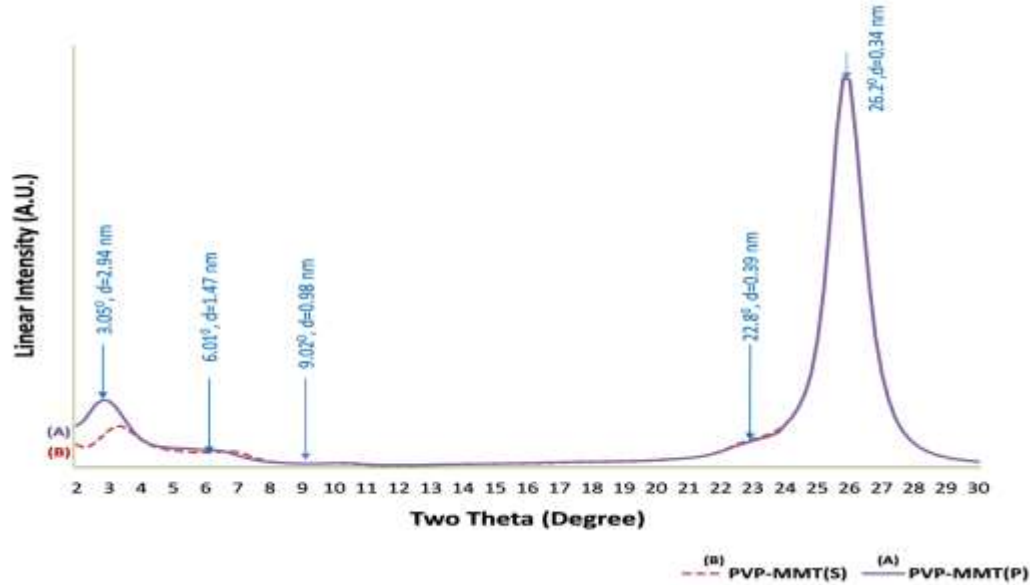


Figure 6. 1: XRD results for PVP-MMT (a) printing, (b) spraying

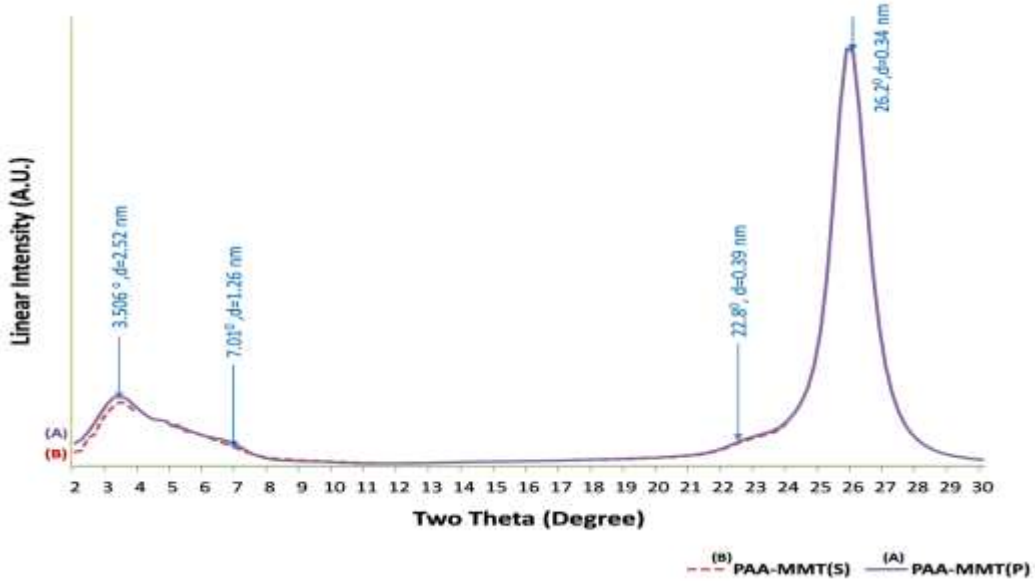


Figure 6. 2: XRD results for PAA-MMT (a) printing, (b) spraying

All the patterns in Figure 6.1 and 6.2 show both polymer nanocomposites are intercalated.

Figure 6.3 shows the average OTR and thickness in printing and spraying with PVP-MMT and PAA-MMT films as a function of different bilayers.

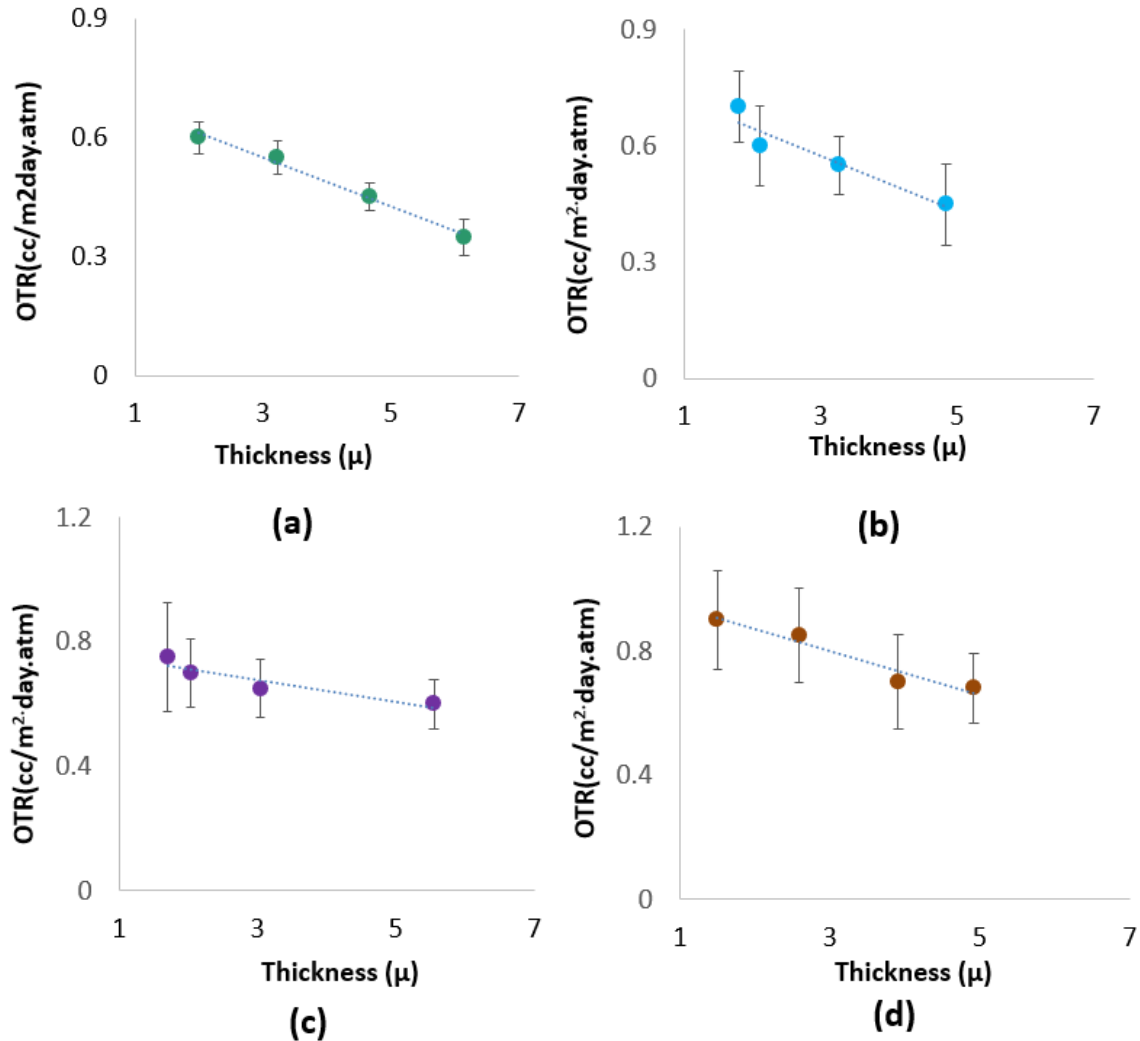


Figure 6. 3: Oxygen Transmission Rate comparison of (a) PVP-MMT_(P), (b) PVP-MMT_(S), (c) PAA-MMTP, and (d) PAA-MMTS.(P: Printing, S: Spraying)

Figure 6.4 shows that PVP-MMT nanocomposite deposited via Inkjet printing has remarkably 40 times better oxygen barrier capability than Mylar (PET) alone. We

conclude that spraying technique is the faster technique than ink jet printing technique, but printing technique are more precise and controllable. The PAA-MMT nanocomposite deposited via Inkjet printing has 23 times better oxygen barrier capability than Mylar (PET) alone. The PVP-MMT nanocomposite created with the ink-jet printer in previous work [46] has a lower molecular weight and increased thickness but less OTR compared to the PVP-MMT nanocomposite in this work. Thickness differences depend on inkjet printer settings, montmorillonite concentration, and polymer molecular weight. The PVOH-MMT nanocomposite has 13 times less thickness than the nanocomposite in the previous work [46] . In Figure 6.5, the effect of each material on OTR was individually investigated in the PVOH-MMT nanocomposite. Figure 6.6, part (a) shows the photograph of deposited film and part (b) shows the cross-section SEM image of our minimum thickness for PVOH-MMT nanocomposite that has zero transmission rate.

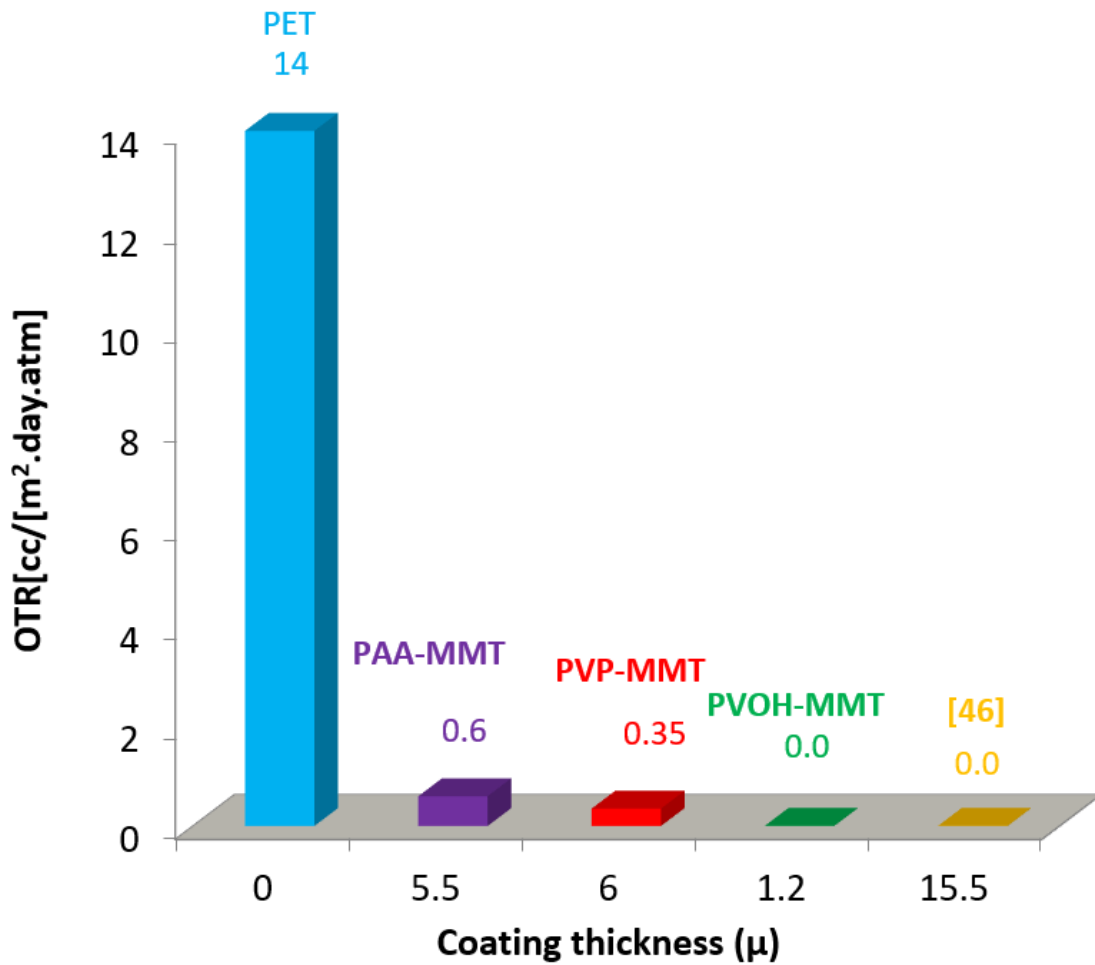


Figure 6. 4: OTR comparison of PET, several deposited nanocomposites and previous [26] work via inkjet-printer

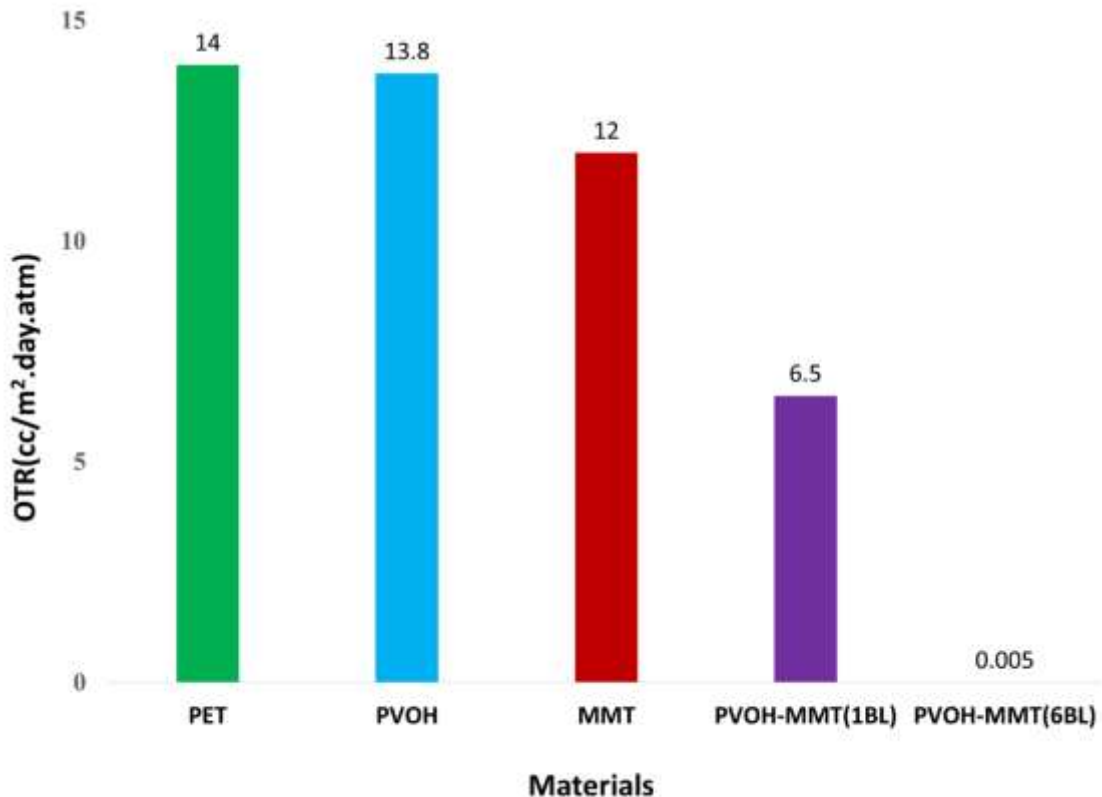


Figure 6. 5: Comparison among materials that affect oxygen barrier

From Figure 6.5, we can understand that the OTR results taken under the exact same humidity conditions that PET coated with pure PVOH has no effect on the gas permeability. Furthermore, PET coated with MMT did not statistically improve the OTR. It is clear then that the intercalated complex behaves quite differently than any prediction of any additive effect of the two pure systems. It is well established that PVOH films are extremely sensitive to humidity when measuring OTR. In the case of the pure PVOH and the MMT the area was printed twice to adjust the thickness to be as close to the same as possible. The drying conditions of humidity and temperature were maintained equally for all the films.



Figure 6. 6:(a) Photograph of PVOH-MMT;(b). Cross-section SEM image of 6 BL PVOH-MMT composite

Figure 6.7 is the surface SEM image of PVOH-MMT PNC film deposited via printing technique. Pictures taken from PNC by SEM has poor quality because of the charging polymer. To solve the charging problem on the surface of films, a 2 μm layer of iridium was deposited. Then we did Ion milling by SEM to see deposited layers (with ions SEM bombards the sample and this milling the pointed place).

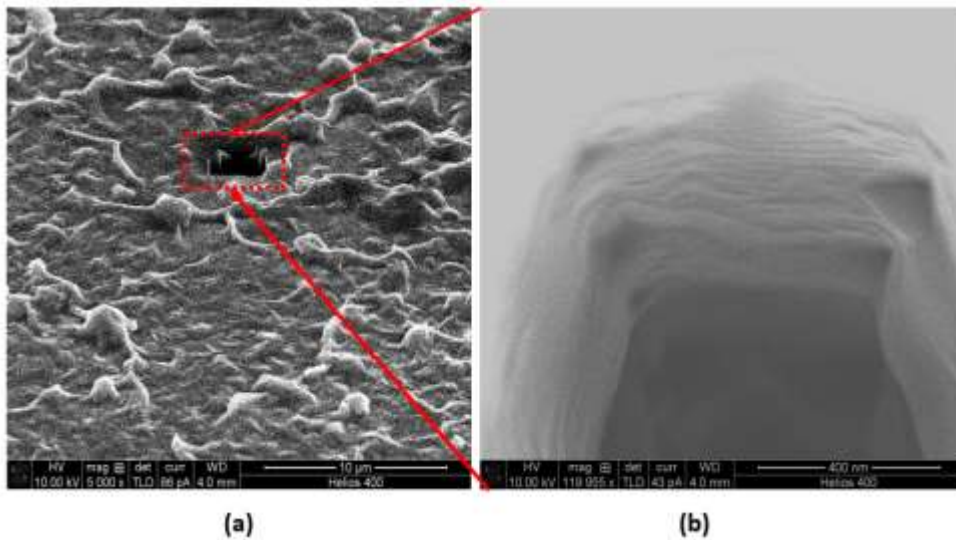


Figure 6.7: (a) SEM surface picture (b) ion milled part of surface

Transmission Electron Microscopy (TEM) can take a high-resolution photograph of PNC. TEM can show the level of exfoliation and the distance between particles. TEM can show the pictures of disordered structures and tactoids. We needed to make a very thin sample by using a microtome (put in epoxy resin to for easy cutting). A thin slice of the sample should be floated onto copper grids. TEM imaging can take several days [56]. Figure 6.8 shows a TEM picture of PVOH-MMT PNC layers and reveals a narrow size of MMT.

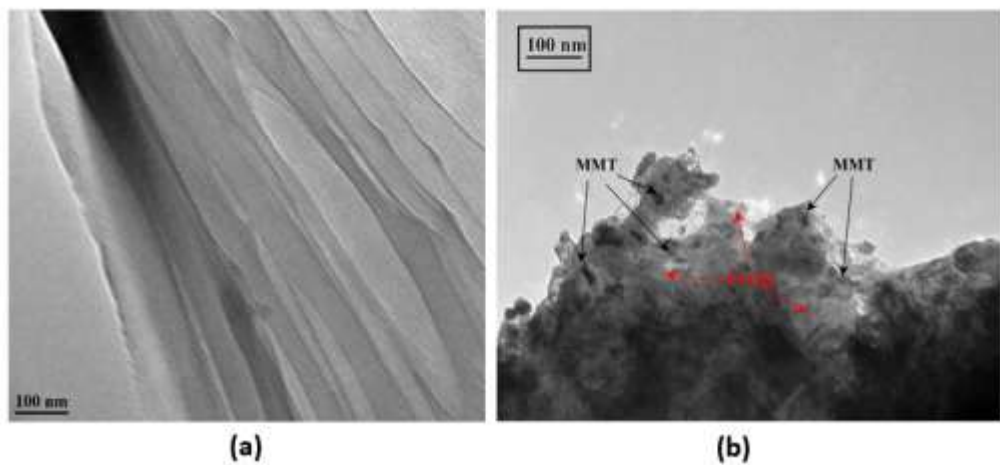


Figure 6.8: Morphological features of (a) 6B PVOH-MMT;(b) narrow size of MMT palates

The last variable of interest in these intercalated system is the effect of film thickness in PVOH-MMT PNC. In these experiments a series of films were printed in successive number of from one to six BL with subsequent measurement of OTR for each film. In Figure 6.9, the results of these experiments are contained. At 6 bilayers the film thickness is 1.2 microns. It is clear from the graph that extremely good gas barrier performance can be obtained with these intercalated systems. To put these values in context the gold standard in packaging is aluminized PET which typically has an OTR just below 1 cc/m² day atm. These films can clearly excel barrier performance and are quite transparent.

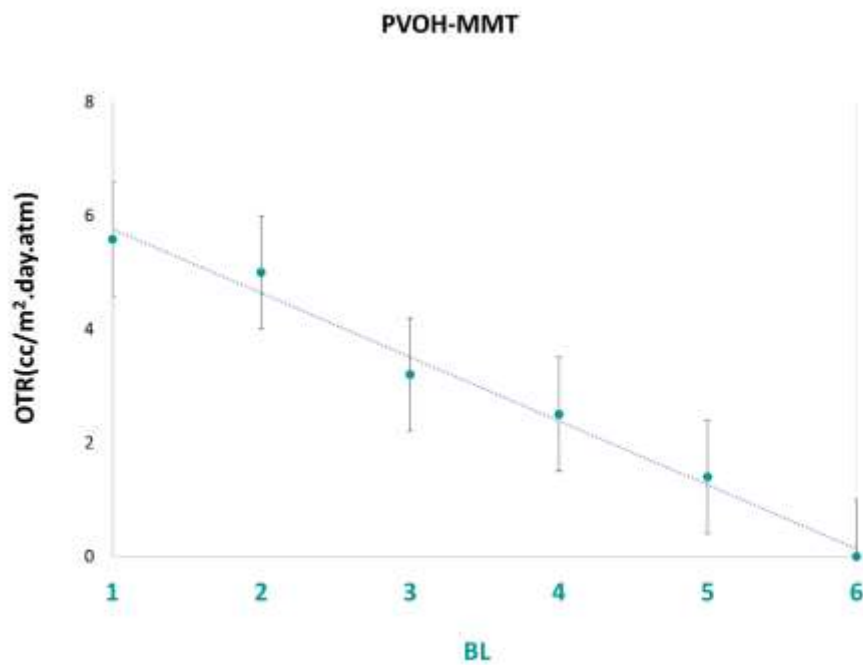


Figure 6. 9: Effect of film thickness on OTR for PVOH-MMT PNC

Figure 6.10 shows the transmittance spectra of different films in a wavelength range of 400 - 700 nanometers (nm) (visible light).

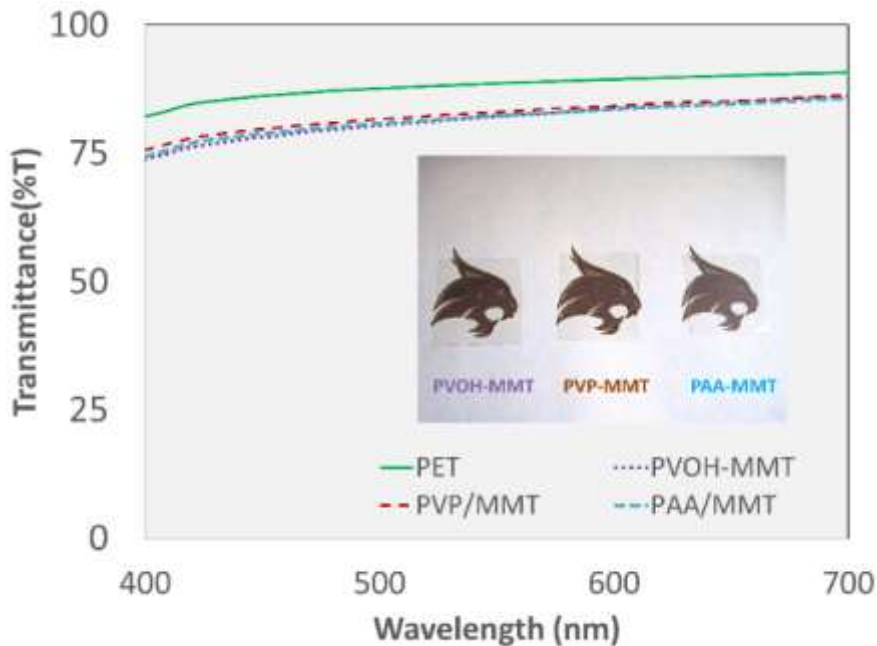


Figure 6. 10: Transparency measurement via UV-Vis spectrometer

We also printed PVOH-Lap in 5 BL with a thickness less than few microns (see Figure 6.11). This PNC obeys “the rule of constrained polymer region.” Therefore, clay size has no influence on having less amount of gas permeation here. Figure 6.12 part (a) shows the effect of having this nanocomposite in 5BL and deposited via the ink-jet printer.

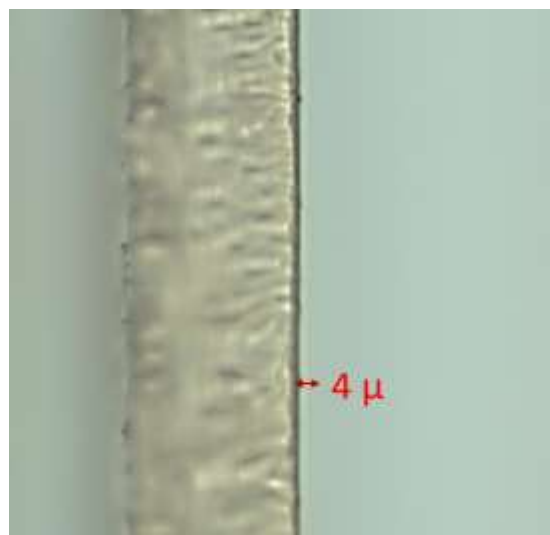


Figure 6. 11: Cross-section picture of PVOH-Lap 5 BL printed

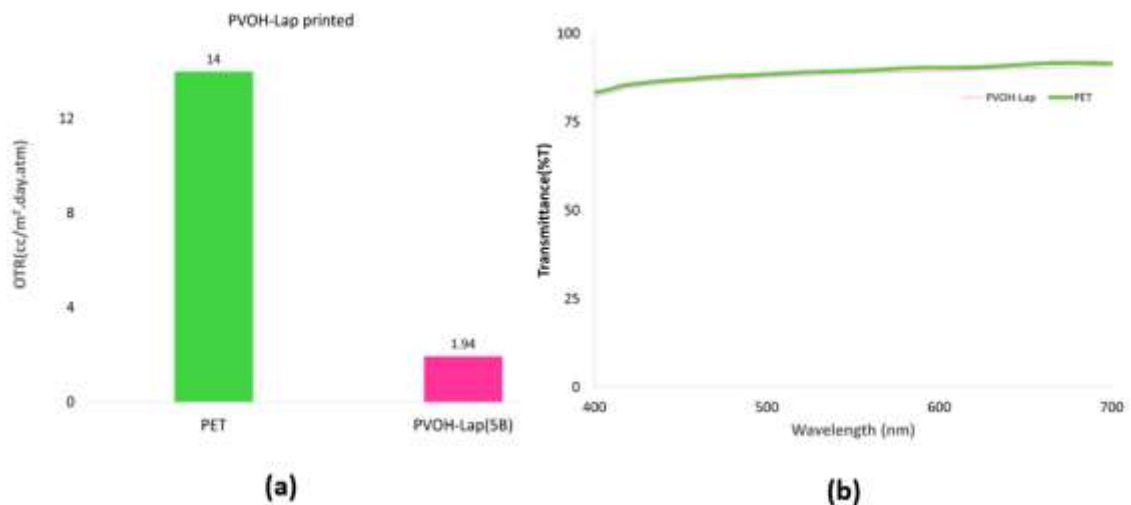


Figure 6. 12: (a) OTR of printed PVOH-Lap in 5 BL;(b) Transparency measurement

We also know that Laponite clay is completely transparent. The light transmission rate for uncoated PET is 85% while the PVOH-LAP coated is also 85%. When observing the coated film from different angles it appears to be more transparent. This effect is most

likely due to surface roughness that exist on the surface of the PET sheets that is largely eliminated with the film drying and nanoparticles filling the imperfections.

We compared PVOH-Lap PNC with PET substrate alone in Figure 6.12 part (b). The result shows the 100% transparency of this polymer nanocomposite.

Table 6.1 compares various gas barrier materials and techniques on transparency in the literature with our nanocomposites. We consider all materials to be evaluated at an average wavelength of 400-700 nm.

Table 6.1 Comparison of composite transmittance films used with various materials, OTR and transparency in range of visible light (400 nm -700 nm) via UV-Vis spectrometer

Materials	Techniques	OTR ($\text{cc m}^{-2} \text{ day}^{-1}$ atm^{-1})	%Transparency
SiO_xN_y [102]	Magnetic	0.71	100
PAM/MMT [103]	sputtering		
	Dipping and drying	0	90
PVOH-LDH [90]	Dipping and drying	0.72	90
PVOH/MMT	Ink-jet printing	0	93
PVP/MMT	Ink-jet printing	0.35	97
PAA/MMT	Ink-jet printing	0.6	96
PVOH/Lap	Ink-jet printing	1.9	100
PEI/PAA/PEI/MMT [26]	Rinsing and drying	0	95
PEI/MMT [22]	Plasma	1.6	88.5

6.3 Transparency and PNCs Thickness

Thicker polymer-clay composite films are less transparent than thinner films [22].

The film thickness of assemblies can be varied by different pH, molecular weight, solution, and environmental factors such as temperature or relative humidity [93]. Figure 6.13 shows a comparison between two PVP and MMT nanocomposites with different molecular weight.

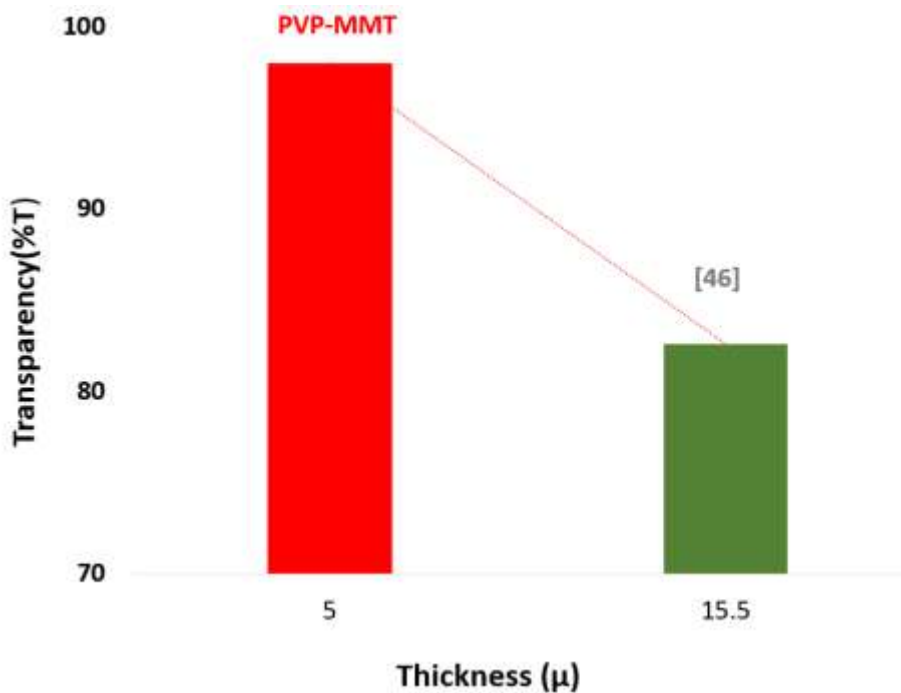


Figure 6. 13: Transparency improvement in less thickness

6.4 Edible Coating Application

We can understand that these intercalated systems could be used as a replacement for food packaging to extend shelf life of food. This intercalated system would be major improving food packaging while it has high barrier property and high transparency. Disposal of the packaging is major problem. This problem has been highlighted recently [104]. For example, more than 78 million metric tons of plastic packaging produced each

year and around 31 million tons go to landfills, only 22 million tons are used for energy recovery or recycled, and 25 million tons are trash in the environment. For decreasing this problem, a more revolutionary approach is to coat fruits and vegetables directly and this will eliminate packaging altogether. This coating must be edible or removable by washing. PVOH and smectite clays are both classified as GRAS (Generally Recognized as Safe) by the Food and Drug Administration. Many products are existing that contain PVOH or MMT and they are consumed daily by consumers. To test this approach, several fruits and vegetables were purchased at the local market and one set of each was coated by spraying them with a solution containing both PVOH and MMT and one set left uncoated. The different fruits and vegetables were then stored at room temperature and observed for discoloration, mold, or rotting. Figure 6.14 includes the results of those tested produces. Each of the bars in the graph display the number of days that the respective fruit or vegetable remained without defect past the point at which the uncoated produce was judged to be unacceptable.

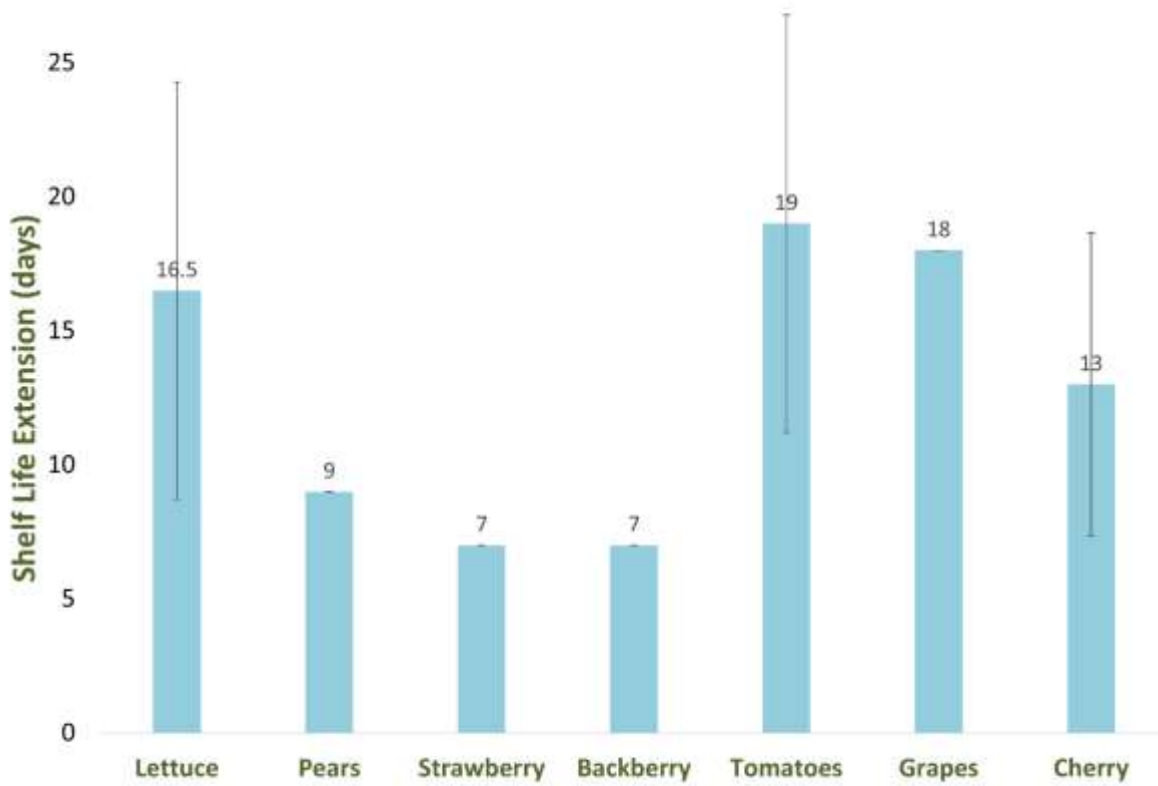


Figure 6. 14: Shelf life extension for selected fruits and vegetables (in days)

The zero point in Figure 6.14 is the time that the uncoated fruit or vegetable was judged to be unacceptable for human consumption. These results show that all cases tested the coated produce lasted longer than the uncoated. The average extension was a factor of two in shelf life. It is rational to expect that produce coated at harvest would exhibit larger extension of shelf life. Figure 6.15 shows a photograph a of typical results for tomatoes.



Figure 6. 15: Comparison of coated and uncoated tomatoes at 35 days after purchase

CHAPTER VII. CONCLUSION AND RECOMMENDATION FOR FURTHER RESEARCH

This chapter provides an overall conclusion on the results and accomplished research. Also, in this chapter suggestions for future work is presented.

7.1 Results and Conclusion

In this research, we found several polymers (PVP, PAA, PVOH, and EVOH) and nanoclays (MMT and LAP) which can give us a remarkable amount of oxygen barrier property. The extension of the self-assembling polymer/clay nanocomposites has been demonstrated for a variety of polymers and smectic clays. These intercalated systems yield extraordinary gas barrier performance that appears to exceed that which would be expected from a simple tortuous path model for gas diffusion. The intercalated systems exhibit behavior that is very different than the individual systems. Moreover, we also found that the constrained region of the amorphous polymer can affect gas barrier property even when we have a small particle size particle in polymer nanocomposite. Because, in Tortuous Path model, the size of the constrained region and the diffusion coefficient within the constrained region were not considered.

Also, we found that lower molecular weight of polymers gives better gas barrier property. However, annealing the polymer nanocomposites will help to have less amount of gas permeation rate. Moreover, a surfactant in polymer nanocomposite structure or having polymer in the different level of hydrolyzation may help to have a more ordering system, but it has a negligible effect on having less amount of OTR. Furthermore, we investigated the impact of humidity on different polymer nanocomposites. We developed

a novel technique and material to protect PVOH from humidity. The effect of a different range of humidity on the oxygen permeation of PVOH-MMT nanocomposite shows that on average, all OTR rate is less than one cc/m².day.atm. Also, this work exhibits excellent results that our self-assembled nanocomposite film has excellent oxygen barrier (zero oxygen transmission rate) without overcoating with another polymer. The thickness amount of this deposited nanocomposite via inkjet printer is 1200 nm, and it provides transparency more than 93%.

We report the novel paint spraying and inkjet printing techniques for having a self-assembling system which eliminates the many rinsing and drying steps in LbL. Overall, comparing of inkjet printing and spraying, each technique has pros and cons. For using the ink-jet printer, the solution should be diluted well and DMC-11601 print head of the Dimatix 2831 designed for particle size less than 0.2 microns. Paint spraying is faster and having lower cost than inkjet printing technique. However, ink jet printing is more controllable and time consuming than spraying technique. Difference of result in these two techniques is only 10-20 %.

These coating materials are approved by the FDA (Food and Drug Administration), and they are generally recognized as safe materials to use. This reason makes them excellent alternative food packaging commercial applications. These intercalated systems applied to produce yield substantial increases in shelf life and eliminated packaging waste and disposal issues. These intercalates could have other potential applications such as protection for organic light emitting diodes that are very sensitive to oxidation.

7.2 Recommendation for Future Research

Further study on constrained polymer model can be done by using complex simulation (theoretical) which can consider the size of the constrained region and the diffusion coefficient within the constrained region.

PVOH/LAP nanocomposite has outstanding amount of transparency and oxygen permeation and this can be a good candidate for Electro-Optical applications ($OTR < 10^{-5}$).

Other substrates and materials should be tested to verify their structure and impact on gas permeability. The effect of manipulating pH amount in polymer solution needs to be analyzed [105].

The effect of other gases such as CO_2 permeability in polymer nanocomposite needs to be investigated. Several more bilayers of a film (different thickness) in both printing and spraying need to be deposited and compared to observe and find which ones have an ascending path of reducing OTR quickly.

The role of surface tension should be considered when studying the ordering that has been observed in the self-assembled films [106].

Other characterization techniques such as TEM needs to be used to see the morphology of polymer nanocomposites in detail. Simulation techniques need to be used to forecast the different behavior of polymers and clays. Other surfactants need to be used to observe their effect on oxygen permeability and ordering of polymer nanocomposite systems.

APPENDIX SECTION

APPENDIX A: ACRONYMS AND PHYSICAL QUANTITIES

PNC	Polymer Nano Composite
Bilayer	BL
DOD	Drop on Demand
XRD	X Ray-Diffraction
OTR	Oxygen Transmission Rate
DLH	Different Level of Humidity
HM	Humidity
CNTs	Carbon Nanotubes
P	Printing
S	Spraying

APPENDIX B: USED MATERIALS AND MANUFACTURERS

Materials	Stated	Characteristic	Manufacturer
Poly (vinylpyrrolidone)	PVP	K-90, MW=360000	SPI Chem
Poly (vinylpyrrolidone)	PVP	K-60, 45% in water MW=160000	Sigma Aldrich
poly (acrylic acid)	PAA	MW=1800	Sigma Aldrich
Poly (vinyl alcohol)	PVOH	3-80 wt% >94 Bulk density 400 - 600 kg/m ³	KURARAY POVAL
Ethyl (vinyl alcohol)	EVOH	Type f (F101B) Density 10 ³ kg/m ³	KURARAY EVAL
Poly (ethylene glycol)	PEG	MW=2000	BASF (pluracol E2000)
Poly (ethylene glycol)	PEG	MW=8000	Fluka
Montmorillonite	MMT	Cloisite Na+	BYK
Laponite	Lap/LAP	XLG	BYK
Hectorite	Hector/HEC	SHCa-1 Contains(CaCo ₃)	Baroid Division- National Lead Co. Clay mineral society
Saponite	Sap/SAP		BYK
Vermiculite	VMT	25.4mm or less than 75 mm.	BYK
Humic Acid	HA	SP-90	1 Lb TeraVita =>87%-93% humic acids
Dimethyl Sulfoxide (methyl sulfoxide)	DMSO	(CH ₃) ₂ SO	Baker Analyzed' reagent

APPENDIX C: USED CHARACTRIZATION DEVICES

Devices	Detail	Model
XRD	X-ray Diffraction	Rigaku smart lab X-ray diffractometer/ Bruker D8 focus powder
Mocon	Oxygen permeation	ox-tran 2/60
UV-Vis spectrometer	Transmittance light	Shimadzu 2501PC
SEM	Scan Electron Microscope	FEI Helios NanoLab 400
TEM	Transmission Electron Microscopy	JELO JEM 1200EXII
Profilometer	Height measuring	Dektak XT
TGA	Thermal gravimetric Analyzer	(TA Q50) during heating in an argon atmosphere at a rate of 10 °C/min from room temperature to 800 °C.
ChemDraw Prime 16	Drawing software	Trial version
PH	Hydrion (PH 1-11)	MicroEssentialLab

APPENDIX D: MEASURD PH OF USED MATERIAL IN DI WATER

Materials	PH
PVOH	5
PAA	4
EVOH	4
PVP (k-15)	5
PVP(k-30)	4.5
PEG 2000	5
PEG 8000	5
SDS	4
MMT(Na)	7
Humic acid	8
Saponite	6
Laponite	7
GO	4
Vermiculite	5
Hectorite	7
Hydrotalcite	10
PVOH-MMT mixed	6
PVOH-SDS	5
MMT(ca)	5
NaCL	4
DI H2O	4

REFERENCES

- [1] G. Decher, J. Hong, and J. Schmitt, “Buildup of ultrathin multilayer films by a self-assembly process: III. Consecutively alternating adsorption of anionic and cationic polyelectrolytes on charged surfaces,” *Thin Solid Films*, vol. 210-211, pp. 831–835, 1992.
- [2] D. Shipp, “Polymer-Layered Silicate Nanocomposites,” *Comprehensive Nanoscience and Technology*, pp. 265–276, 2011.
- [3] W. T. Brydges, S. T. Gulati, and G. Baum, “Permeability of glass ribbon-reinforced composites,” *Journal of Materials Science*, vol. 10, no. 12, pp. 2044–2049, 1975.
- [4] Y. Ke and P. Stroeve, “Polymer-Layered Silicate and Silica Nanocomposites,” *Polymer-Layered Silicate and Silica Nanocomposites*, pp. 119–209, 2005.
- [5] S. C. Tjong and Y. W. Mai, *Physical properties and applications of polymer nanocomposites*. Cambridge: Woodhead Publishing, 2010.
- [6] A. Kalendova, D. Merinska, J. F. Gerard, and M. Slouf, “Polymer/clay nanocomposites and their gas barrier properties,” *Polymer Composites*, vol. 34, no. 9, pp. 1418–1424, 2013.
- [7] Y. Wu, “Nanoparticle filled polymeric systems for gas barrier and flame-retardant properties,” dissertation, 2013.
- [8] T. Lan and T. Lan, “Polymer-clay nanocomposites,” in *Polymer-clay nanocomposites*, 1994.
- [9] P. Anadão, “Polymer/ Clay Nanocomposites: Concepts, Researches, Applications and Trends for The Future,” in *Nanotechnology and Nanomaterials*, INTCH, 2012.
- [10] P. Meneghetti and S. Qutubuddin, “Synthesis, thermal properties and applications of polymer-clay nanocomposites,” *Thermochimica Acta*, vol. 442, no. 1-2, pp. 74–77, Mar. 2006.

- [11] G. Choudalakis and A. D. Gotsis, “Permeability of polymer/clay nanocomposites: A review,” European Polymer Journal, pp. 967–984, Apr. 2009.
- [12] K. Jlassi, M. M. Chehimi, and S. Thomas, Clay-polymer nanocomposites. Amsterdam: Elsevier, 2017.
- [13] “Introduction to Polymer–Clay Nanocomposites,” CRC Press. [Online]. Available: <https://www.crcpress.com/Introduction-to-PolymerClay-Nanocomposites/Gurses/p/book/9789814613026>. [Accessed: 08-Oct-2017].
- [14] K. Müller, E. Bugnicourt, M. Latorre, M. Jorda, Y. E. Sanz, J. Lagaron, O. Miesbauer, A. Bianchin, S. Hankin, U. Bötz, G. Pérez, M. Jesdinszki, M. Lindner, Z. Scheuerer, S. Castelló, and M. Schmid, “Review on the Processing and Properties of Polymer Nanocomposites and Nanocoatings and Their Applications in the Packaging, Automotive and Solar Energy Fields,” *Nanomaterials*, vol. 7, no. 4, p. 74, 2017.
- [15] I. Soltani, S. D. Smith, and R. J. Spontak, “Effect of polyelectrolyte on the barrier efficacy of layer-by-layer nanoclay coatings,” *Journal of Membrane Science*, vol. 526, pp. 172–180, 2017.
- [16] S. Pira, “Global Growth Ahead for Flexible Packaging,” *The National Provisioner*, 01-Oct-2015.
- [17] A. Zurutuza and C. Marinelli, “Challenges and opportunities in graphene commercialization,” *Nature Nanotechnology*, vol. 9, no. 10, pp. 730–734, 2014.
- [18] A. S. H. Makhlouf, Nanocoatings and ultra-thin films: technologies and applications. Cambridge: Woodhead Publishing Ltd, 2011.
- [19] A. Al-Abduljabbar, “Modeling Gas Barrier Property Improvements in Polymer-Clay Nano-Composites,” *Journal of Nano Research*, vol. 29, pp. 75–84, 2014.
- [20] L. Wu and J. Baghdachi, Functional polymer coatings: principles, methods and applications. Hoboken, NJ: Wiley, 2015.
- [21] Y. Wu, “Nanoparticle filled polymeric systems for gas barrier and flame retardant properties,” dissertation, 2013.

- [22] M. A. Priolo, D. Gamboa, K. M. Holder, and J. C. Grunlan, “Super Gas Barrier of Transparent Polymer–Clay Multilayer Ultrathin Films,” *Nano Letters*, vol. 10, no. 12, pp. 4970–4974, 2010.
- [23] A. J. Svagan, A. Åkesson, M. Cárdenas, S. Bulut, J. C. Knudsen, J. Risbo, and D. Plackett, “Transparent Films Based on PLA and Montmorillonite with Tunable Oxygen Barrier Properties,” *Biomacromolecules*, vol. 13, no. 2, pp. 397–405, 2012.
- [24] T. V. Duncan, “Applications of nanotechnology in food packaging and food safety: Barrier materials, antimicrobials and sensors,” *Journal of Colloid and Interface Science*, vol. 363, no. 1, pp. 1–24, 2011.
- [25] D. Rawtani and Y. K. Agrawal, “Emerging Strategies and Applications of Layer-by-Layer Self-Assembly,” *Nanobiomedicine*, vol. 1, p. 8, 2014.
- [26] M. A. Priolo, D. Gamboa, and J. C. Grunlan, “Transparent Clay–Polymer Nano Brick Wall Assemblies with Tailorable Oxygen Barrier,” *ACS Applied Materials & Interfaces*, vol. 2, no. 1, pp. 312–320, 2010.
- [27] G. Findenig, S. Leimgruber, R. Kargl, S. Spirk, K. Stana-Kleinschek, and V. Ribitsch, “Correction to Creating Water Vapor Barrier Coatings from Hydrophilic Components,” *ACS Applied Materials & Interfaces*, vol. 6, no. 2, pp. 1337–1337, 2014.
- [28] Y. Cui, S. Kundalwal, and S. Kumar, “Gas barrier performance of graphene/polymer nanocomposites,” *Carbon*, vol. 98, pp. 313–333, 2016.
- [29] E. Dunkerley and D. Schmidt, “Effects of Composition, Orientation and Temperature on the O₂Permeability of Model Polymer/Clay Nanocomposites,” *Macromolecules*, vol. 43, no. 24, pp. 10536–10544, 2010.
- [30] R. Bharadwaj, A. Mehrabi, C. Hamilton, C. Trujillo, M. Murga, R. Fan, A. Chavira, and A. Thompson, “Structure–property relationships in cross-linked polyester–clay nanocomposites,” *Polymer*, vol. 43, no. 13, pp. 3699–3705, 2002.

- [31] D. Adame and G. Beall, “Direct measurement of the constrained polymer region in polyamide/clay nanocomposites and the implications for gas diffusion,” *Applied Clay Science*, vol. 42, no. 3-4, pp. 545–552, 2009.
- [32] W.-S. Jang, I. Rawson, and J. C. Grunlan, “Layer-by-layer assembly of thin film oxygen barrier,” *Thin Solid Films*, vol. 516, no. 15, pp. 4819–4825, 2008.
- [33] C.-W. Chiu and J.-J. Lin, “Self-assembly behavior of polymer-assisted clays,” *Progress in Polymer Science*, vol. 37, no. 3, pp. 406–444, 2012.
- [34] S. Nazarenko, P. Meneghetti, P. Julmon, B. G. Olson, and S. Qutubuddin, “Gas barrier of polystyrene montmorillonite clay nanocomposites: Effect of mineral layer aggregation,” *Journal of Polymer Science Part B: Polymer Physics*, vol. 45, no. 13, pp. 1733–1753, 2007.
- [35] K. Yano, A. Usuki, A. Okada, T. Kurauchi, and O. Kamigaito, “Synthesis and properties of polyimide–clay hybrid,” *Journal of Polymer Science Part A: Polymer Chemistry*, vol. 31, no. 10, pp. 2493–2498, 1993.
- [36] Y. Ye, H. Chen, J. Wu, and L. Ye, “High impact strength epoxy nanocomposites with natural nanotubes,” *Polymer*, vol. 48, no. 21, pp. 6426–6433, 2007.
- [37] E. Picard, A. Vermogen, J. Gerard, and E. Espuche, “Barrier properties of nylon 6-montmorillonite nanocomposite membranes prepared by melt blending: Influence of the clay content and dispersion state Consequences on modelling,” *Journal of Membrane Science*, vol. 292, no. 1-2, pp. 133–144, 2007.
- [38] T. Guin, M. Krecker, D. A. Hagen, and J. C. Grunlan, “Thick Growing Multilayer Nanobrick Wall Thin Films: Super Gas Barrier with Very Few Layers,” *Langmuir*, vol. 30, no. 24, pp. 7057–7060, 2014.
- [39] G. A. Choudalakis, H. Kalo, J. Breu, and A. D. Gotsis, “CO₂ gas barrier properties in polymer nanocomposite coatings containing Li-hectorite clays,” *Journal of Applied Polymer Science*, vol. 131, Apr. 2014.

- [40] N. Boutroy, Y. Pernel, J. Rius, F. Auger, H. Bardeleben, J. Cantin, F. Abel, A. Zeinert, C. Casiraghi, A. Ferrari, and J. Robertson, “Hydrogenated amorphous carbon film coating of PET bottles for gas diffusion barriers,” *Diamond and Related Materials*, vol. 15, no. 4-8, pp. 921–927, 2006.
- [41] M. D. Amiri, S. Das, G. W. Beall, “Improvement Approach for Gas Barrier Behavior of Polymer/Clay Nanocomposite Films” *MRS Advances*, Accepted, 2017.
- [42] D. A. Kunz, J. Schmid, P. Feich, J. Erath, A. Fery, and J. Breu, “Clay-Based Nanocomposite Coating for Flexible Optoelectronics Applying Commercial Polymers,” *ACS Nano*, vol. 7, no. 5, pp. 4275–4280, Apr. 2013.
- [43] K. Tulysyan, S. Toshniwal, G. Dorairaju, D. F. Schmidt, and E. Reynaud, “Thermomechanical Assessment of Plastic Deformation in Model Amorphous Polyamide/Clay Nanocomposites,” *Journal of Nanomaterials*, 2010.
- [44] Ahmed M. Youssef, “Polymer Nanocomposites as a New Trend for Packaging Applications,” *Journal Polymer-Plastics Technology and Engineering*, vol. 52, no. 7, pp. 635–660, 2013.
- [45] “Oxygen Transmission Rate,” Poly Print: Oxygen Transmission Rate. [Online]. Available: <http://www.polyprint.com/flexographic-otr.htm>. [Accessed: 09-Feb-2017].
- [46] R. Cook, Y. Chen, and G. W. Beall, “Highly Ordered Self-Assembling Polymer/Clay Nanocomposite Barrier Film,” *ACS Applied Materials & Interfaces*, vol. 7, no. 20, pp. 10915–10919, 2015.
- [48] M. Wong, R. Ishige, K. L. White, P. Li, D. Kim, R. Krishnamoorti, R. Gunther, T. Higuchi, H. Jinnai, A. Takahara, R. Nishimura, and H.-J. Sue, “Large-scale self-assembled zirconium phosphate smectic layers via a simple spray-coating process,” *Nature Communications*, vol. 5, 2014.
- [49] P. C. Suarez-Martinez, J. Robinson, H. An, R. C. Nahas, D. Cinoman, and J. L. Lutkenhaus, “Spray-On Polymer-Clay Multilayers as a Superior Anticorrosion Metal Pretreatment,” *Macromolecular Materials and Engineering*, p. 1600552, 2017.

- [50] N. Reis, C. Ainsley, and B. Derby, “Ink-jet delivery of particle suspensions by piezoelectric droplet ejectors,” *Journal of Applied Physics*, vol. 97, no. 9, p. 094903, 2005.
- [51] “Industrial Inkjet Printheads,” Fujifilm Value from Innovation. [Online]. Available: http://www.fujifilmusa.com/products/industrial_inkjet_printheads/index.html. [Accessed: 03-Jun-2017].
- [52] yoshinorikato, “FUJIFILM Group's inkjet printhead and technology,” *FUJIFILM RESEARCH AND DEVELOPMENT*, vol. 59, pp. 27–31, 2014.
- [53] A. B. Morgan and J. W. Gilma, “Characterization of Polymer-Layered Silicate (Clay) Nanocomposites by Transmission Electron Microscopy and X-Ray Diffraction: A Comparative Study,” *Journal of Applied Polymer Science*, vol. 87, no. 6, pp. 1330–1338, 2002.
- [55] A. Greco, A. Timo, and A. Maffezzoli, “Development and Characterization of Amorphous Thermoplastic Matrix Graphene Nanocomposites,” *Materials*, vol. 5, pp. 1972–1985, 2012.
- [56] G. W. Beall and C. E. Powell, *Fundamentals of Polymer-Clay Nanocomposites*. Cambridge: Cambridge University Press, 2011.
- [57] R. Jenkins and R. L. Snyder, *Introduction to x-ray powder diffractometry*. New York: John Wiley & Sons, 1996.
- [58] A. Reyna-Valencia, Y. Deyrail, and M. Bousmina, “In Situ Follow-Up of the Intercalation Process in a Clay/Polymer Nanocomposite Model System by Rheo-XRD Analyses,” *Macromolecules*, vol. 43, no. 1, pp. 354–361, Dec. 2010.
- [59] X. Deng and R. Srinivasan, “When Do Transparent Packages Increase (or Decrease) Food Consumption?” *Journal of Marketing*, vol. 77, no. 4, pp. 104–117, 2013.
- [60] J. Y. Kim, H. Kim, B. H. Kim, T. Chang, J. Lim, H. M. Jin, J. H. Mun, Y. J. Choi, K. Chung, J. Shin, S. Fan, and S. O. Kim, “Highly tunable refractive index visible-light metasurface from block copolymer self-assembly,” *Nature Communications*, vol. 7, p. 12911, 2016.

- [61] F. J. Stevenson, *Humus chemistry: genesis, composition, reactions*. New York: Wiley, 1994.
- [62] Q. Yang, T. Saito, and A. Isogai, “Transparent, flexible, and high-strength regenerated cellulose/saponite nanocomposite films with high gas barrier properties,” *Journal of Applied Polymer Science*, vol. 130, no. 5, pp. 3168–3174, Jul. 2013.
- [63] J. H. Koo, *Fundamentals, properties, and applications of polymer nanocomposites*. Cambridge: Cambridge University Press, 2016.
- [64] S. Kaufhold, M. Pohlmann-Lortz, R. Dohrmann, and R. Nüesch, “About the possible upgrade of bentonite with respect to iodide retention capacity,” *Applied Clay Science*, vol. 35, no. 1-2, pp. 39–46, 2007.
- [65] P. Lebaron, “Polymer-layered silicate nanocomposites: an overview,” *Applied Clay Science*, vol. 15, no. 1-2, pp. 11–29, 1999.
- [66] R. P. Singh, M. Khait, S. C. Zunjarao, C. S. Korach, and G. Pandey, “Environmental Degradation and Durability of Epoxy-Clay Nanocomposites,” *Journal of Nanomaterials*, vol. 2010, pp. 1–13, 2010.
- [67] “Polymer-Clay Nanocomposites: Design and Application of Multi-Functional Materials,” Sigma-Aldrich. [Online]. Available: <http://www.sigmaaldrich.com/technical-documents/articles/material-matters/polymer-clay-nanocomposites.html>. [Accessed: 08-Oct-2017].
- [68] H. Khalil, D. Mahajan, and M. Rafailovich, “Polymer-montmorillonite clay nanocomposites. Part 1: Complexation of montmorillonite clay with a vinyl monomer,” *Polymer International*, vol. 54, no. 2, pp. 423–427, 2004.
- [69] R. G. Cook, “Layer-by-Layer films via 3D drop on demand printing,” dissertation.
- [70] V. Korampally, M. Yun, T. Rajagopalan, P. K. Dasgupta, K. Gangopadhyay, and S. Gangopadhyay, “Entropy driven spontaneous formation of highly porous films from polymer–nanoparticle composites,” *Nanotechnology*, vol. 20, no. 42, p. 425602, 2009.

- [71] J. K. Roberts and W. J. C. Orr, “Induced dipoles and the heat of adsorption of argon on ionic crystals,” *Transactions of the Faraday Society*, vol. 34, p. 1346, 1938.
- [72] P. W. Labuschagne, W. A. Germishuizen, S. M. C. Verryn, and F. S. Moolman, “Improved oxygen barrier performance of poly (vinyl alcohol) films through hydrogen bond complex with poly (methyl vinyl ether-co-maleic acid),” *European Polymer Journal*, vol. 44, no. 7, pp. 2146–2152, 2008.
- [73] Boundless, “Synthesis of Biological Macromolecules,” *Synthesis of Biological Macromolecules | Boundless Biology*. [Online]. Available: <https://courses.lumenlearning.com/boundless-biology/chapter/synthesis-of-biological-macromolecules/>. [Accessed: 28-Sep-2017].
- [74] Admin, “Selvol™ Polyvinyl Alcohol,” Sekisui Specialty Chemicals-PVOH, 20-Jan-2016. [Online]. Available: <http://www.sekisui-sc.com/products/polyvinyl-alcohol/>. [Accessed: 28-Sep-2017].
- [75] B. K. G. Theng, G. Yuana, and H. Hashizume , “Clay Minerals and Polymers: From Soils to Nanocomposites,” *Clay science 12 Supplement* , pp. 69–73, 2005.
- [76] G. H. Fredrickson and J. Bicerano, “Barrier properties of oriented disk composites,” *The Journal of Chemical Physics*, vol. 110, no. 4, pp. 2181–2188, 1999.
- [77] T. J. Pinnavaia and G. W. Beall, *Polymer-clay nanocomposites*. Chichester: John Wiley, 2002.
- [78] A. Benhammou, B. Tanouti, L. Nibou, A. Yaacoubi, and J.-P. Bonnet, “Mineralogical and Physicochemical Investigation of Mg-Smectite from Jbel Ghassoul, Morocco,” *Clays and Clay Minerals*, vol. 57, no. 2, pp. 264–270, Jan. 2009.
- [79] J. W. Jordan, B. J. Hook, and C. M. Finlayson, “The Organophilic Bentonites. II. Organic Liquid Gels.,” *The Journal of Physical and Colloid Chemistry*, vol. 54, no. 8, pp. 1196–1208, 1950.

- [80] L. E. Nielsen, “Models for the Permeability of Filled Polymer Systems,” *Journal of Macromolecular Science: Part A - Chemistry*, vol. 1, no. 5, pp. 929–942, 1967.
- [81] T. Ebina and F. Mizukami, “Flexible Transparent Clay Films with Heat-Resistant and High Gas-Barrier Properties,” *Advanced Materials*, vol. 19, no. 18, pp. 2450–2453, 2007.
- [82] M. A. Priolo, K. M. Holder, S. M. Greenlee, and J. C. Grunlan, “Transparency, Gas Barrier, and Moisture Resistance of Large-Aspect-Ratio Vermiculite Nanobrick Wall Thin Films,” *ACS Applied Materials & Interfaces*, vol. 4, no. 10, pp. 5529–5533, 2012.
- [83] U. Tritschler, I. Zlotnikov, P. Fratzl, H. Schlaad, S. Grüner, and H. Cölfen, “Gas barrier properties of bio-inspired Laponite–LC polymer hybrid films,” *Bioinspiration & Biomimetics*, vol. 11, no. 3, p. 035005, 2016.
- [84] G. Yeh, R. Hosemann, J. Loboda-Čačković, and H. Čačković, “Annealing effects of polymers and their underlying molecular mechanisms,” *Polymer*, vol. 17, no. 4, pp. 309–318, 1976.
- [85] U. S. Kestur, H. Lee, D. Santiago, C. Rinaldi, Y.-Y. Won, and L. S. Taylor, “Effects of the Molecular Weight and Concentration of Polymer Additives, and Temperature on the Melt Crystallization Kinetics of a Small Drug Molecule,” *Crystal Growth & Design*, vol. 10, no. 8, pp. 3585–3595, 2010.
- [86] A. Zhuk, R. Mirza, and S. Sukhishvili, “Multiresponsive Clay-Containing Layer-by-Layer Films,” *ACS Nano*, vol. 5, no. 11, pp. 8790–8799, 2011.
- [87] Q. Sun, F. Joseph Schork, and Y. Deng, “Water-based polymer/clay nanocomposite suspension for improving water and moisture barrier in coating,” *Composites Science and Technology*, vol. 67, pp. 1823–1829, Jul. 2007.
- [88] A. D. Drozdov, J. C. Christiansen, R. K. Gupta, and A. P. Shah, “Model for anomalous moisture diffusion through a polymer–clay nanocomposite,” *Journal of Polymer Science Part B: Polymer Physics*, vol. 41, no. 5, pp. 476–492, Apr. 2003.

- [89] W.-S. Jang, I. Rawson, and J. C. Grunlan, “Layer-by-layer assembly of thin film oxygen barrier,” *Thin Solid Films*, vol. 516, no. 15, pp. 4819–4825, 2008.
- [90] OX-TRAN® Model 2/61 Operator’s Manual. Minneapolis: MOCON.
- [91] A. J. Nolte, N. D. Treat, R. E. Cohen, and M. F. Rubner, “Effect of Relative Humidity on the Young’s Modulus of Polyelectrolyte Multilayer Films and Related Nonionic Polymers,” *Macromolecules*, vol. 41, no. 15, pp. 5793–5798, 2008.
- [92] K. M. Holder, M. A. Priolo, K. E. Secrist, S. M. Greenlee, A. J. Nolte, and J. C. Grunlan, “Humidity-Responsive Gas Barrier of Hydrogen-Bonded Polymer–Clay Multilayer Thin Films,” *The Journal of Physical Chemistry C*, vol. 116, no. 37, pp. 19851–19856, 2012.
- [93] F. L. Marten, “Vinyl Alcohol Polymers,” *Encyclopedia of polymer science and engineering*, pp. 167–96, 1989.
- [94] Y. Dou, A. Zhou, T. Pan, J. Han, M. Wei, D. G. Evans, and X. Duan, “Humidity-triggered self-healing films with excellent oxygen barrier performance,” *Chemical Communications*, vol. 50, no. 54, p. 7136, 2014.
- [95] Y. Xianda, W. Anlai, and C. Suqin, “Water-vapor permeability of polyvinyl alcohol films,” *Desalination*, vol. 62, pp. 293–297, 1987.
- [96] M. Schmid, S. Sängerlaub, O. Miesbauer, V. Jost, J. Werthan, C. Stinga, D. Samain, C. Stramm, K. Noller, and K. Müller, “Water Repellence and Oxygen and Water Vapor Barrier of PVOH-Coated Substrates before and after Surface Esterification,” *Polymers*, vol. 6, no. 11, pp. 2764–2783, Mar. 2014.
- [97] V. Korampally, M. Yun, T. Rajagopalan, P. K. Dasgupta, K. Gangopadhyay, and S. Gangopadhyay, “Entropy driven spontaneous formation of highly porous films from polymer–nanoparticle composites,” *Nanotechnology*, vol. 20, no. 42, p. 425602, 2009.
- [98] M. R. Kamal, I. A. Jinnah, and L. A. Utracki, “Permeability of oxygen and water vapor through polyethylene/polyamide films,” *Polymer Engineering and Science*, vol. 24, no. 17, pp. 1337–1347, 1984.

- [99] “Barrier Properties of Ordered Multilayer Polymer Nanocomposites Part 2(Nanotechnology),” whatwhenhow RSS. [Online]. Available: <http://what-when-how.com/nanoscience-and-nanotechnology/barrier-properties-of-ordered-multilayer-polymer-nanocomposites-part-2nanotechnology/>. [Accessed: 26-Sep-2017].
- [100] Messersmith P.B., Giannelis E.P. Synthesis and barrier properties of poly(ϵ -caprolactone)-layered silicate nanocomposites. *J. Polym. Sci. A–Polym. Chem.* 1995; 33:1047–1057. doi: 10.1002/pola.1995.080330707.
- [101] K. M. Holder, M. A. Priolo, K. E. Secrist, S. M. Greenlee, A. J. Nolte, and J. C. Grunlan, “Humidity-Responsive Gas Barrier of Hydrogen-Bonded Polymer–Clay Multilayer Thin Films,” *The Journal of Physical Chemistry C*, vol. 116, no. 37, pp. 19851–19856, 2012.
- [102] G. Laufer, C. Kirkland, A. A. Cain, and J. C. Grunlan, “Clay–Chitosan Nanobrick Walls: Completely Renewable Gas Barrier and Flame-Retardant Nanocoatings,” *ACS Applied Materials & Interfaces*, vol. 4, no. 3, pp. 1643–1649, 2012.
- [103] W.-S. Jang, I. Rawson, and J. C. Grunlan, “Layer-by-layer assembly of thin film oxygen barrier,” *Thin Solid Films*, vol. 516, no. 15, pp. 4819–4825, 2008.
- [104] A. E. Tullo, “Chemical and engineering news,” 2016, 33-37.
- [105] H. J. Bae, H. J. Park, S. I. Hong, Y. J. Byun, D. O. Darby, R. M. Kimmel, and W. S. Whiteside, “Effect of clay content, homogenization RPM, pH, and ultrasonication on mechanical and barrier properties of fish gelatin/montmorillonite nanocomposite films,” *LWT - Food Science and Technology*, vol. 42, pp. 179–1186, 2009.
- [106] Z. Zhao, “Controlling Self-assembled Surface Features in Thin Films by Surface Tension and Elasticity,” dissertation, 2013.